

# Master's thesis

**NTNU**  
Norwegian University of Science and Technology  
Faculty of Engineering  
Department of Geoscience and Petroleum

Alireza Mohsenifesegandis

## Exploring the Transferability of Optimization Methods from Production to Storage: A Case Study of CO<sub>2</sub> Injection at Smeaheia

Master's thesis in Petroleum Engineering

Supervisor: Carl Fredrik Berg

Co-supervisor: Amir Ghaderi

June 2024



Norwegian University of  
Science and Technology



Alireza Mohsenifesegeandis

# **Exploring the Transferability of Optimization Methods from Production to Storage: A Case Study of CO2 Injection at Smeaheia**

Master's thesis in Petroleum Engineering  
Supervisor: Carl Fredrik Berg  
Co-supervisor: Amir Ghaderi  
June 2024

Norwegian University of Science and Technology  
Faculty of Engineering  
Department of Geoscience and Petroleum



Norwegian University of  
Science and Technology



---

*To my beloved parents.*



---

# Abstract

The primary objective of this research was to develop a workflow for optimizing injection well placement using reservoir simulation techniques. This study focuses on the Smeaheia CO<sub>2</sub> storage project and employs the GAS\_WATER mode of the Pflotran-OGS reservoir simulator.

To achieve this goal, several tasks were undertaken. Initially, pressure matching was performed using a system of dummy production wells and pore volume multipliers to simulate the effects of production from the Troll field which is situated near Smeaheia. The pressure matching procedure achieved an accuracy of within 4% of the measured pressures. Simulations with and without the production wells simulating the pressure drawdown from Troll gave significantly different results. The NPV for pressure-matched cases was up to 6.3% higher in some instances.

In the context of CO<sub>2</sub> sequestration, containment and storage safety were addressed by identifying spill points within the reservoir, using a method to classify regions as safe or unsafe for free CO<sub>2</sub>. Data availability challenges were managed by conducting a sensitivity analysis on four key parameters: porosity, permeability, relative permeability, and compressibility factor. This analysis highlighted the significant impact of relative permeability on the results, particularly the residual gas saturation and the slope of the relative permeability curve.

Well placement optimization was carried out following three approaches: lateral optimization with one well, with two wells, and combined lateral and perforation interval optimization. The derivative-free compass search method was used for this purpose. The results indicated that higher injection rates led to increased NPVs, with lateral optimization of one well improving NPV by up to 4.5%. However, poor initial guesses for the optimization could lead to negative NPVs, demonstrating the importance of the initial guess in the optimization process.

This research highlights the importance of initial reservoir conditions, safety considerations in CO<sub>2</sub> sequestration, and the impact of key parameters on injection strategies. Furthermore, the developed method, with some modifications, can be adapted for other CO<sub>2</sub> storage projects or similar subsurface injection scenarios. Future work should explore joint optimization of well placement and well control, and consider limiting the reservoir domain to critical areas to reduce computational costs.



---

# Sammendrag

Hovedmålet med denne forskningen var å utvikle en arbeidsflyt for optimalisering av plassering av injeksjonsbrønner ved bruk av reservoarsimuleringssteknikker. Denne studien fokuserer på Smeaheia CO<sub>2</sub>-lagringsprosjektet og benytter GAS\_WATER-modusen til Pflotran-OGS reservoarsimulatoren.

For å oppnå dette målet ble flere oppgaver utført. Først ble trykkmatching utført ved hjelp av et system av dummy produksjonsbrønner og porevolummultiplikatorer for å simulere effektene av produksjon fra Troll-feltet. Trykkmatchingprosedyren oppnådde en nøyaktighet innenfor 4% av de målte trykkene. Simuleringer med og uten produksjonsbrønnene som simulerer trykkreduksjonen fra Troll ga betydelig forskjellige resultater. NPV for trykkmatchede tilfeller var opptil 6,3% høyere i noen tilfeller.

I sammenheng med CO<sub>2</sub>-sekvestrering ble sikkerhet for innestengning og lagring adressert ved å identifisere utløpspunkter innenfor reservoaret, ved bruk av en ny metode for å klassifisere regioner som trygge eller utsikte for fri CO<sub>2</sub>. Datatilgjengelighetsutfordringer ble håndtert ved å gjennomføre en sensitivitetsanalyse på fire viktige parametere: porøsitet, permeabilitet, relativ permeabilitet og kompressibilitetsfaktor. Denne analysen fremhevet den betydelige påvirkningen av relativ permeabilitet på resultatene, spesielt residual gassmetning og stigningen på den relative permeabilitetskuren.

Optimalisering av brønnplassering ble utført i tre tilnærminger: lateral optimalisering med én brønn, med to brønner, og en kombinert lateral og perforasjonsintervaloptimalisering. Den de-riveringsfrie kompass-søk metoden ble brukt til dette formålet. Resultatene indikerte at høyere injeksjonsrater førte til økt NPV, med lateral optimalisering av én brønn som forbedret NPV med opptil 4,5%. Imidlertid førte noen startspunkt i optimeringsrutinen til negativ NPV, noe som demonstrerte viktigheten av startbetingelser i optimalisingsprosessen.

Denne forskningen fremhever viktigheten av initiale reservoarbetingelser, sikkerhetsvurderinger i CO<sub>2</sub>-sekvestrering, og påvirkningen av nøkkelparametere på injeksjonsstrategier. Videre kan den utviklede metoden, med noen modifikasjoner, tilpasses andre CO<sub>2</sub>-lagringsprosjekter eller lignende injeksjonsscenarier. Fremtidig arbeid bør utforske felles optimalisering av brønnplassering og brønnkontroll, og vurdere å begrense reservoar domenet til kritiske områder for å redusere beregningskostnadene.

---

## Preface

This thesis is the culmination of my research work for the Master's degree in Petroleum Engineering at NTNU, focusing on Exploring the Transferability of Optimization Methods from Production to Storage: A Case Study of CO<sub>2</sub> Injection at Smeaheia. The journey has been both challenging and rewarding, and I am grateful for the support and guidance I received along the way.

First and foremost, I would like to express my deepest gratitude to my supervisor, Carl Fredrik Berg, for his invaluable guidance, patience, and support throughout this research. He helped me develop a new way of thinking, for which I am profoundly grateful.

I am also thankful to Amir Ghaderi, and Bamshad Nazarian for their contributions and constructive feedback, which greatly enhanced the quality of this work.

I am grateful to SINTEF Industry for providing the data that was essential for this study.

I am particularly grateful to my family and friends for their unwavering support and encouragement throughout my academic journey. Their belief in me kept me motivated during the most challenging times.

My interest in the topic of optimization began when I took the course on advanced computer methods for petroleum engineering, where Carl taught us about optimization methods. This interest was furthered during the reservoir simulation course, also taught by Carl, where I became more familiar with reservoir simulation techniques. The final project of this course opened my path to optimization in CCS projects, solidifying my passion for this area of research.

Completing this thesis has been an enriching experience, filled with learning and growth. I hope that this work will contribute to the advancement of knowledge in Petroleum Engineering and inspire future research.

Alireza Mohsenifesegandis

Trondheim, Norway

June, 2024

---

# Table of Contents

|   |           |
|---|-----------|
| <b>List of Figures</b>  | <b>ix</b> |
| <b>List of Tables</b>   | <b>x</b>  |
| <b>1 Introduction</b>   | <b>1</b>  |
| 1.1 Global Warming . . . . .  | 1         |
| 1.2 Climate Change Mitigation: The Role of Carbon Capture and Storage . . . . . | 1         |
| 1.3 Smeaheia Exploration license . . . . .                                      | 2         |
| 1.4 Research Motivation . . . . .   | 3         |
| 1.5 Research Objective . . . . .  | 4         |
| 1.6 Outline . . . . .   | 5         |
| <b>2 Geological CO<sub>2</sub> Storage</b>                                      | <b>6</b>  |
| 2.1 CO <sub>2</sub> Properties . . . . .  | 6         |
| 2.2 Capture . . . . .   | 7         |
| 2.3 Transportation . . . . .  | 8         |
| 2.4 CO <sub>2</sub> Storage . . . . .   | 10        |
| 2.4.1 Stratigraphic and Structural Trapping Mechanism . . . . .                 | 10        |
| 2.4.2 Residual Trapping Mechanism . . . . .                                     | 10        |
| 2.4.3 Dissolution Trapping Mechanism . . . . .                                  | 11        |
| 2.4.4 Mineralization Trapping Mechanism . . . . .                               | 11        |
| 2.5 Storage Capacity . . . . .  | 11        |
| 2.6 Storage Safety and Post-injection Monitoring . . . . .                      | 12        |
| 2.7 Review of Optimization Techniques in CCS Projects . . . . .                 | 14        |
| 2.8 CCS projects . . . . .  | 18        |
| <b>3 Case Study: Smeaheia</b>   | <b>20</b> |
| 3.1 Geological Model . . . . .  | 20        |
| 3.2 Model setup and Data File . . . . .   | 22        |
| 3.3 Model Uncertainties . . . . .   | 26        |
| <b>4 Background and methodology</b>   | <b>28</b> |
| 4.1 Reservoir Simulator . . . . .   | 28        |
| 4.1.1 Gas_Water Mode . . . . .  | 28        |
| 4.1.2 Parallelization . . . . .   | 29        |
| 4.1.3 Implementation . . . . .  | 30        |

---

---

|          |  |           |
|----------|--|-----------|
| 4.2      | History Matching . . . . .   | 31        |
| 4.2.1    | Pressure Matching Implementation . . . . .                             | 31        |
| 4.3      | Spill-point . . . . .  | 33        |
| 4.3.1    | Spill-point Identification . . . . .                                   | 34        |
| 4.4      | Optimization . . . . .   | 35        |
| 4.4.1    | Optimization Methods . . . . .   | 35        |
| 4.5      | Objective Function . . . . .   | 35        |
| 4.5.1    | Net Present Value (NPV) Calculation . . . . .                          | 36        |
| 4.6      | Well Placement Optimization . . . . .                                  | 39        |
| 4.6.1    | Lateral Well Placement Optimization . . . . .                          | 39        |
| 4.6.2    | Coupled Well Placement and Perforation Length Optimization . . . . .   | 40        |
| 4.6.3    | Lateral Well Placement Optimization with Two Injection Wells . . . . . | 40        |
| <b>5</b> | <b>Results and Discussion</b>  | <b>42</b> |
| 5.1      | Parallelization . . . . .  | 42        |
| 5.2      | Pressure Matching . . . . .  | 43        |
| 5.3      | Spill Point Identification . . . . .                                   | 44        |
| 5.4      | Sensitivity Analysis . . . . .   | 45        |
| 5.4.1    | Porosity . . . . .   | 47        |
| 5.4.2    | Saturation Functions . . . . .   | 48        |
| 5.4.3    | Permeability . . . . .   | 49        |
| 5.4.4    | Compressibility Factor . . . . .                                       | 50        |
| 5.5      | Optimization . . . . .   | 50        |
| 5.5.1    | Lateral Well Placement Optimization . . . . .                          | 50        |
| 5.5.2    | Effect of Starting Point . . . . .                                     | 52        |
| 5.5.3    | Effect of Pressure Matching . . . . .                                  | 54        |
| 5.5.4    | Coupled Well Placement and Perforation Length Optimization . . . . .   | 55        |
| 5.5.5    | Lateral Well Placement Optimization with Two Injection Wells . . . . . | 55        |
| <b>6</b> | <b>Conclusion</b>  | <b>58</b> |
| 6.1      | Key Findings and Implications . . . . .                                | 58        |
| 6.2      | Limitations . . . . .  | 58        |
| 6.3      | Recommendations for Future Work . . . . .                              | 59        |
| 6.4      | Final Thoughts . . . . .   | 59        |
|          | <b>Bibliography</b>  | <b>60</b> |

---

---

## List of Figures

|    |  |    |
|----|--|----|
| 1  | Global amount of carbon released into the atmosphere by different sources of fossil fuels. This plot is generated using data gathered from [41]  | 1  |
| 2  | Global land and ocean temperature since 1850 [35]  | 2  |
| 3  | Overveiw of CCS technologies[55]   | 2  |
| 4  | Smeaheia storage site location [29]  | 3  |
| 5  | CO <sub>2</sub> Phase diagram. This plot is generated using data from [8].   | 6  |
| 6  | CO <sub>2</sub> density at different pressures and temperatures. This plot is generated using data gathered from [16].   | 7  |
| 7  | CO <sub>2</sub> viscosity at different pressures and temperatures. This plot is generated using data gathered from [16].   | 7  |
| 8  | Various CO <sub>2</sub> Capture Methods within the Combustion Category [25]  | 8  |
| 9  | cost and capacity of each transportation method at the distance of 250 km [63]   | 9  |
| 10 | General Transport Systems [67]   | 10 |
| 11 | CO <sub>2</sub> trapping mechanism over time [36]  | 11 |
| 12 | Possible leakage pathways around the well [54]   | 12 |
| 13 | Idealised sketch of a storage site monitoring programme [55]   | 14 |
| 14 | Depth map of the Smeaheia filed with Alpha and Beta structures shown with red polygons [11].   | 20 |
| 15 | Viking group outline on the lithostratigraphic illustration of the North Sea [15]  | 21 |
| 16 | CO <sub>2</sub> movement from Alpha to Beta structure [21]   | 22 |
| 17 | Gas saturation distribution at the end of the eighth year [45]   | 23 |
| 18 | Porosity distribution in two different layers in the model   | 24 |
| 19 | Permeability distribution in two different layers in the model   | 25 |
| 20 | Probability distribution of porosity and cumulative probability distribution of permeability in the model  | 25 |
| 21 | Saturation functions for water and CO <sub>2</sub>   | 26 |
| 22 | Neighbouring fluxes into a control volume in a 2D vertex-centred, structured finite volume method discretisation [20]  | 29 |
| 23 | Domain decomposition where the domain is split between two processes [20]  | 30 |
| 24 | Simple illustration of spill-point   | 33 |
| 25 | Steps of compass search optimization method (illustration from [39])   | 39 |
| 26 | Simulation time versus number of cores requested. Here $n$ is the number of CPUs.  | 42 |
| 27 | Lines showing pressure drawdown from start of production from Troll field in five different cells in the model and the points show the measured pressure points of the Gladsheim well. | 43 |
| 28 | Reservoir divided into two main parts, safe and non safe regoins for CO <sub>2</sub> storage   | 44 |
| 29 | Field Average Pressure and Total Injected CO <sub>2</sub> over 25 Years  | 45 |

---

---

|    |   |    |
|----|---|----|
| 30 | NPV vs Time for CASE 1 . . . . .  | 46 |
| 31 | Field average pressure for a 560-year period, including production from Troll field, CO <sub>2</sub> injection, and post-injection for two cases, with injection rate of 3, and 4.5 MT/y. . . . . | 46 |
| 32 | Total mass of CO <sub>2</sub> dissolved in the aqueous phase for a case with injection rate of 3 million ton per year . . . . .   | 47 |
| 33 | Field average pressure build-up versus time, for three cases with different porosity values. . . . .  | 48 |
| 34 | Field average pressure build-up during the injection period, and bottom-hole pressure for two cases with different saturation functions . . . . .   | 49 |
| 35 | NPV values for all of well locations in the optimization loop for CASE 2 . . . . .  | 51 |
| 36 | Well movement for CASE 1,2, and 3 plotted on the average permeability map . . . . .   | 52 |
| 37 | Results from CASE 3 and CASE 4, blue for positive NPV, red for negative NPV, and yellow for cells outside the reservoir domain. . . . .   | 53 |
| 38 | Results of well movement for CASE3 and 4 plotted on the map of the penalty of CO <sub>2</sub> leakage for each location . . . . .   | 54 |
| 39 | CO <sub>2</sub> plume shape at the end of injection for CASE 2, showing cells with gas saturation higher than zero. . . . .   | 56 |
| 40 | CO <sub>2</sub> saturation 500 years after injection cessation in the safe region map, demonstrating effective containment within the designated area . . . . .                                   | 57 |

## List of Tables

|   |  |    |
|---|--|----|
| 1 | Research questions and corresponding tasks . . . . .                       | 4  |
| 2 | Trapping Mechanisms . . . . .  | 10 |
| 3 | Eclipse keywords and their applications . . . . .                          | 24 |
| 4 | Effect of Porosity on NPV and Field Average Pressure . . . . .             | 48 |
| 5 | Effect of Saturation Function on NPV and Field Average Pressure . . . . .  | 48 |
| 6 | Effect of Permeability on NPV and Bottom-hole Pressure . . . . .           | 49 |
| 7 | Effect of Compressibility Factor on NPV and Bottom-hole Pressure . . . . . | 50 |
| 8 | Optimization Results for different cases . . . . .                         | 56 |

---

# 1 Introduction

## 1.1 Global Warming

The most important current environmental issue is global warming. Global warming affects human life, natural ecosystems, and our climate. Climate changes like frequent heat waves, higher precipitation, and more frequent and intense climate events are in this category [34]. The Earth's atmospheric composition comprises approximately 78% nitrogen and 21% oxygen. The remaining fraction, constituting around one percent, includes greenhouse gases like carbon dioxide, methane, nitrous oxide, and ozone. These gases trap heat in the atmosphere, and lead to higher surface temperature. Since approximately 1800, there has been a notable surge in human utilization of fossil fuels, commencing with coal during the industrial revolution, followed by the incorporation of petroleum liquids and hydrocarbon gases. This has resulted in a substantial uptick in the pace of fossil fuel consumption post-1950[55].

Figure 1 shows the amount of carbon released to the atmosphere by different sources of fossil fuels between 1750 and 2014.

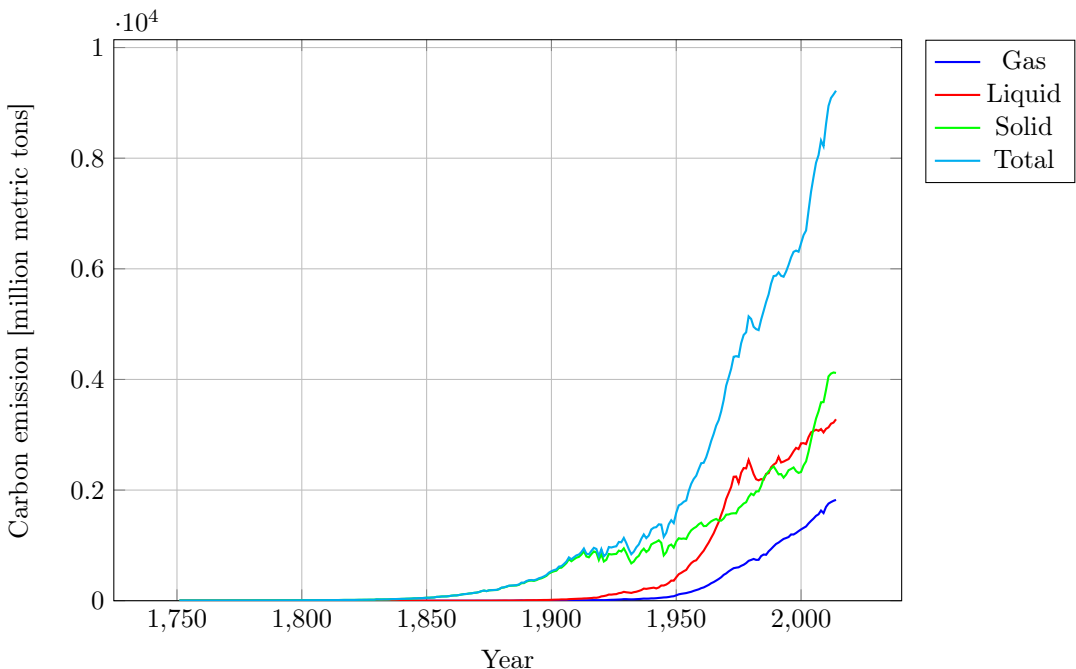


Figure 1: Global amount of carbon released into the atmosphere by different sources of fossil fuels. This plot is generated using data gathered from [41]

In addition to carbon released from the burning of fossil fuels, less carbon dioxide is stored in biological material due to massive deforestation. The combined carbon release from fossil fuels and deforestation has resulted in higher temperatures on the planet's surface. This temperature rise is captured in Figure 2, which shows the global land and ocean September temperature anomalies from 1850 till 2023 [35].

## 1.2 Climate Change Mitigation: The Role of Carbon Capture and Storage

Global warming and climate change can have numerous negative effects on the environment, such as intense heatwaves, droughts, wildfires, short water supply, decreased agricultural productivity, species extinction, and conflicts over resources. To mitigate these impacts, we must move towards more sustainable solutions. This includes using environmentally friendly energy resources like solar,

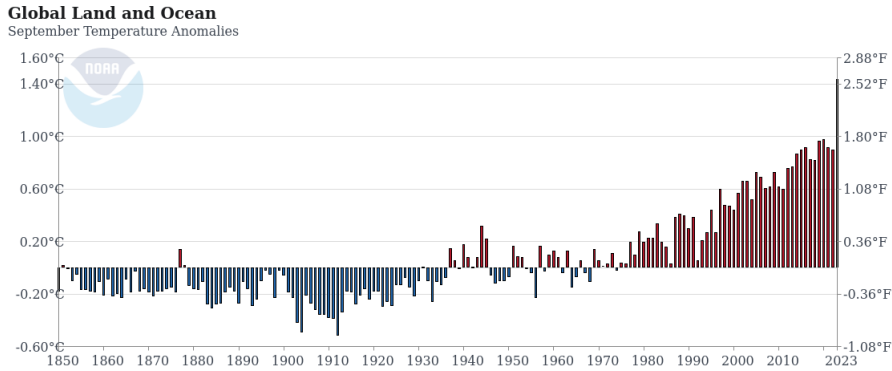


Figure 2: Global land and ocean temperature since 1850 [35]

wind, hydro, nuclear, and bio-fuels, as well as adopting lifestyles with a smaller carbon footprint. Additionally, carbon capture and storage (CCS) is a proven method with several successful projects around the world such as Sleipner and Snøhvit projects in offshore Norway, and Quest CCS project in Canada. It is important to note that while CCS is not a standalone solution, it supplements other strategies. Together, these solutions can effectively combat climate change, and reach the net zero CO<sub>2</sub> emissions by 2050. CCS projects encompass three primary components: capture, transport, and storage of carbon dioxide (CO<sub>2</sub>). This study will provide a brief overview of the capture and transport phases, with a predominant focus on the storage component. Specifically, the research will concentrate on the storage of CO<sub>2</sub> in an offshore area located in the North Sea, known as Smeaheia. Figure 3 shows an overview of the CCS technologies.

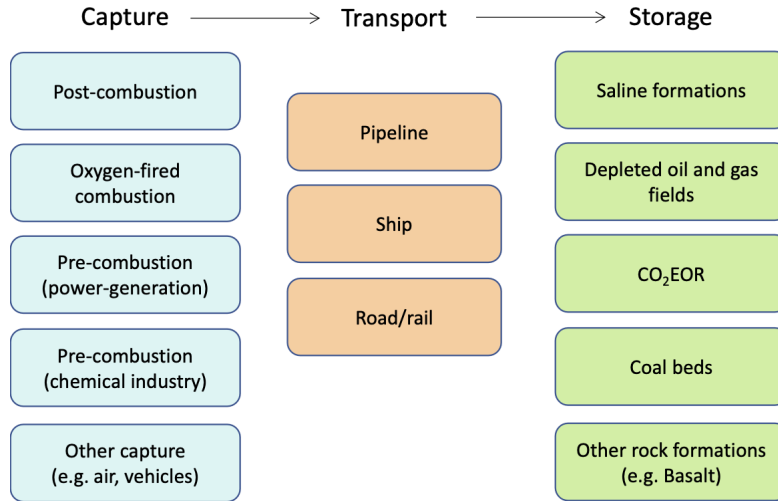


Figure 3: Overveiw of CCS technologies[55]

### 1.3 Smeaheia Exploration license

The methodology employed in this study, while particularly focuses on the Smeaheia CO<sub>2</sub> storage site, aims to offer insights that could be applicable to other CO<sub>2</sub> storage fields as well. Smeaheia Exploration license is positioned within the Horda Platform east of the Troll field, predominantly within Blocks 32/4 and 32/1 as depicted in 4, this area holds strategic significance for carbon dioxide storage exploration. Approximately 20 kilometers east of the Troll A platform and 40 kilometers northwest of the Kollsnes gas terminal, it serves as an good case for the broader analysis of CO<sub>2</sub> storage prospects.[21]

The license history traces a timeline of exploration efforts conducted by various operators and

---

partners from the mid-1990s to the early 2010s. Notably, licenses PL205 (1996-99) and PL369 (2006-11), operated by Phillips and Talisman (later DnO) respectively, alongside partners such as Statoil, Hydro, Total, Wintershall, Petro-Canada, Revus Energy, and Noil Energy, witnessed drilling activities aimed at evaluating targeted structures. However, the outcomes were disappointing, with two dry wells, 32/4-1 and 32/2-1 drilled in an attempt to discover hydrocarbon reserves within these areas, resulting in the eventual relinquishment of these licenses[21]. In recent years, the oil and gas industry has undergone a significant shift in its objectives. Previously focused solely on maximizing the production of oil and gas, the sector's priorities have evolved. Today, alongside conventional production endeavors, there is a notable engagement in CCS projects. Unlike traditional production projects, CCS initiatives may not yield equivalent economic returns. However, they play a crucial role in the global fight against climate change. This transition reflects a growing recognition within the industry of its responsibility to address environmental concerns and contribute to sustainable practices on a global scale. Fortunately, starting from mid-2022, Equinor has been awarded operator-ship for the development of the CO<sub>2</sub> storage site, marking a new chapter in the exploration and potential development of the area.

The closest production license currently is the PL085 Troll East license situated in block 31/6.

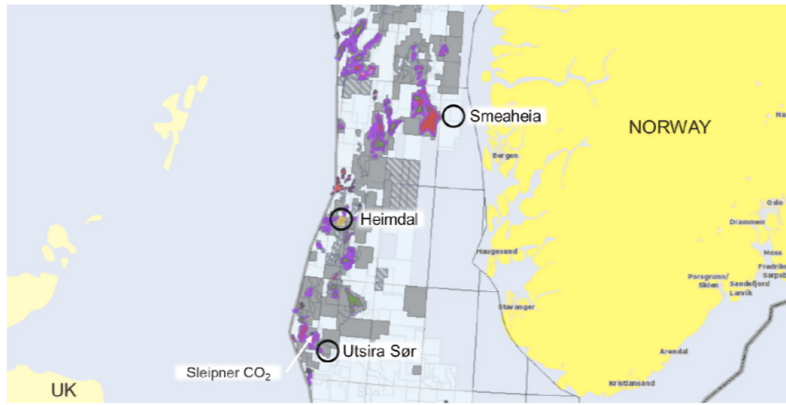


Figure 4: Smeaheia storage site location [29]

## 1.4 Research Motivation

The urgent problem of global warming demands effective solutions including storing carbon dioxide underground. In addition to storing carbon dioxide underground, expanding the use of renewable energy sources and improving energy efficiency are crucial strategies for reducing greenhouse gas emissions. Long-term underground carbon dioxide storage could be done either in depleted hydrocarbon reservoirs or saline aquifers. This method has already been tested and there are several successful projects around the world. Our research focuses on the Smeaheia saline aquifer in the northern North Sea, which was briefly discussed in the previous section.

One of the primary challenges in underground CO<sub>2</sub> storage projects is their economic viability. Despite comparable costs to conventional hydrocarbon production projects, the revenue generated is not as substantial. Thus, ensuring the economic feasibility of these projects is paramount. Optimizing factors such as well location, injection rate, and the number of wells is essential to achieve profitability. Additionally, maintaining control over the CO<sub>2</sub> underground and tracking its location and trapping mechanisms over time are critical aspects. These factors underscore the significance of our thesis research, as we aim to address these challenges and contribute to the development of economically sustainable solutions for carbon capture and storage initiatives. This serves as our primary motivation for undertaking this study.

---

## 1.5 Research Objective

The main objective of this work is to develop a workflow for optimizing CO<sub>2</sub> injection in a Carbon Capture and Storage project. The proposed workflow is intended to be adaptable to other CCS projects with appropriate modifications. The Smeaheia storage site was used as a case study to identify challenges with current workflows adopted from more traditional (hydrocarbon) production optimization. To achieve the overarching objective, several sub-objectives were identified from work on the Smeaheia case study. These questions, and how they were addressed, are all summarized in Table 1.

Table 1: Research questions and corresponding tasks

| Question   | Task to be conducted   |
|--|--|
| How does the pressure decrease from nearby production activities affect the injection capacity of the formation?   | <b>Pressure Matching</b><br>Using Smeaheia as an example case, we will study the effects of including pressure drawdown from the neighboring Troll field.<br>This process aims to reconcile the initial injection pressure with the prevailing conditions at the site, accounting for deviations from hydrostatic equilibrium.   |
| How can mapping the alpha structure and finding the spill point influence the overall CO <sub>2</sub> storage strategy?  | <b>Structure Mapping and Spill Point Identification</b><br>Given the inherent uncertainties and limitations in available data, a self-developed methodology is employed to map the Alpha structure and identify potential spill points in the current case. This process is essential for delineating the boundaries of the containment structure and assessing the likelihood of CO <sub>2</sub> migration beyond acceptable thresholds.  |
| What is the optimal placement of wells to maximize CO <sub>2</sub> injection efficiency and storage security?  | <b>Well Placement Optimization</b><br>Recognizing the critical influence of well placement and injection period on CCS efficiency, the subsequent phase focuses on optimizing the placement of injection wells. To achieve this goal, several optimization approaches could be employed. This step aims to maximize CO <sub>2</sub> injection rates while minimizing the risk of leakage or migration from the Alpha structure.  |
| What is the optimal number of wells required to achieve the desired CO <sub>2</sub> sequestration targets while maintaining economic and operational efficiency? | <b>Optimizing the number of wells</b><br>Determining the optimal number of wells is crucial for achieving efficient and cost-effective CO <sub>2</sub> sequestration. An insufficient number of wells may lead to inadequate distribution of CO <sub>2</sub> within the formation, resulting in lower storage efficiency and potential pressure build-ups around the wells due to the high injection rate from a lower number of wells. Conversely, too many wells can escalate costs and operational complexities without proportional benefits. This research will employ reservoir simulation models to evaluate different scenarios and determine the optimal number of wells required to achieve the desired sequestration targets. |
| What is the optimal perforation interval for injecting CO <sub>2</sub> to maximize storage efficiency and ensure formation integrity?                            | <b>Optimizing the perforation interval</b><br>Selecting the optimal perforation interval for CO <sub>2</sub> injection is essential to ensure efficient storage and maintain the integrity of the formation. The perforation interval determines the depth at which CO <sub>2</sub> is injected, which can significantly influence the distribution and containment of the gas.  |

---

The overarching objective of this research is to enhance the efficiency, safety, and long-term viability of CCS operations. The case study at the Smeaheia storage site integrated pressure matching, well placement optimization, and structural mapping techniques. This study specifically focuses on the Smeaheia site by developing detailed models and methodologies tailored to Smeaheia, the research also contributes to the general knowledge on how to effectively model CCS projects. These insights can be applied to other CCS initiatives, thereby supporting the broader goal of mitigating greenhouse gas emissions through effective carbon capture and storage strategies.

## 1.6 Outline

This section provides an overview of the structure and content of the thesis. Each chapter is briefly introduced, outlining the key topics and discussions covered in the subsequent sections. The outline serves as a roadmap for navigating through the research, highlighting the progression of ideas and methodologies explored in the following chapters.

- **Geological CO<sub>2</sub> Storage**

In the chapter, fundamental aspects of geological CO<sub>2</sub> storage is discussed. CO<sub>2</sub> properties, most importantly its density and viscosity which play important roles in CO<sub>2</sub> plume movement. Different methods of CO<sub>2</sub> capture which are commercially available are briefly presented afterward. CO<sub>2</sub> transportation and the pros and cons of each method, which is one of the most challenging parts of CCS projects, is also reviewed. Trapping mechanisms, safety, and monitoring are explored in this chapter. In the final two sections, a review of optimization techniques in CCS projects is provided, along with a comprehensive overview of previous CCS projects. This section also serves as a continuation of my specialization project, with some material directly sourced from that work.

- **Case Study: Smeaheia** This chapter focuses on a detailed examination of the Smeaheia site. It encompasses three key components: firstly, the geological model, which delineates the geological characteristics and structures of the site. Secondly, the model setup and data files used in simulations, detailing the computational framework and input data sources. Lastly, the section addresses model uncertainties, discussing the inherent variability.

- **Background and Methodology** The "Methodology" chapter provides a detailed account of the techniques and tools employed in this study. It begins by introducing the reservoir simulator utilized in the research, along with the governing equations. The chapter then delves into the parallelization of simulations, highlighting how this process enhances the pace and efficiency of the modeling efforts. Furthermore, history matching and pressure matching techniques are discussed in detail, underscoring their significance in refining simulation results to match observed data. Additionally, the chapter addresses the optimization aspect of the study, outlining the methodologies employed to optimize well placement and injection strategies. Notably, the section concerning reservoir simulation constitutes a continuation of my previous work, sourced from my specialization project.

- **Results and Discussion** This chapter includes five sections: parallelization results, pressure matching outcomes, spill point identification findings, sensitivity analysis results, and optimization findings. Each section discusses specific aspects related to the corresponding topic, providing a comprehensive analysis and discussion based on the results obtained.

- **Conclusion** In the conclusion chapter, we synthesize the findings from the results and discussion chapter, offering insights and interpretations based on our analysis. Additionally, we propose several avenues for future research to enhance the current work and address potential limitations.

---

## 2 Geological CO<sub>2</sub> Storage

### 2.1 CO<sub>2</sub> Properties

With a density of 1.87 kg/m<sup>3</sup> at atmospheric conditions, CO<sub>2</sub> is a thermodynamically stable gas that is heavier than air and compressible. A CCS project involves various operations under differing pressure and temperature scenarios. Given that CO<sub>2</sub> properties undergo significant changes with alterations in pressure and temperature, understanding these variations is critical for the project's success. CO<sub>2</sub> properties are functions of pressure and temperature. In deep saline aquifers, due to overburden pressure and thermal gradient, both the pressure and temperature are high. In this circumstance, CO<sub>2</sub> will be in a liquid phase. After the critical point, CO<sub>2</sub> will move to a supercritical state, which can have a density variation between 150 to around 800 kg/m<sup>3</sup>. The critical point for CO<sub>2</sub> is at T = 30.98 °C and P = 73.8 bar. CO<sub>2</sub> viscosity also changes significantly with pressure and temperature. In the liquid phase, it can have a viscosity of 0.18 cP, and in the gas phase, it could be as low as 0.02 cP [59]. Figure 5 shows the phase diagram of CO<sub>2</sub>.

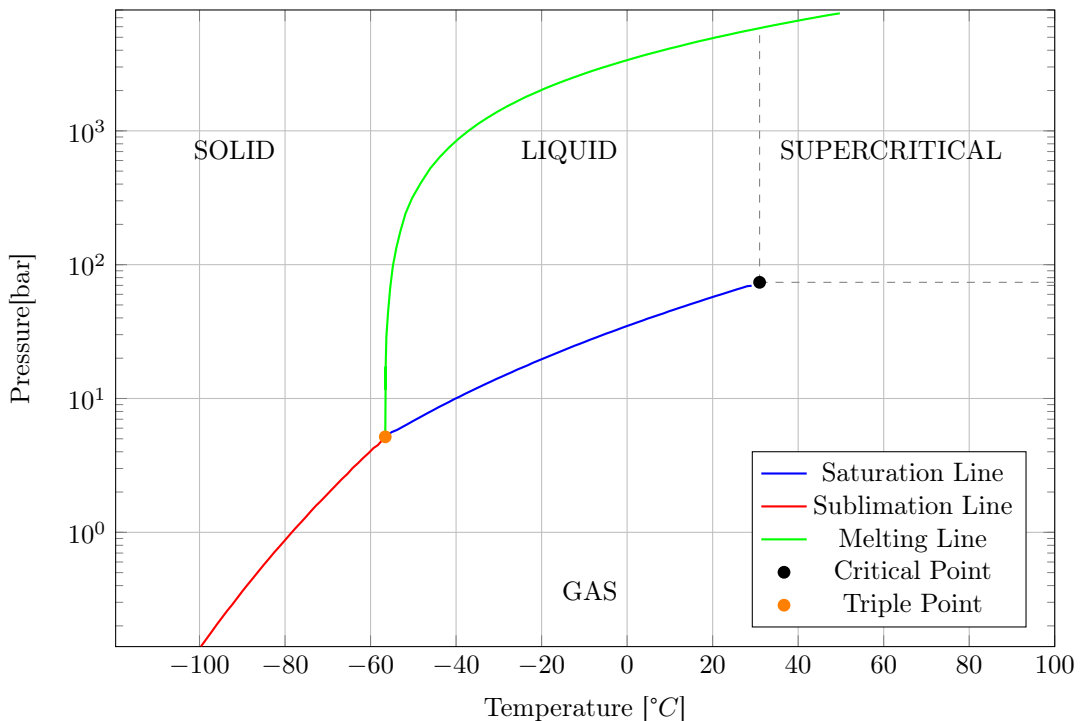


Figure 5: CO<sub>2</sub> Phase diagram. This plot is generated using data from [8].

The density and viscosity of CO<sub>2</sub> play crucial roles in both the injection and post-injection phases of a CCS project. During the injection phase, these properties dictate the amount of CO<sub>2</sub> that can be injected into the subsurface reservoir. The viscosity of CO<sub>2</sub> influences the rate at which it can be injected, as it determines how easily the CO<sub>2</sub> can flow through the reservoir rock. Additionally, the density contrast between CO<sub>2</sub> and the in-situ fluid determines the buoyancy of the injected CO<sub>2</sub>, affecting its upward movement within the reservoir. In the post-injection phase, the density of CO<sub>2</sub> determines its phase state within the reservoir—whether it remains as a single-phase fluid or transitions into a two-phase flow with the in-situ fluid. Understanding these properties is crucial for predicting the behavior of injected CO<sub>2</sub> over time, including its migration away from the injection well and potential interactions with the surrounding fluids, such as dissolution processes. Figure 6 and Figure 7 illustrate CO<sub>2</sub> density and viscosity respectively, at different pressure and temperatures.

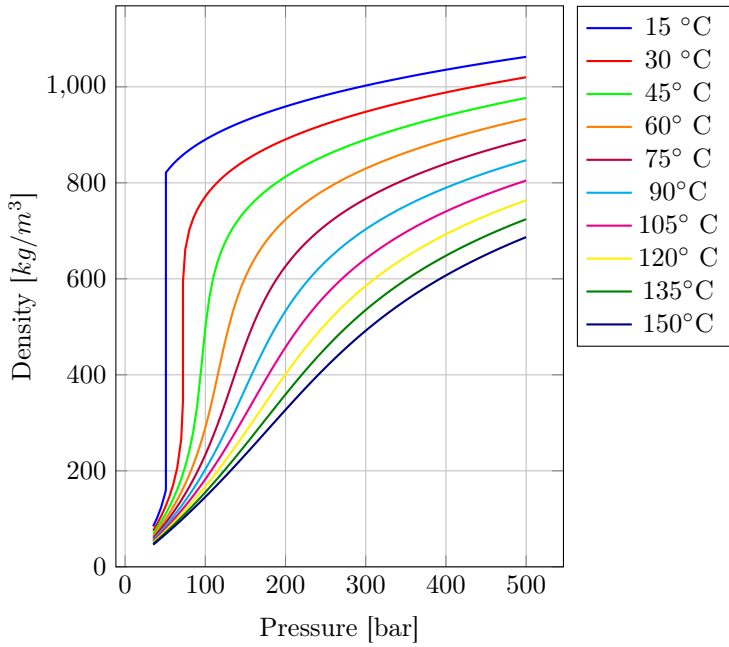


Figure 6: CO<sub>2</sub> density at different pressures and temperatures. This plot is generated using data gathered from [16].

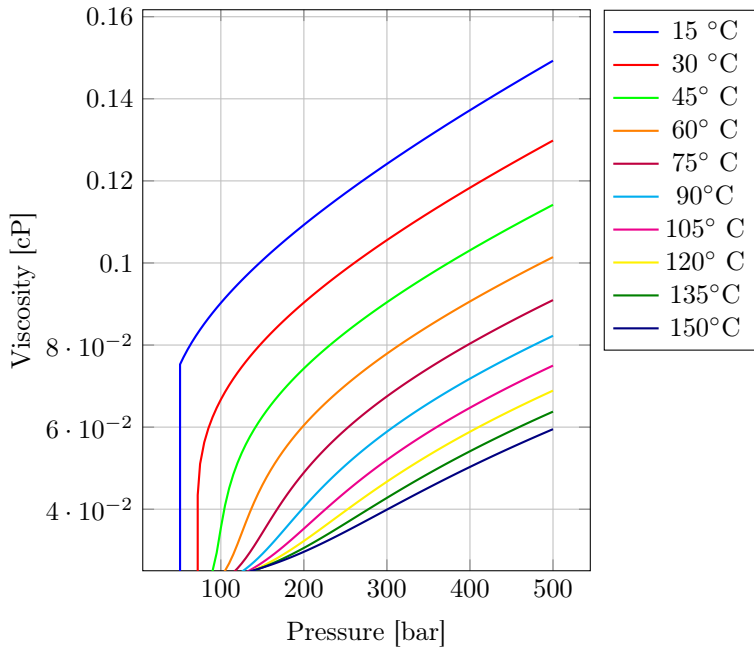


Figure 7: CO<sub>2</sub> viscosity at different pressures and temperatures. This plot is generated using data gathered from [16].

## 2.2 Capture

The first step in every CCS project is CO<sub>2</sub> capture. CO<sub>2</sub> capture can be separated into three main categories, capture from combustion, direct CO<sub>2</sub> capture from the air, and stripping CO<sub>2</sub> from the produced natural gas. The first category can also be divided into three smaller groups, namely, pre-combustion, post-combustion, and oxy-combustion, which are briefly explained below [24].

- **Pre-combustion:** In the pre-combustion method, CO<sub>2</sub> is captured before the fuel and oxygen entering the combustion turbine. Oxygen and fuel enter a gasifier unit, and H<sub>2</sub> and CO<sub>2</sub> exit this unit at high pressure and temperature. Following this unit, CO<sub>2</sub> is captured, and finally H<sub>2</sub> and air enter the combustion turbine [24].
- **Post-combustion:** In this procedure, CO<sub>2</sub> is captured after combustion. Produced flue gas passes through different solvents, and CO<sub>2</sub> is removed from the flow before being released into the atmosphere. The captured CO<sub>2</sub> is isolated and stored for future uses [24].
- **Oxy-combustion:** Unlike the two previous procedures, the air is replaced with pure oxygen as a reactant. In this kind of reaction, the products would be carbon dioxide and water in the vapor phase. The flue gas will be extremely hot, and can therefore be utilized again, due to its high energy content [24].

Figure 8 illustrates the different capture methods from combustion.

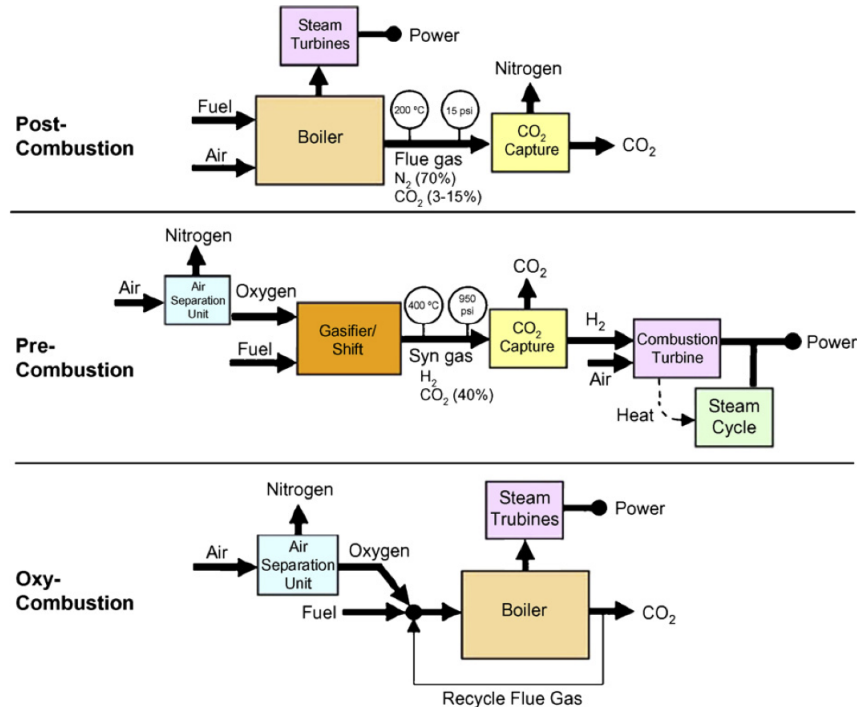


Figure 8: Various CO<sub>2</sub> Capture Methods within the Combustion Category [25]

The other approach which is direct capture from air needs a higher amount of air to be treated, because of the low concentration of CO<sub>2</sub> in the air. In this process, a sorbent is used to absorb CO<sub>2</sub> from the air.

Captured CO<sub>2</sub> undergoes a compression process to reach the desired pressure and temperature. Initially, it is pressurized using multi-stage compressors, with intercoolers reducing the temperature between stages to manage heat buildup. This ensures the CO<sub>2</sub> is efficiently compressed to the high pressures needed for transport.

## 2.3 Transportation

Transporting the captured CO<sub>2</sub> to the intermediate storage site, and finally to the injection point is among the most challenging parts of CCS projects. As mentioned previously, the physical properties of CO<sub>2</sub> are highly dependent on its pressure and temperature. Moreover, captured CO<sub>2</sub> is not always 100% pure, and could have impurities, like hydrocarbons, nitrogen, oxygen, and

water. These impurities change the properties significantly and make transportation even more challenging. Water in the mixture can increase corrosion, especially in pipeline systems, due to the formation of carbonic acid when CO<sub>2</sub> dissolves in water. This acidic environment accelerates the electrochemical reactions that cause corrosion of metal surfaces. Moreover, a combination of water and methane in the mixture can also form hydrates. There are several methods of transportation, using pipelines, trucks, ships, and railways. Next, we will delve into the advantages and disadvantages of various CO<sub>2</sub> transportation methods. Transportation with pipelines has higher capital costs, but lower operational costs [2]. This method has been used for several years in the oil and gas industry for gas transportation and even CO<sub>2</sub> transportation for EOR uses. Moreover, in some cases, the currently available pipelines can also be used, which decreases capital costs.

On the other hand, unlike pipeline transportation, using ships has lower capital costs and higher operational costs. This transport system is widely used in the food and brewery industries, but it should be mentioned that quantities and conditions are completely different. If this transportation method is used up to the injection point, the injection system will be batch-wise, and the injection will not be constant in time [2].

The third method is transportation via railway. In this system, a loading and unloading infrastructure is necessary, and an intermediate storage site must be built. Economic-wise, this system is only feasible with the existing railways. So this method is more advantageous for long-distance cases.

The last method is the utilization of trucks. This method has a limitation of the amount of CO<sub>2</sub> being transported in each batch, which could vary between 2 to 30 tonnes of CO<sub>2</sub> per batch [2]. Moreover, the emitted CO<sub>2</sub> during transportation could be up to 10% of the load [68]. Consequently, this method is not applicable to large-scale CCS project .

Figure 9 briefly illustrates the cost and capacity of each transportation method at a distance of 250 km, and figure 10 shows the general capture-to-storage systems.

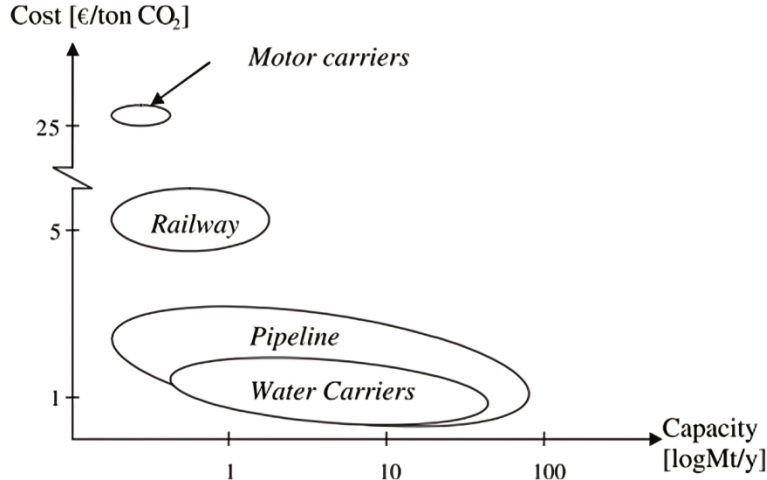


Figure 9: cost and capacity of each transportation method at the distance of 250 km [63]

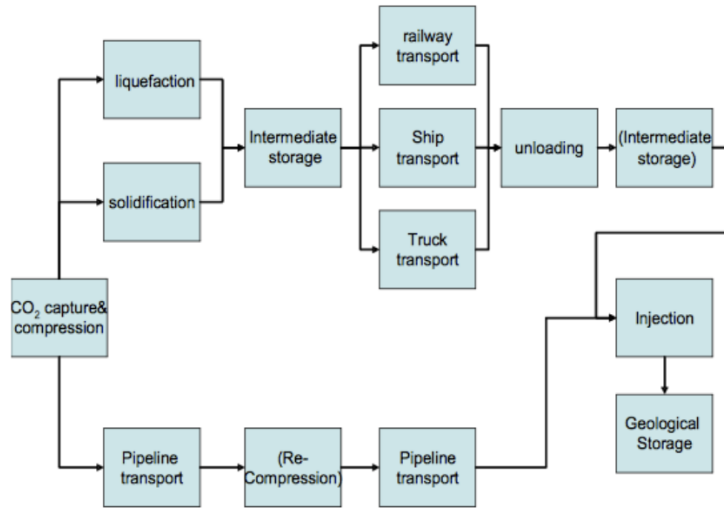


Figure 10: General Transport Systems [67]

## 2.4 CO<sub>2</sub> Storage

Captured CO<sub>2</sub> is transported to the designated injection location by one of the methods discussed above, and via the injection well it is injected into the subsurface formations.

Carbon dioxide is injected into the subsurface, and stored in the interconnected pore system. After injection, carbon dioxide starts moving in the system due to pressure differences or gravitational forces. The injected CO<sub>2</sub> will be trapped due to different mechanisms, which could be physical or chemical, which control the CO<sub>2</sub> leakage, too. Physical and chemical trapping mechanisms occur simultaneously but in different time scales. Table 2 summarizes these mechanisms. In this section, these mechanisms are briefly explained.

Table 2: Trapping Mechanisms

| Physical                                 | Chemical                      |
|--|-------------------------------|
| Stratigraphic and Structural<br>Residual | Dissolution<br>Mineralization |

### 2.4.1 Stratigraphic and Structural Trapping Mechanism

This mechanism works exactly the same way as the trapping mechanism for hydrocarbon reservoirs. An impermeable layer, which could be a shale layer or a salt bed over a permeable zone. Fluid with the lower density, which is CO<sub>2</sub> in this case, moves upwards. Due to the very low permeability or very high entry pressure of the overlying layer due to very small pore size, fluid is stopped and trapped. This mechanism plays an important role in the early stages of the injection [55].

### 2.4.2 Residual Trapping Mechanism

One well-known phenomenon in the oil and gas industry, which has considerable influence on the recoverable amount of hydrocarbon in oil and gas-bearing formations, is residual trapping. As the CO<sub>2</sub> plume moves through the rock, small part of it snaps off the plume and is left behind in the

---

pores, because of pore scale trapping. The magnitude of residual trapping is a function of the pore throat size, the interfacial tension, and the wettability [55].

#### 2.4.3 Dissolution Trapping Mechanism

Injected CO<sub>2</sub> ascends to the top of the permeable layer, where it will be stored. The CO<sub>2</sub> plume comes into contact with the brine and begins to dissolve into the aqueous phase. Brine containing dissolved CO<sub>2</sub> has a higher density compared to brine without CO<sub>2</sub>. Consequently, the denser brine at the interface moves downward due to gravitational forces, and is replaced by fresher brine. This ongoing process, known as convective mixing, occurs. Although this mechanism is slower compared to physical storage methods, it is more significant for long-term storage

#### 2.4.4 Mineralization Trapping Mechanism

Dissolved CO<sub>2</sub> in the brine makes the environment acidic. When the acidic phase is in contact with the grains and the elements present in the rock, they react and start to deposit, and also it can dissolve the grains due to its acidity. This mechanism is dominant in the late-time storage phases, even after dissolution.

Figure 11 illustrates the contribution of each mechanism over time.

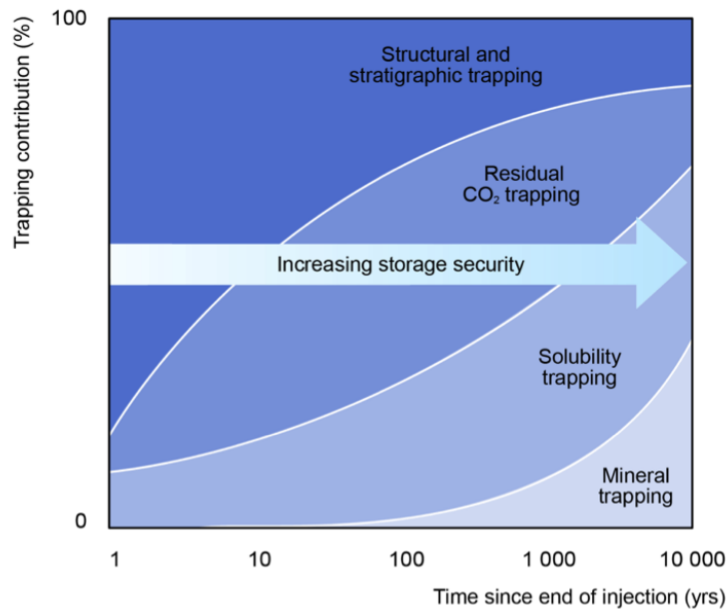


Figure 11: CO<sub>2</sub> trapping mechanism over time [36]

### 2.5 Storage Capacity

Even though storage capacity is inherently unpredictable, estimating it before to injection is critical. This attribute is a key indicator of the economic feasibility of the project. By estimating the possible volume of CO<sub>2</sub> that a formation might hold, stakeholders can determine if the project is financially viable. Additionally, this estimation allows for improved planning and resource management throughout the project's life-cycle. Despite the inherent uncertainties, having an approximate figure for storage capacity enables better informed investment, resource allocation, and risk assessment, ultimately contributing to the overall success and sustainability of CO<sub>2</sub> storage programs.

Capacity refers to the pore volume available for storing CO<sub>2</sub> in a given formation, representing

the quantity of CO<sub>2</sub> that the formation can hold. This capacity is influenced by various factors, including the thickness of the formation, its porosity, the density of CO<sub>2</sub>, the surface area of the storage structure, and the efficiency of storage [14].

An approximation of storage capacity can be calculated using the equation below:

$$M_s = V_{\text{trap}} \times \text{Net}_r \times \phi_r \times S_g \times \rho_g \quad (1)$$

Where:

- $M_s$  represents the mass of CO<sub>2</sub> stored in the formation (in units of mass).
- $V_{\text{trap}}$  denotes the bulk rock volume of the trapping mechanism (in units of volume).
- $\text{Net}_r$  Net to gross ratio (unitless).
- $\phi_r$  stands for the porosity of the reservoir (unitless).
- $S_g$  represents the gas saturation in the reservoir (unitless).
- $\rho_g$  denotes the density of the gas (in units of mass per volume).

## 2.6 Storage Safety and Post-injection Monitoring

Although CO<sub>2</sub> storage presents itself as a promising long-term solution for mitigating greenhouse gas emissions, it is imperative to acknowledge the associated risks and plan for them accordingly in injection projects. One significant risk is the potential for CO<sub>2</sub> leakage to the surface. This could occur through fractures and faults in the geological formations or, in cases where the well cementing has not been done properly, via pathways between the casings and the formations, and from the abandoned wells in the vicinity of the injection location. Figure 12 illustrates the possible leakage pathways around a plugged well which could be in the vicinity of the injection well.

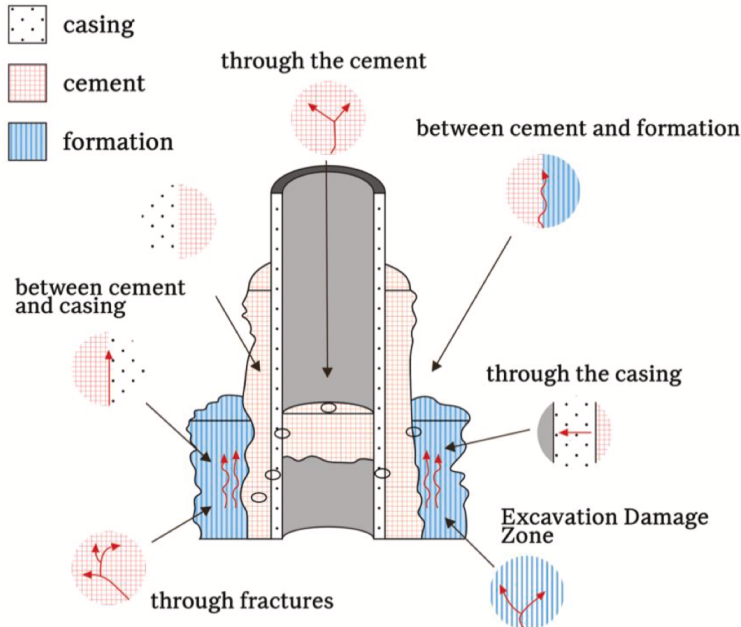


Figure 12: Possible leakage pathways around the well [54]

Therefore, robust monitoring measures are essential to detect and address any signs of leakage promptly. By proactively addressing these risks and implementing comprehensive monitoring plans, we can enhance the safety and effectiveness of CO<sub>2</sub> storage projects. Given that CO<sub>2</sub> injection projects share similarities with oil and gas production, many of the techniques and methodologies

---

employed in the oil and gas industry can also be adapted for use in CO<sub>2</sub> storage projects [42]. Some of the monitoring techniques are listed and explained briefly below:

- 4D Seismic: Seismic surveys are a crucial tool in geophysics used to image subsurface structures and identify geological features such as oil and gas reservoirs, fault lines, and rock formations. Using 3D seismic technology provides a comprehensive understanding of the subsurface, which is especially valuable in assessing the distribution of different phases within formations. In the context of CO<sub>2</sub> storage, acquiring a 3D seismic map of the injection formation before commencing injection activities, and subsequently conducting another 3D seismic survey post-injection, allows for a comparison between the two maps. This comparative analysis enables us to discern any changes that have occurred within the reservoir, including the movement of the CO<sub>2</sub> plume.

By examining these seismic maps, we can determine whether the injected CO<sub>2</sub> remains within the intended structure or if any leakage has occurred. This method proves to be instrumental in monitoring CO<sub>2</sub> storage projects, providing insights into the effectiveness of containment measures and the overall integrity of the storage site. In essence, 4D seismic mapping serves as a powerful tool in assessing and managing the safety and efficiency of CO<sub>2</sub> storage operations.

- Gravimetric and controlled-source electromagnetic surveys: Gravimetric and controlled-source electromagnetic (CSEM) surveys are geophysical methods for investigating subsurface structures and variations in Earth's characteristics. Gravimetric surveys, in particular, measure the gravitational field at specified locations on the Earth's surface.

Gravity is a fundamental force that depends on the mass of two objects and the distance between them. In the context of CO<sub>2</sub> injection, one of the objects is the Earth itself. By measuring gravity before and after CO<sub>2</sub> injection and analyzing the changes that occur, we can gain insights into the amount of CO<sub>2</sub> injected into the subsurface. When CO<sub>2</sub> is injected, the initial fluid in the reservoir is displaced by the CO<sub>2</sub>. Gravity measurements can be used to determine the change in mass distribution since CO<sub>2</sub> and the initial fluid have different densities. Through the comparison of pre- and post-injection gravity measurements, we are able to approximate the height or volume of the CO<sub>2</sub> plume within the reservoir.

It is noteworthy that, although gravimetric surveys offer significant insights into subsurface alterations, their resolution is typically inferior to that of methods such as seismic surveys. However, gravimetric surveys serve as a valuable supplement to existing monitoring techniques and advance our understanding of the dynamics of CO<sub>2</sub> storage.

- Pressure Measurement: In CCS projects, monitoring pressure is paramount for ensuring the safe and effective storage of CO<sub>2</sub> underground. During the injection process, the bottom-hole pressure is highly dependent on the reservoir pressure. Leakage in the formation would change the reservoir pressure and consequently injection pressure. Therefore, leakage can be detected using the pressure measurement. Sun et al. demonstrated in a real-world trial that leakage from the reservoir could be identified due to its impact on injection pressure [62].
- InSAR : Synthetic Aperture Radar (SAR) systems operate by emitting electromagnetic waves and capturing the energy reflected back from targets, which allows for detailed surface imaging. Interferometric Synthetic Aperture Radar (InSAR) utilizes phase measurements to detect variations between two SAR images [50]. The injection of CO<sub>2</sub> into the subsurface can elevate reservoir pressure, potentially leading to measurable surface deformation if the pressure change is substantial. A highly valuable and somewhat unexpected monitoring technique has been the use of satellite-based InSAR to identify minor ground deformation by comparing phase differences from successive satellite observations. By utilizing data from multiple satellite passes, deformation detection can achieve measurement accuracy of approximately 5 mm/year, with long-term averages reaching up to 1 mm/year [44].

Figure 13 depicts an idealized outline of a storage site monitoring program, where various techniques are employed. These include seismic imaging, wellhead data analysis, near-surface geochemistry assessments, gravimetry measurements, micro-seismic monitoring, and strain measurements, as well as the utilization of down-hole gauges and fiber optic sensing methods.

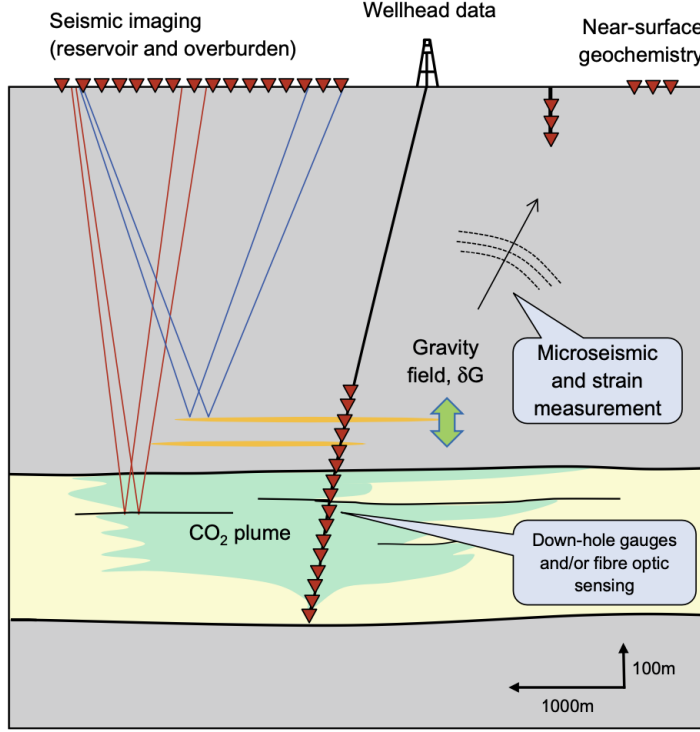


Figure 13: Idealised sketch of a storage site monitoring programme [55]

## 2.7 Review of Optimization Techniques in CCS Projects

Optimization techniques have been extensively applied to CCS projects, with objective functions that either mirror those in traditional oil and gas applications or address specific challenges unique to CCS. The following paragraphs provide a review of various studies and methodologies employed in the optimization of CCS processes.

Kumar's master's thesis [40], focused on optimizing the geological sequestration of carbon dioxide to enhance residual trapping in saline aquifers, thereby minimizing structural trapping risks. The study employs the conjugate gradient (CG) method and utilizes a commercial simulator for numerical gradient calculations. Through 2-D simulations and optimizations on heterogeneous models, Kumar demonstrates that optimized well settings significantly increase CO<sub>2</sub> residual trapping compared to unoptimized scenarios. The thesis explores various factors' impacts on optimization outcomes, including aquifer heterogeneity and capillary pressure hysteresis, highlighting opportunities for algorithmic refinement and enhanced computational efficiency in optimizing CO<sub>2</sub> sequestration strategies.

Nghiem et al. [47] investigated CO<sub>2</sub> storage mechanisms in saline aquifers, focusing on residual gas trapping and solubility trapping. Their study explores the placement of a water injector above a CO<sub>2</sub> injector to enhance trapping efficiency. Through simulation, they determine optimal locations and operating conditions for the water injector in both low- and high-permeability aquifers. Their results indicate that in low-permeability aquifers and deeper water injection scenarios, residual gas trapping is favored, whereas solubility trapping benefits from shallower injection in high-permeability aquifers. Furthermore, they found that in high-permeability aquifers, water injection does not increase total CO<sub>2</sub> trapping efficiency.

Nghiem et al. [48] focused on modeling CO<sub>2</sub> trapping processes in saline aquifers, highlighting solubility trapping, residual gas trapping, and mineral trapping mechanisms. They explore the impact of injecting brine above the CO<sub>2</sub> injector on enhancing both soluble and residual CO<sub>2</sub> trapping. Instead of employing optimization techniques due to the scale of their study, they systematically investigate all feasible cases. The study evaluates the security of the trapping

---

process by considering potential leakage of mobile CO<sub>2</sub> through the caprock. Furthermore, they investigate the long-term potential of CO<sub>2</sub> conversion into minerals, emphasizing the role of pre-existing minerals in aquifers that facilitate these conversion reactions.

Shamshiri and Jafarpour [57] introduced a novel framework for optimizing waterflooding sweep efficiency in reservoir engineering and its application to geological CO<sub>2</sub> sequestration. Their approach focused on equalizing and delaying breakthrough times of injected fluids at production wells, crucial for improving hydrocarbon recovery and minimizing bypassed oil. They extended this method to CO<sub>2</sub> sequestration, introducing pseudo production wells to simulate breakthrough curves in the absence of actual producers. By applying this method to heterogeneous reservoir models, they demonstrated enhanced sweep efficiency in waterflooding and improved CO<sub>2</sub> storage capacity through optimized residual and solubility trapping in geological formations. Their study underscores the effectiveness of their algorithm in optimizing CO<sub>2</sub> storage by facilitating better contact between injected CO<sub>2</sub> and fresh brine in aquifers.

Cameron and Durlofsky [10] used computational optimization to minimize the mobile fraction of CO<sub>2</sub> in a 1000-year carbon sequestration operation in a brine aquifer. They apply a noninvasive gradient-free direct search technique and explore different scenarios, including CO<sub>2</sub> injection and brine cycling, demonstrating that optimization can significantly reduce mobile CO<sub>2</sub> compared to base cases.

Zhang's PhD dissertation [70] introduced a genetic algorithm (GA)-based optimization tool, GA-TOUGH2, tailored for optimizing CCS operations. GA-TOUGH2 is validated through optimization studies on injection strategies like water-alternating-gas (WAG) injection, optimal time-dependent injection rates, and well placement designs to enhance CO<sub>2</sub> sequestration capacity and reduce in situ CO<sub>2</sub> footprint. Zhang's research demonstrates significant improvements in CO<sub>2</sub> dissolution efficiency and well injectivity, underscoring GA-TOUGH2's potential for addressing diverse optimization challenges in CCS applications.

Petvipusit et al. [53] presented a surrogate-assisted optimization technique using Adaptive Sparse Grid Interpolation (ASGI) for optimizing CO<sub>2</sub> injection strategies in deep saline aquifers under geological uncertainty. This method adaptively refines the surrogate model to balance accuracy and computational cost. A utility function incorporating statistical moments is used for robust design. Numerical tests demonstrate the method's efficiency in optimizing CO<sub>2</sub> injection strategies.

Goda and Sato [30] tackled the complex task of globally optimizing the placement of injection wells for CO<sub>2</sub> geological storage. They emphasize the challenges posed by the interaction of unknown parameters and the lack of prior information on the function to be minimized. Traditional gradient-based methods are deemed insufficient due to their local focus, prompting the authors to adopt population-based search algorithms. Specifically, they introduce the iterative Latin hypercube sampling (ILHS) method, noted for its ability to explore parameter spaces effectively while mitigating the risk of getting trapped in local minima. Their research underscores ILHS as a promising approach for achieving optimal injection well placement, demonstrating faster convergence rates compared to other popular optimization techniques like particle swarm optimization and differential evolution.

Pan et al. [51] focused on maximizing CO<sub>2</sub> trapping in a reservoir with heterogeneous and uncertain petrophysical properties. They employed a multi-period injection strategy and optimization algorithm to determine optimal injection quantities across different wells over time spans. To address uncertainty, multiple realizations of permeability and porosity were generated and integrated into the optimization framework. The algorithm utilizes a kriging-based meta-modeling technique to optimize sampling points efficiently, significantly reducing computational time by minimizing function calls to the flow solver. Compared to Genetic Algorithms, this methodology demonstrates superior performance in terms of computational efficiency and convergence characteristics.

The study by Cihan,et al. [13] presented a Constrained Differential Evolution (CDE) algorithm tailored for global optimization in CCS projects, specifically focusing on pressure management in a deep sandstone reservoir in the Southern San Joaquin Basin, California, USA. The study addresses concerns of induced seismicity due to CO<sub>2</sub> injection-induced pressure buildup and aims to optimize brine extraction well placements to mitigate these risks. Using a vertically-averaged reservoir

---

---

simulator coupled with CDE optimization, the authors successfully identify optimal extraction strategies that maintain pressure below specified thresholds along surrounding faults. Their findings highlight the significant impact of reservoir heterogeneity on optimal extraction rates and well locations, underscoring the need for iterative reservoir modeling to refine optimization decisions as project data accumulates. The CDE methodology also shows promise for addressing broader CCS optimization challenges, including enhancing storage efficiency through improved injectivity and trapping mechanisms.

Babaei et al. [5] address robust optimization for CO<sub>2</sub> injection well placement in saline aquifers, considering parametric and spatial uncertainties. The uncertainties include interfacial tension, Land's trapping coefficient, and aquifer permeability. The optimization aims to maximize residually trapped CO<sub>2</sub>, using a risk-averse objective function derived from the cumulative density function of trapped gas. Monte Carlo simulations and Polynomial Chaos Expansion (PCE) methods were employed for uncertainty quantification. PCE is more efficient for up to two parametric uncertainties, while Monte Carlo simulations are preferred for spatial uncertainties. The robust optimization successfully identifies optimal CO<sub>2</sub> injection well locations.

Tarrahi and Afra [66] proposed a novel objective function to optimize CO<sub>2</sub> flooding in heterogeneous formations by equalizing breakthrough times from injection wells to equidistant cell pairs. Applied to the PUNQ-S3 benchmark model, their method significantly enhanced CO<sub>2</sub> distribution uniformity, boosting solubility and residual trapping efficiency. Their results demonstrate substantial increases in total trapped CO<sub>2</sub> compared to traditional methods, highlighting its potential to optimize geological carbon storage effectively.

Babaei et al. [6] focused on optimizing well rate in CO<sub>2</sub> storage in saline aquifers, addressing operational objectives among uncertainties. They use a 3D geological model based on the Forties and Nelson fields, exploring coarse grid resolutions to reduce computational costs without compromising accuracy. The study aims to find optimal CO<sub>2</sub> injection rates among existing wells, balancing simulation intensity with model resolution to enhance efficiency in CO<sub>2</sub> storage design.

Stopa et al. [60] developed and employed an optimization approach aimed at reducing the potential for CO<sub>2</sub> leakage in a heterogeneous aquifer by minimizing the volume of free CO<sub>2</sub> gas near top of the aquifer. Their study utilized genetic algorithm and particle swarm optimization techniques to determine optimal placements for CO<sub>2</sub> injection wells and time-dependent injection rates. They evaluated the efficacy of genetic algorithm and particle swarm optimization in optimizing scenarios involving structural and residual trapping within the aquifer.

Jeong et al. [37] addressed the challenge of leakage from geologic faults and abandoned wells in large-scale CCS projects. They propose a binary integer programming approach to optimize the design of pressure monitoring networks, which is crucial due to the high costs of deploying deep pressure monitoring wells. Their method aims to create a cost-effective monitoring network that ensures coverage of all potentially leaky locations, adheres to CO<sub>2</sub> storage performance criteria, and accounts for geological uncertainty. Unlike other studies using cost surrogates, their approach directly evaluates total costs, including monitoring and potential leakage damages. Numerical examples show that this optimal design can significantly reduce costs, with key influencing factors being unit leakage damage costs, pressure detection thresholds, and geological uncertainty.

The study by Gonzalez-Nicolas et al. [31] aims to demonstrate the application of adaptive optimization methods in planning brine extraction and assess the impact of initial site characterization quality and ongoing monitoring data on optimization effectiveness. By integrating continuous monitoring, calibration, and optimization of brine extraction rates to meet pressure constraints, the research highlights the importance of early and frequent pressure monitoring, especially under uncertain initial reservoir conditions. Effective adaptive pressure management minimizes extracted brine volumes while controlling reservoir pressures, essential for optimizing reservoir operations.

Jun et al. in [38] studied the optimal injection strategies in the Pohang Basin, Korea, which has complex aquifer layers, faults, and varying reservoir properties. They explore four well patterns—single vertical injection well, two vertical injection wells, single horizontal injection well, and two wells for brine extraction and CO<sub>2</sub> injection (TVEI). Their findings highlight that TVEI, with optimized placement and fluid rates, can store nearly eight times more CO<sub>2</sub> compared to the

---

base case. This research demonstrates the effectiveness of different well patterns in enhancing CO<sub>2</sub> storage capacity and ensuring pressure security in the Pohang Basin.

A.Y. Sun [61] used deep reinforcement learning for optimal multiperiod planning in geosystem energy management. A deep Q-learning network (DQN) agent is trained to maximize rewards and deep multitask learning is used to approximate transition functions. Applied to carbon sequestration reservoir planning, the framework identifies optimal policies for monitoring and brine extraction strategies, demonstrating effective risk and cost management.

In [46], Musayev et al. utilized Artificial Neural Network (ANN)-based proxy models to optimize CO<sub>2</sub> injection and brine extraction well placements in the upper aquifer of the Pohang Basin. By integrating ANN models with a genetic algorithm, the research aims to maximize cumulative CO<sub>2</sub> injection efficiently. Several ANN models with different input features are developed and tested against full physics reservoir simulations. The approach reduces computational demands significantly, achieving comparable results with an 80.7% reduction in simulation runs compared to conventional methods, demonstrating its effectiveness and efficiency in optimizing well placements for CO<sub>2</sub> storage.

Park et al. in [52] introduced a Pareto-based multi-objective optimization approach for optimizing CO<sub>2</sub> sequestration operations using a multi-well system under geological uncertainty. The study focuses on minimizing operational pressure while maximizing sequestration efficiency through optimal allocation of CO<sub>2</sub> injection rates at multiple wells.

Zheng et al. in [71] explored the optimization strategies for CO<sub>2</sub> storage in geologic formations, emphasizing the inclusion of geomechanical risks such as reservoir expansion, ground surface uplift, and induced seismicity during injection. They propose a multi-objective optimization framework that integrates coupled flow-geomechanics simulations to assess risks and optimize CO<sub>2</sub> storage while minimizing geomechanical impacts. Their study highlights that optimal injection well locations differ significantly when geomechanical risks are considered, compared to traditional flow-only simulations. This approach underscores the importance of balancing CO<sub>2</sub> storage capacity with geomechanical safety considerations in optimizing injection strategies for geological CO<sub>2</sub> storage.

In [4] Arouri and Sayyafzadeh, introduced the use of the adaptive moment estimation (ADAM) framework with stochastic gradient approximation for optimizing well location and trajectory. ADAM enhances optimization by utilizing previous gradient information for variable-specific steps, accelerating convergence. This method, suited for computational budget constraints, incorporates nonlinear constraints for practical applicability. Comparing ADAM with steepest descent and generalized pattern search in case studies involving vertical and nonconventional wells, results show ADAM's superior computational efficiency and optimal outcomes.

Espinoza et al. in [22] introduced a methodology for optimizing injector location and injection rates in faulted and compartmentalized reservoirs using integrated reservoir and geomechanics simulations, cash flow analysis, and neural networks. The optimization aims to prevent fault shear failure by stopping injection when a safety factor-determined distance to faults is reached. The study applies this method to a faulted sand reservoir model based on the Gulf of Mexico Coast. It finds that moderate injection rates maximize net present value by balancing storage volume and injection period, avoiding both excessively low and high injection rates that lead to suboptimal economic and operational outcomes. Neural networks facilitate comprehensive exploration of injector scenarios, ensuring an optimal solution across all feasible locations and injection rates.

Zou and Durlofsky in [72] presented a framework for optimizing monobore well locations and time-varying injection rates in geological carbon storage. They consider two objective functions: minimizing mobile CO<sub>2</sub> fraction and maximizing storage efficiency. Linear and nonlinear constraints are managed with derivative-free algorithms like particle swarm optimization and differential evolution. A multifidelity optimization approach, adjusting grid resolution during optimization, outperforms high-resolution methods in both solution quality and computational efficiency. Results show significant improvements in mobile CO<sub>2</sub> fraction and storage efficiency, with distinct well configurations tailored to each objective function.

In a recent work [28], Fotias et al. presented a framework utilizing Bayesian Optimization to optim-

---

ize well placement in CCS operations. The study focuses on scenarios without flow boundaries in aquifers, where production wells manage pressure buildup and injection wells sequester CO<sub>2</sub>. Emphasizing group control, predefined targets and constraints guide well operations throughout the project. The study explores Bayesian Optimization's effectiveness under permutation in-variance, highlighting its rapid optimization capabilities. Overall, the research underscores Bayesian Optimization as a promising approach for enhancing sustainability in energy sectors through optimized well placement in CCS operations .

In conclusion, optimization techniques are commonly used in CCS projects, with varied approaches and objective functions designed to meet unique project objectives. Researchers have investigated several techniques to optimizing CCS processes, highlighting the varied character of these endeavors and the need for efficient and effective carbon capture and storage solutions.

## 2.8 CCS projects

In this section, we will discuss the history of CCS. This section is primarily based on the latest report from the International Energy Agency (IEA). According to the report, the total number of projects with an announced capacity exceeding 100 000 tonne per year (or 1000 tonne per year for direct air capture facilities) reported since the 1970s exceeds 800. This number encompasses both operational projects and those in the planning or construction phase. This number encompasses a wide range of projects, including those focused on EOR, carbon capture, Carbon Capture and Utilization (CCU), full chain integration, storage, transport, and storage, as well as projects dedicated solely to storage.

In this section, we will narrow our focus to CCS projects that do not involve EOR, or other forms of utilization. We will specifically discuss projects that are currently operational or have been suspended or decommissioned.

With this refined focus, it's noteworthy to mention that the first-ever CCS project started in 1996 is Sleipner, located in Norway. Sleipner involves the storage of CO<sub>2</sub> in saline aquifers situated 800 to 1100 m beneath the seabed. Operations commenced in 1996, boasting a capacity of 1 million tonnes per year [43]. By the end of 2020, Sleipner has successfully stored approximately 19 million tonnes of CO<sub>2</sub> <sup>1</sup>.

The second-ever CCS project, the In Salah project in Algeria, stands as a pioneering onshore endeavor. Operationalized in 2004, this initiative was undertaken in the In Salah Gas Field by BP (Algeria) to inject the extracted CO<sub>2</sub> from natural gas back into the subsurface [9]. However, operations were suspended in 2011 due to concerns regarding the integrity of the seal. The process involved the separation of CO<sub>2</sub> from natural gas, followed by injection into a 20-meter thick Carboniferous interval within a saline aquifer situated approximately 2 kilometers below the surface. Utilizing three long-reach horizontal injection wells, the CO<sub>2</sub> was injected into the down-dip aquifer leg of the gas reservoir [56]. Despite its early suspension, the In Salah project managed to inject a total of 3.8 million tonnes of CO<sub>2</sub> during its operational period [43].

The third CCS project chronologically is the Snøhvit Capture and Storage project in Norway, announced in 2002, and the operation started in 2008, with an annual capacity of 0.7 million tonnes of CO<sub>2</sub> storage. Initially, CO<sub>2</sub> injection occurred in the Tubåen formation, mainly comprised of fluvial sandstone. The injection well at Snøhvit is situated in waters approximately 318 meters deep. For better monitoring, both the well-head and down-hole gauges are installed. The down-hole gauge is positioned approximately 1782 meters below sea level and around 800 meters above the sand face [33]. However, due to faster-than-anticipated pressure buildup, an intervention was necessary to prevent seal fracturing after 1.1 million tons of CO<sub>2</sub> injection <sup>2</sup>. Consequently, injection into the Tubåen formation ceased in 2011, with the shallower Stø formation serving as the new CO<sub>2</sub> storage reservoir. By the end of 2019, Snøhvit has successfully stored approximately 3 million tonnes of CO<sub>2</sub> <sup>3</sup>.

---

<sup>1</sup><https://www.equinor.com/energy/sleipner>

<sup>2</sup><https://www.sodir.no/en/whats-new/publications/co2-atlases/co2-atlas-for-the-norwegian-continental-shelf/6-the-barents-sea/6.2-storage-options-of-the-barents-sea/6.2.1-saline-aquifers/storage-capacity-snöhvit-area/>

<sup>3</sup><https://ccreservoirs.com/the-snöhvit-ccs-project-from-over-pressurisation-to-successful-sequestration/>

---

The Illinois Basin- Decatur Project commenced operations in 2011 and operated until 2014 in the USA. With an initial plan to inject 1000 tonnes per day, the project successfully injected approximately one million tonnes of CO<sub>2</sub> into the Mount Simon Sandstone, which has a porosity in the range of 5 - 17 %, during this period [26]. The injected CO<sub>2</sub>, sourced as a byproduct of corn fermentation for ethanol production, boasted a purity exceeding 99%. The project involved a 2190-meter-deep injection well and a 2201-meter-deep observation well. Insights gained from this endeavor are now being applied to the neighboring Illinois Industrial CCS Project, leveraging the lessons learned for enhanced effectiveness [27].

Started in 2015, the Quest Carbon Capture and Storage project in Canada represents the world's first large-scale commercial implementation of CCS at an oil sands operation. This project captures over one million tonnes of CO<sub>2</sub> annually. The captured CO<sub>2</sub> is compressed to its supercritical phase and transported via 12-inch underground pipelines over a distance of 65 km to the injection wells. The CO<sub>2</sub> is then injected into a deep saline aquifer known as the Basal Cambrian Sand, which is approximately 45 meters thick via three injection wells. This storage formation is securely sealed by multiple layers, including the Middle Cambrian Shale (around 50 meters thick) and the Lotsberg Salts (approximately 120 meters thick) [19]. By July 2020, 5 million tonnes of CO<sub>2</sub> has been successfully stored in this project <sup>4</sup>.

The Tomakomai CCS project in Japan is the first industrial-scale project in Asia, which ran from 2016 to 2019, and is a notable example of carbon capture and storage integrated with industrial operations. The project captured CO<sub>2</sub> from a hydrogen production unit at an oil refinery. Throughout its duration, the project injected 300 012 tonne of CO<sub>2</sub> into a primary reservoir about 1,000 meters below the seabed with a thickness of roughly 200 meters. A secondary reservoir, located approximately 2,400 meters deep and 600 meters thick, received less than 100 tonne of CO<sub>2</sub> due to its low permeability, which led to the cessation of injection into this formation [65, 64]. One of the key achievements of the Tomakomai project was its innovative use of onshore drilling platforms to access offshore reservoirs, significantly lowering the CO<sub>2</sub> emissions associated with the drilling process [64]. This method, along with the successful storage and thorough monitoring, highlights the importance of the in demonstrating the feasibility and environmental advantages of CCS technology in coastal and industrial settings.

The Gorgon CCS project in Australia captures CO<sub>2</sub> naturally occurring in offshore gas reservoirs and injects it into a vast sandstone formation located two kilometers beneath Barrow Island, ensuring permanent containment. The project began operations in 2019 with an announced capacity of 4 million tonnes per year. By the end of 2023, it had successfully injected 9 million tonnes of CO<sub>2</sub>. To regulate pressure, water is reinjected into a formation situated 1 kilometer above the CO<sub>2</sub> injection depth<sup>5</sup>.

In summary, the projects discussed above represent significant milestones in the history of carbon capture and storage. They highlight the progress and successes achieved over the years. However, it is important to note that there is a substantial number of CCS projects currently in the planning or construction phases worldwide. These upcoming projects indicate a growing commitment to CCS technology and its potential to play a crucial role in reducing global CO<sub>2</sub> emissions.

---

<sup>4</sup>[https://www.shell.ca/en\\_ca/media/news-and-media-releases/news-releases-2020/quest-ccs-facility-captures-and-stores-five-million-tonnes.html](https://www.shell.ca/en_ca/media/news-and-media-releases/news-releases-2020/quest-ccs-facility-captures-and-stores-five-million-tonnes.html)

<sup>5</sup><https://australia.chevron.com/-/media/australia/publications/documents/gorgon-CCS--fact-sheet.pdf?a>

---

### 3 Case Study: Smeaheia

In this section, we will delve into a comprehensive examination of the Smeaheia storage area, beginning with a detailed discussion on the geological model. Subsequently, attention will be directed towards elucidating the model setup on the reservoir simulator, followed by an exploration of the inherent uncertainties within the model.

#### 3.1 Geological Model

In discussing the geological model of the Smeaheia storage area, it is pertinent to provide an overview of the project's context. Smeaheia stands as a significant CCS initiative situated within the expansive reaches of the northern North Sea in Norway. Positioned approximately 50 kilometers eastward from the shoreline, the site is flanked by the prominent Troll field, a substantial oil and gas reservoir in operation since 1991, situated roughly 20 kilometers to its west. Within the Smeaheia field, two distinct geological structures are discernible: the Alpha structure occupies the western sector, proximal to the Troll field, while the Beta structure is situated to the east. Notably, the Alpha structure boasts greater depth, reaching approximately 1200 meters, whereas the Beta structure ranges between 800 and 900 meters in depth [11]. Figure 14 shows the depth map of the Smeaheia field, and Alpha and Beta structures.

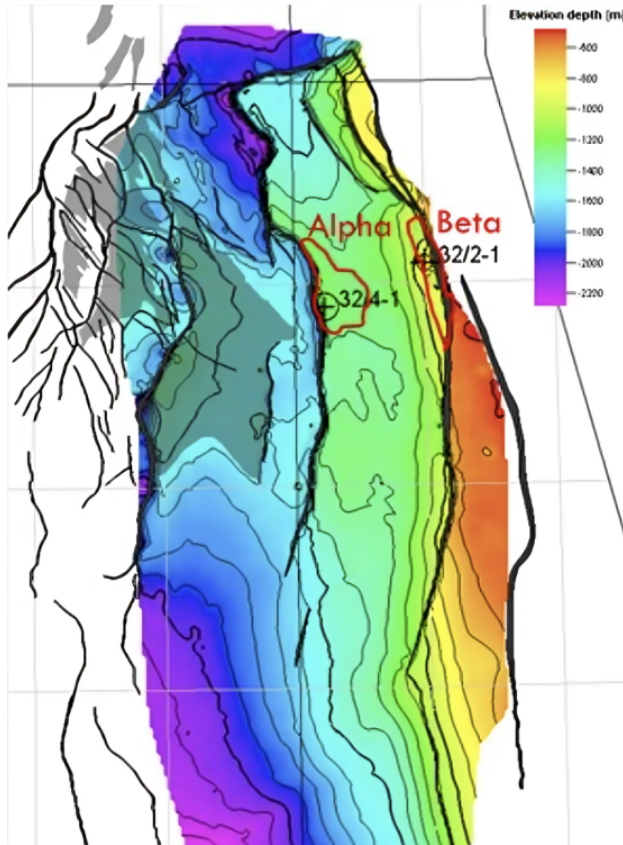


Figure 14: Depth map of the Smeaheia field with Alpha and Beta structures shown with red polygons [11].

This storage field is found in the Viking group, Smeaheia storage site is more specifically found in the Viking group on the Horda platform located in the Stord basin [21]. Sandstones categorized within the Viking group are commonly known as the Sognefjord delta aquifer, encompassing formations such as the Sognefjord, Fensfjord, and Krossfjord formations which are coastal-shallow marine sandstone, which are separated by thin shale layers. These shale layers play the role of

internal barriers [32]. Moreover, the main cap rock of the storage site is the thick shaly layer of Draupne formation. A lithostratigraphic illustration of the North Sea is shown in the figure 15, in which the Viking group is outlined by the blue square.

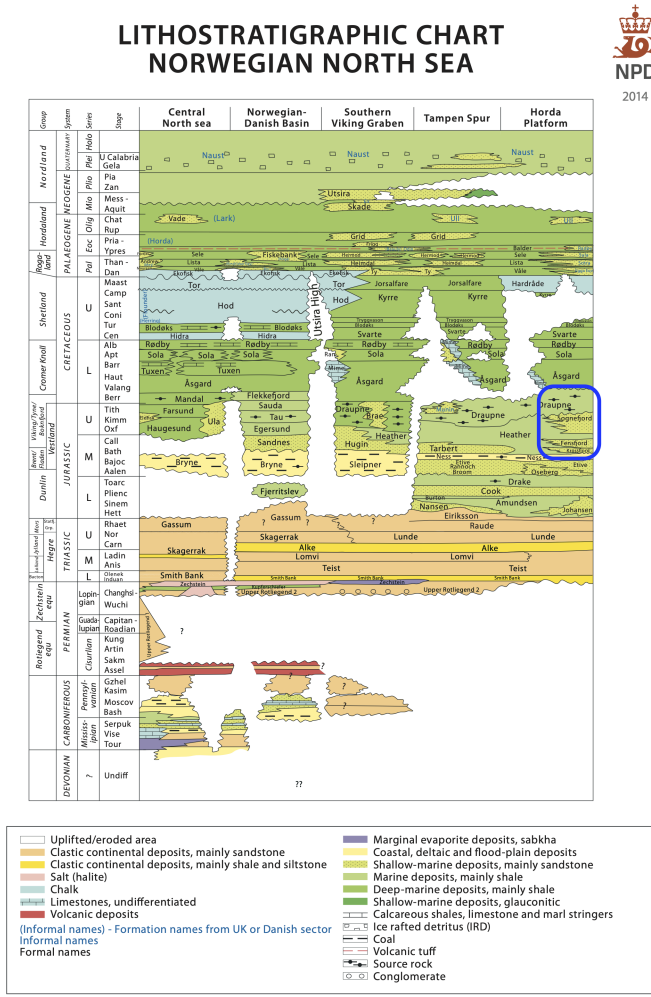


Figure 15: Viking group outline on the lithostratigraphic illustration of the North Sea [15]

The Krossfjord formation, located at the deepest level, exhibits thinner characteristics compared to the overlying formations. Additionally, it demonstrates relatively lower porosity and permeability. Conversely, the Fensfjord formation represents the thickest layer, measuring 300 meters in thickness [3], and is characterized by high permeability. The porosity within this formation typically ranges from 25 to 30 percent. At the shallower end, the Sognefjord formation emerges as the shallowest layer. It boasts notably high permeability, ranging between 1 to 30 darcy, and exhibits porosity levels varying from 26 to 35 percent. The maximum thickness of this formation reaches 220 meters [3, 23].

The storage site comprises two primary structures: Alpha and Beta. Alpha is situated in the western portion of the site, adjacent to the Troll field, and is separated from it by the Vette fault. Conversely, Beta occupies the eastern portion of the site and is bounded by the Øygarden fault to its east. As mentioned earlier, Alpha is positioned at a deeper level compared to Beta, but shallower than the Troll field. Additionally, it's worth noting that the vertical extension of the Øygarden fault increases the risk of CO<sub>2</sub> leakage to the surface in the vicinity of Beta. Based on these reasons, Alpha emerges as the most preferable structure for CO<sub>2</sub> injection. Firstly, it

is shallower than the Troll field, mitigating the risk of CO<sub>2</sub> migration towards Troll. Secondly, its deeper position relative to Beta enhances containment. Thirdly, the presence of the Øygarden fault increases the likelihood of CO<sub>2</sub> vertical leakage to the surface near Beta, further emphasizing the advantages of Alpha.

Considering that Alpha and Beta are connected to each other, it's imperative to identify the spill point and carefully study the total amount of CO<sub>2</sub> and injection rate. This is essential to prevent CO<sub>2</sub> migration towards the Beta structure. Figure 16 illustrates the path between Alpha and Beta structures.

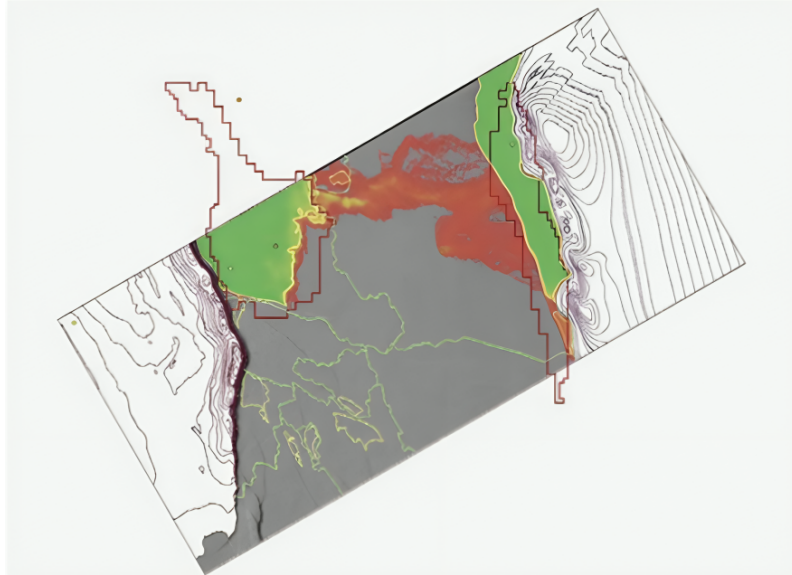


Figure 16: CO<sub>2</sub> movement from Alpha to Beta structure [21]

### 3.2 Model setup and Data File

The reservoir model used in this study was developed by SINTEF and is based on surfaces and faults received from Equinor in 2020. The model features a gridblock size of 300 by 300 meters, with layers thinned below low permeable layers to accurately resolve CO<sub>2</sub> saturation. Permeability and porosity are randomly distributed according to a simple facies model that includes several low permeability layers. The model comprises a total of 25 layers. In the simulation model, regions in the north and south have been deactivated to focus on the areas of interest.

Below, different parts of the Input deck for the Pflotran-OGS will be discussed, and more specifically for the current work.

- **Simulation:** In this part, the flow model to simulate is defined. There are several options to choose between, based on the purposes of the study, and also the availability of the data. As mentioned in the previous sections, Pflotran-OGS has multiple modes, which should be chosen based on the fluids and number of the phases in the reservoir. GAS\_WATER is used in our work, because it is the most suitable one for CO<sub>2</sub> sequestration cases in aquifers, which will be discussed in the next chapter. Next keyword used is RESERVOIR\_DEFAULTS. If this keyword is added to the input deck, some commonly used values will be automatically set in the simulation.

The next keyword used is ISOTHERMAL. Activating this option will keep the simulation isothermal, meaning that the temperature in the cells will stay constant as the initialized temperature during the simulation. It should be noted that for most of the modes in the simulator, thermal is the default.

After careful consideration, we have opted to utilize the isothermal mode in our reservoir simulation. This decision is underpinned by extensive analyses conducted during my specialization project. In [45], we examined 16 different scenarios characterized by variations in injection temperature, injection pattern, brine salinity, the presence of thief layers, and permeability anisotropy. Each scenario was simulated using both thermal and isothermal modes with the current simulator.

Our findings indicated that the differences between the thermal and isothermal simulations were minimal and did not significantly influence the plume movement or its shape. Additionally, the thermal mode demanded substantially more computational resources. Given the constraints on computational power and time, and considering the negligible impact on the simulation outcomes, the choice to adopt the isothermal mode is both practical and efficient. This approach ensures computational efficiency while maintaining the accuracy of the simulation results.

For instance, Figure 17 illustrates the distribution of free CO<sub>2</sub> using both thermal and isothermal modes, with no discernible differences.

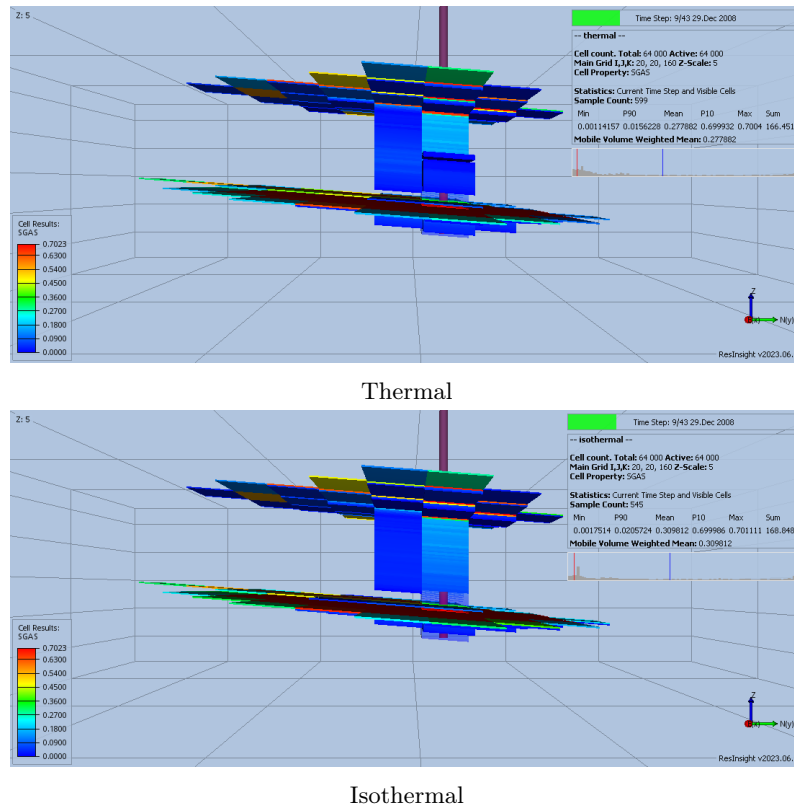


Figure 17: Gas saturation distribution at the end of the eighth year [45]

It is important to note that we do not imply that the thermal mode is without merit. In scenarios where reservoir pressure and temperature conditions are near the CO<sub>2</sub> critical point, the thermal mode is essential. However, in our case, based on the temperature and pressure conditions of the reservoir, it is not necessary.

If there is a previous state of the simulation that is meant to be added to the simulation, and to start the new case from that condition, the keyword ERESTART must be used. ERESTART takes a file name and a date to start. The application of the specific keyword in our reservoir simulation is crucial in scenarios where pressure matching has been conducted, and the commencement of CO<sub>2</sub> injection is predicated on the existing pressure distribution.

- **Grid:** This block is used for defining the computational model. Pflotran-OGS supports three different types of grids. It is common to add the grids to the input deck using an external

file. In this study, GRDECL is used, which defines the grid cell using Eclipse keywords. In this study, the keywords in Table 3 are used in grid block.

Table 3: Eclipse keywords and their applications

| Eclipse Keyword | Application  |
|-----------------|--|
| PINCH           | Handles the inactive layers between active cells               |
| MAPAXES         | Location of the grid is set to the true space                  |
| MAPUNITS        | Unit used for the MAPAXES is defined using this keyword        |
| GRIDUNIT        | The units of the grid data are set                             |
| COORD           | Always comes with the ZCORN, and sets the coordinate lines     |
| ZCORN           | Defines the depth of each node on the coordinate lines         |
| ACTNUM          | Specifies the active and non-active cells                      |
| FAULTS          | Defines the faults in the reservoir                            |
| MULTFLT         | Assigns a transmissibility multiplier to the predefined faults |
| PERMX           | Sets the cell permeability in X direction                      |
| PERMY           | Sets the cell permeability in Y direction                      |
| PERMZ           | Sets the cell permeability in Z direction                      |
| PORO            | Sets the cell porosity   |
| MULTV           | Multiplies the volume of the cell to the given number          |
| FIPNUM          | Used for dividing the reservoir into smaller regions           |

Porosity and permeability distribution in two different layers of the model are illustrated in Figures 18, 19, respectively.

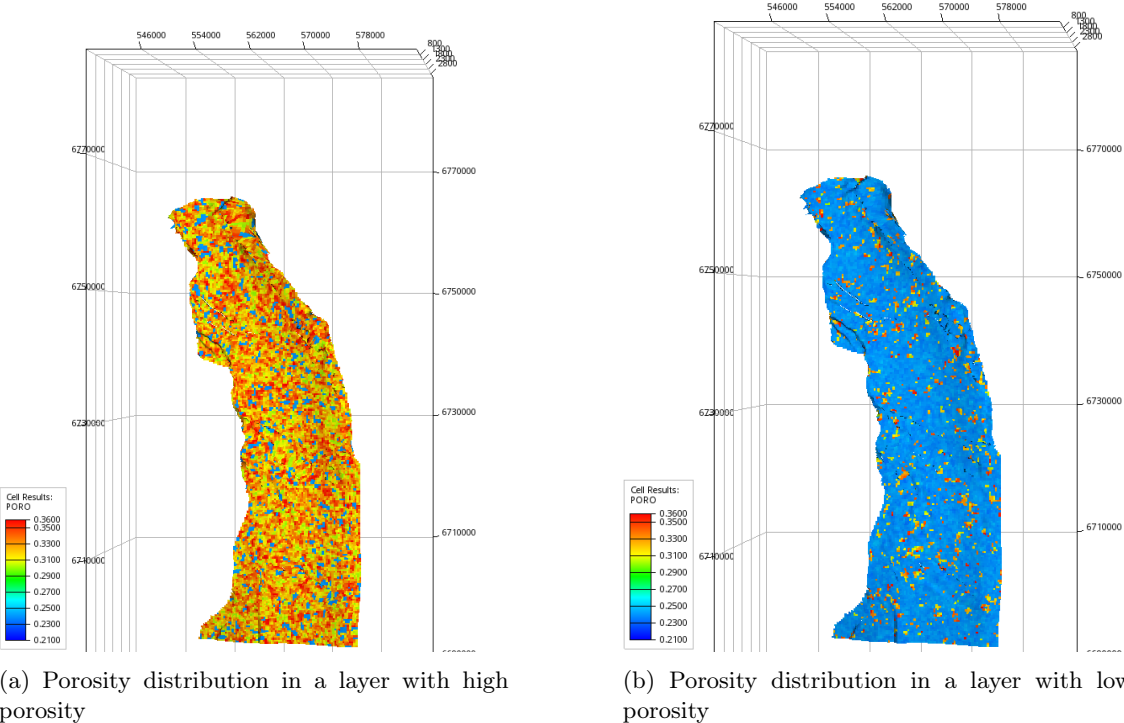


Figure 18: Porosity distribution in two different layers in the model

Moreover, the probability density function (PDF) of porosity and the cumulative distribution function (CDF) of permeability for the entire reservoir are shown in Figure 20.

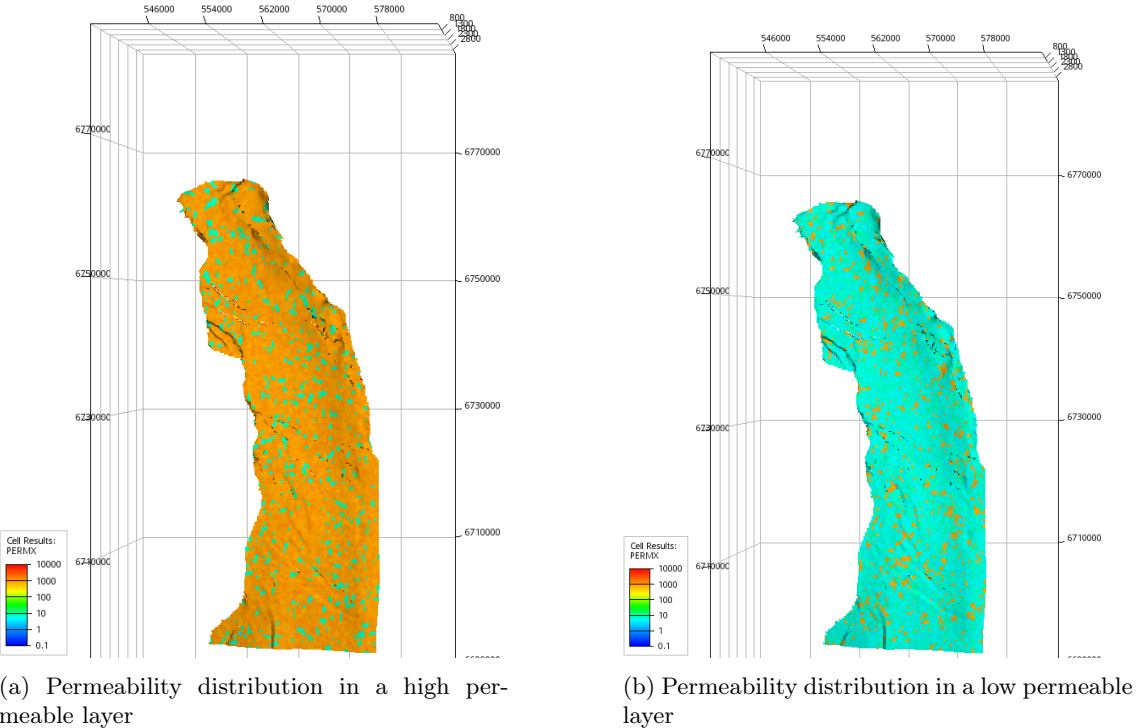


Figure 19: Permeability distribution in two different layers in the model

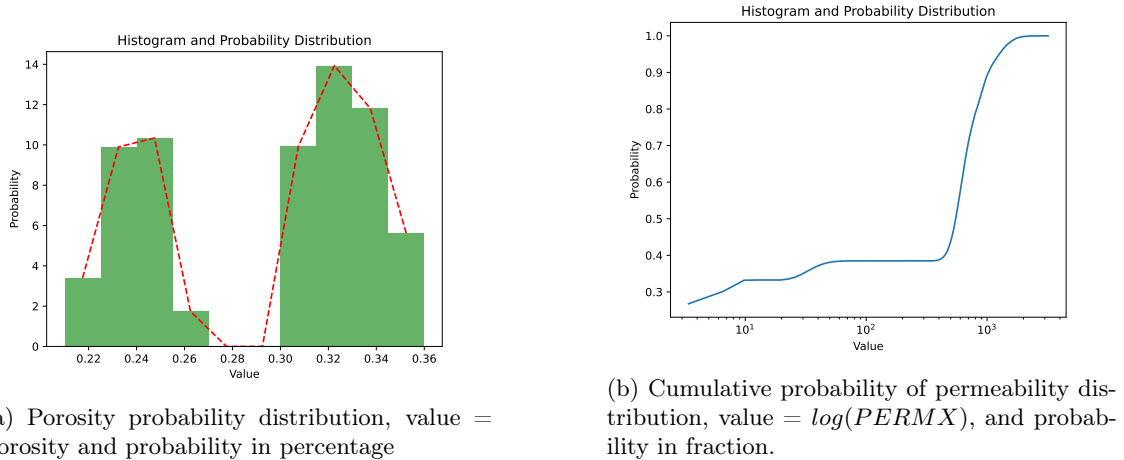


Figure 20: Probability distribution of porosity and cumulative probability distribution of permeability in the model

- **TIME:** In this block, the start and final dated are specified. Moreover, initial and maximum time-step sizes are defined. Multiple maximum time-step sizes can be defined. Among all the keywords, only the FINAL\_TIME is obligatory to be set. If no START\_DATE is set, the default date of 1 January 2000 will be used.
- **OUTPUT:** In this block, the variables to be reported in output, and the type of output file is determined. In this work, two types of output files are requested, MASS\_BALANCE\_FILE in ASCII format, and ECLIPSE textunderscore FILE, which is an unformatted unified Eclipse file. These files are visualized in the ResInsight software in this work.
- **MATERIAL PROPERTY:** In this block, the properties of the reservoir are defined by the simulator. Saturation functions (relative permeability and capillary pressure) are added under the CHARACTERISTIC\_CURVES keyword. Rock compressibility and a reference

pressure to compute the compressibility effects are defined in this block. Most of the keywords in this block like, rock density, specific heat capacity, and dry and wet thermal conductivity of the rock are only required for non-isothermal simulations. Figure 21 illustrates the saturation function used in this work.

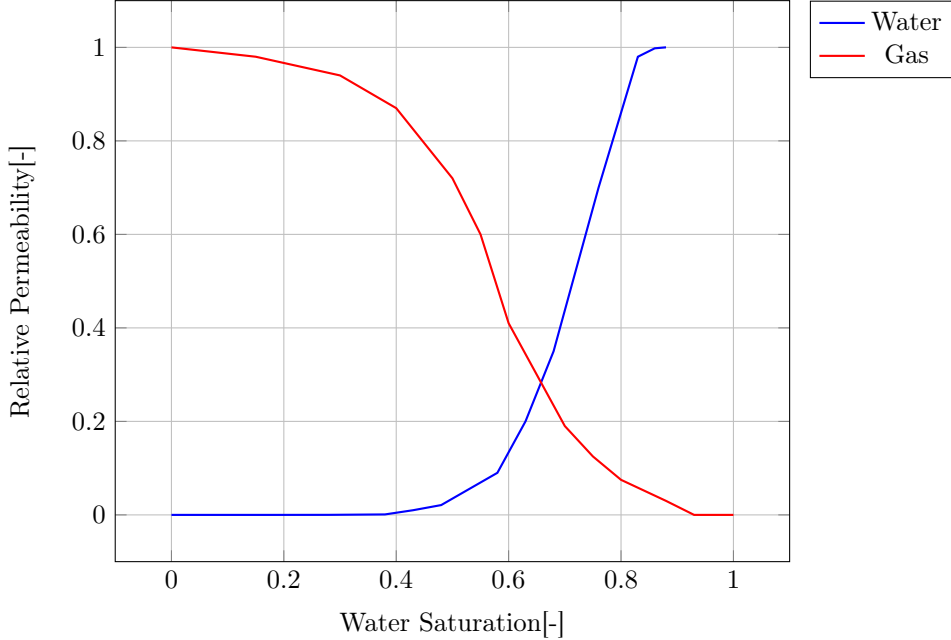


Figure 21: Saturation functions for water and  $\text{CO}_2$

- **FLUID \_ PROPERTY:** In this block, properties of the fluids present in the reservoir are given to the simulator. Diffusion coefficients of liquid and gas phases in each other are defined. Moreover, surface densities of the phases are obligatory to be given. Furthermore, salinity of the liquid phase can be determined in this block.
- **WELL \_ DATA:** In this block, information regarding each well is determined. Name, location, size, type, either injector or producer, which fluid to inject, operating mode of the well, which could be either rate or bottom-hole pressure, and dates regarding opening and shutting of the well are given to the simulator in this block.
- **FLOW \_ CONDITION:** Initial temperature, pressure and saturation distribution, and mole fraction of gas in liquid of the reservoir are defined in this block.

### 3.3 Model Uncertainties

One significant distinction between conventional oil and gas projects and CCS projects lies in the extent of available data and characterization methods. In oil and gas production cases, numerous wells are typically drilled in the area, complemented by extensive core tests, special core analysis (SCAL), logging, and petrophysical studies. These comprehensive datasets provide detailed insights into reservoir layers and their properties. However, in CCS projects, especially those injecting in aquifers like the one under consideration, the number of drilled wells and conducted tests is often limited. Consequently, the available data for CCS reservoirs are comparatively sparse. In this study, the porosity and permeability distribution used in the reservoir model are generated randomly due to the scarcity of available data. This inherent uncertainty in the reservoir properties may significantly impact the results of the study and should be acknowledged and carefully considered in the interpretation of findings. Moreover, it should be mentioned that the saturation functions for the Smeaheia aquifer have been measured, but are not publicly available. The saturation functions of a neighboring aquifer is used in this study, which could also be a ground for variation of results between the reality and the simulation.

---

In this study, we employ a comprehensive model to investigate the various trapping mechanisms in our reservoir system. Among the four primary trapping mechanisms, structural/stratigraphic trapping, residual trapping, solubility trapping, and mineralization trapping, our simulations successfully capture the first three. Structural/stratigraphic trapping and residual trapping are effectively modeled, allowing us to analyze their impact on CO<sub>2</sub> sequestration. Additionally, solubility trapping is incorporated to account for the dissolution of CO<sub>2</sub> into the reservoir fluids over time. However, the mineralization trapping mechanism is not included in our simulations. This exclusion is due to the limitations of the simulator, as it does not support modeling mineralization processes. Moreover, the effects of mineralization trapping typically manifest over extended timescales far beyond the duration of our simulations. Consequently, while our study provides a robust analysis of the initial three trapping mechanisms, mineralization trapping remains beyond the scope of our current modeling efforts.

---

## 4 Background and methodology

### 4.1 Reservoir Simulator

In this project, we use the reservoir simulator Pflotran [1]. US labs started the development of the Pflotran Parallel Flow Transport Simulator as an open-source project, with a background in environmental science and groundwater flow. OpenGoSim has further developed the reservoir simulator with capabilities that are optimized for Carbon Capture and Storage, called pflotran-OGS. Pflotran-OGS is mainly modern Fortran, Petsc, and Hypre, and are largely C, some C++, and Python. Pflotran-OGS solves the flow equations fully implicit and uses the two-point flux approximation. This simulator has different modes that can be used based on the case that is being studied.

- Gas\_Water Mode, which is suitable for CO<sub>2</sub> storage in aquifer
- Compositional Modes
  1. COMP, which works for the cases with water and any number of components.
  2. COMP3, which can be used for CO<sub>2</sub> storage in depleted gas fields.
  3. COMP4, for CO<sub>2</sub> storage in depleted hydrocarbon fields that contain small amounts of residual oil
- Black-oil, which is similar to other reservoir simulators, and accounts for gas dissolving in the oil phase, with oil properties.

For CO<sub>2</sub> injection in saline aquifers, the Gas\_Water Mode is the best fit, and describes a two-phase flow model. As this study is considering CO<sub>2</sub> into an aquifer, the Gas\_Water solution mode will be used in this study.

#### 4.1.1 Gas\_Water Mode

As mentioned previously, the Gas\_Water Mode describes a two-phase flow model. In this module, each of the components could be in both phases, so CO<sub>2</sub> can be dissolved in the aqueous phases, and water can be evaporated in the gas phase. The molar balance equation is solved for each component, and for the thermal effects, the energy equation is used. Equation 2 describes the molar balance for each phase, in which,  $\alpha$  is the component, in our case water or CO<sub>2</sub>, and  $\beta$  is the phase, in our case gaseous (the CO<sub>2</sub>-rich phase) or liquid (the water-rich phase):

$$\frac{\partial}{\partial t} \phi \sum_{\beta} (x_{\beta}^{\alpha} S_{\beta} \eta_{\beta}) + \nabla \cdot \sum_{\beta} (x_{\beta}^{\alpha} q_{\beta} \eta_{\beta} + \phi S_{\beta} D_{\beta} \eta_{\alpha} \nabla x_{\beta}^{\alpha}) = Q_i \quad (2)$$

where:

- $\phi$  is porosity;
- $x_{\beta}^{\alpha}$  is mole fraction of  $\alpha$  in the phase  $\beta$ ;
- $S_{\beta}$  represents the saturation of phase  $\beta$ ;
- $\eta_{\beta}$  is molar density of phase  $\beta$ ;
- $q_{\beta}$  is the Darcy velocity of the phase  $\beta$ ;
- $D_{\beta}$  is the diffusion coefficient of phase  $\beta$ ;
- $Q_i$  is a source term.

For phase  $\beta$ , the Darcy velocity is calculated as below:

$$q_\beta = \frac{K k_\beta}{\mu_\beta} \nabla(P_\beta - \rho_\beta g z) \quad (3)$$

In equation (3),  $K$  is rock permeability,  $k_\beta$ ,  $\mu_\beta$ ,  $P_\beta$ ,  $\rho_\beta$  are the relative permeability, viscosity, pressure and density of the phase  $\beta$  respectively,  $g$  is the gravitational constant, and  $z$  is height. In pflotran-OGS, the default mode is non-isothermal, and equation (4) shows the energy balance, in which the internal energy of each phase, density, heat capacity, and thermal conductivity of the formation is used:

$$\frac{\partial}{\partial t} [\phi \sum_\beta S_\beta \eta_\beta U_\beta + (1 - \phi) \rho_r c_r T] + \nabla \cdot \sum_\beta [q_\beta \eta_\beta H_\beta + \kappa \nabla T] = Q_e \quad (4)$$

For CO<sub>2</sub> properties the Span and Wagner [58] correlation is used in Pflotran-OGS, and the simulator uses the Duan and Sun [17] and the Sun, Duan, Hu, Li, and Mao [18] correlations for the properties of the CO<sub>2</sub>-H<sub>2</sub>O and CO<sub>2</sub>-H<sub>2</sub>O-NaCl systems.

Various approaches are used to discretize fluid flow simulations, including different variants of the Finite Element Method (FEM) and the Finite Volume Method (FVM). PFLOTRAN uses the Finite Volume Method to discretize reservoirs. This technique conserves flow into and out of Control Volumes (CVs) by directly integrating the governing equations and monitoring flux across cell surfaces, as shown in 22. This has the advantage of boosting accuracy through two main methods: grid reorganisation and increasing the number of integration points [20].

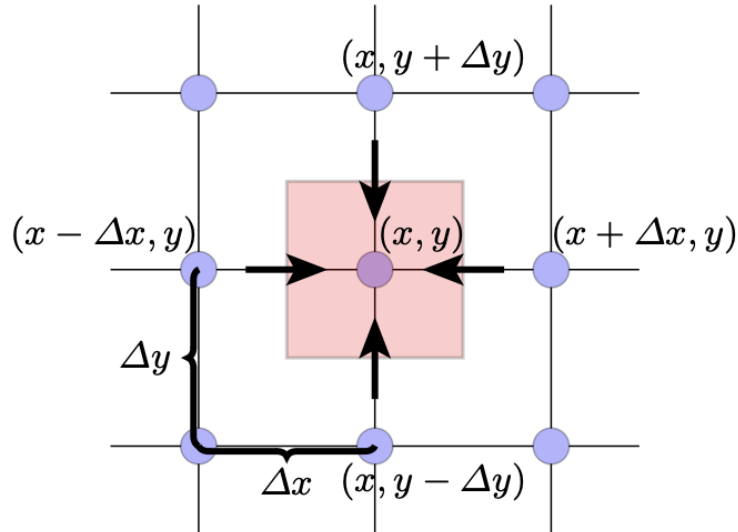


Figure 22: Neighbouring fluxes into a control volume in a 2D vertex-centred, structured finite volume method discretisation [20]

#### 4.1.2 Parallelization

PFLOTRAN is parallelized, using domain decomposition with message passing interface (MPI) to efficiently compute flux across subdomains, enhancing performance for complex simulations. Figure 23 illustrates an example of a domain that is split into smaller subdomains. In domain decomposition, a simulation domain is divided into smaller subdomains for parallel computation. Each subdomain is assigned to a different process, and border information between subdomains is exchanged using ghost vectors. This ensures that each process has the necessary boundary data from neighboring subdomains, facilitating efficient and accurate parallel computations.

However, it should be noted that increasing the number of CPUs does not necessarily result in a proportional decrease in simulation time. In parallel computing, the phenomenon of diminishing

---

returns on performance with increasing core count is often observed, attributed to multiple factors. Amdahl's Law posits that the sequential portion of a program limits speedup, hindering performance gains from additional cores. Communication overhead escalates as core count rises, offsetting potential speedup by increasing coordination complexities. Memory bandwidth contention ensues as multiple cores access shared memory, diminishing returns in simulation time reduction. Load imbalance further exacerbates inefficiencies, with some cores underutilized while others are active. Additionally, simulation-specific constraints, such as dependencies between computations, impede parallelization effectiveness.

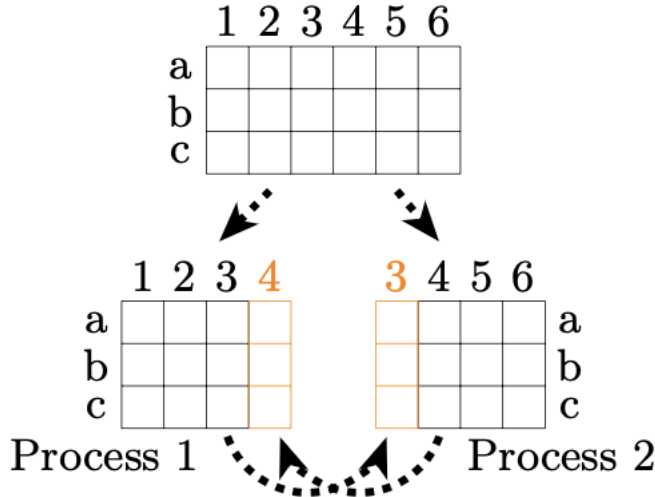


Figure 23: Domain decomposition where the domain is split between two processes [20]

PFLOTTRAN combines PETSc for solvers, data structures, and communication with hypre for its Algebraic Multigrid (AMG) preconditioner, BoomerAMG, which PETSc may use.

#### 4.1.3 Implementation

In order to optimize the computational efficiency of the reservoir simulation process, a benchmark study was conducted. This study involved running the reservoir simulation with varying numbers of CPUs requested at the outset. Specifically, simulations were performed with 1, 2, 4, 8, 16, and 32 CPUs to explore the impact of parallelization on performance. The objective was to identify the optimal number of CPUs to be requested for subsequent simulations, ensuring a balance between computational resources and runtime efficiency.

---

##### Algorithm 1 Simulation Time Measurement

---

```

1: Initialize the core counts: cores = [32, 16, 8, 4, 2, 1]
2: Initialize an empty list to store times: Times = []
3: Initialize an empty list to store durations: Length = []
4: Append the current time to Times: Times.append(time.time())
5: for each core count i in cores do
6:   Record the start time: start = time.time()
7:   Run the simulation with i cores
8:   Record the finish time: finish = time.time()
9:   Calculate the duration: duration = finish - start
10:  Append the duration to Length: Length.append(duration)
11: end for
12: Save the Length to a file: np.save('Duration.npy', Length)

```

---

---

The algorithm for testing how well the simulator can be parallelized is used and the results are discussed in subsection 5.1.

## 4.2 History Matching

While the major goal of reservoir simulation in petroleum engineering is to anticipate the reservoir's future behavior, getting a satisfactory history match is important. History matching entails altering reservoir model parameters to closely match previous production and pressure data. Pressure matching is a crucial consideration in CCS projects, particularly when dealing with reservoirs such as depleted gas reservoirs or saline aquifers adjacent to producing fields, where the reservoir pressure is often below hydrostatic pressure. The variance from initial hydrostatic pressure can significantly impact the CCS operation in several ways:

- Fracture Pressure Management: One of the critical constraints is the maximum allowable pressure, often determined by the fracture pressure of the reservoir. Accurate knowledge of the initial pressure provides a reliable estimation of the permissible pressure increment, ensuring operations remain within safe limits.
- CO<sub>2</sub> Physical Properties: The physical properties of CO<sub>2</sub>, particularly its density and viscosity, are highly pressure-dependent. Misjudging initial reservoir conditions can lead to incorrect predictions of CO<sub>2</sub> behavior and movement within the reservoir, potentially compromising the storage integrity and efficiency.
- Surface Facility Design: The design of surface facilities is influenced by the required injection pressure, which in turn is determined by the bottom-hole pressure—a function of the reservoir pressure. Inaccurate pressure data can lead to suboptimal design choices, affecting the overall effectiveness and safety of the project.
- Operational Expenses: Overestimating reservoir pressure can lead to unnecessary CO<sub>2</sub> pressurization, directly increasing operational costs. Accurate pressure assessment is essential for minimizing these costs and ensuring the economic feasibility of the project.
- Revenue Impact: Revenue in CCS projects is contingent upon the volume of CO<sub>2</sub> injected. Incorrectly assuming higher reservoir pressure in simulations can result in reaching the bottom-hole pressure limit prematurely, thereby reducing the injection rate. This reduction translates to lower CO<sub>2</sub> storage volumes and, consequently, diminished revenue, potentially impacting the economic viability of the project.

Therefore, precise pressure matching is vital for optimizing CCS project design, operation, and financial performance, ensuring both safety and economic success.

### 4.2.1 Pressure Matching Implementation

The Smeaheia storage site, situated in close proximity to the Troll field, has been operational since 1991. Notably, the Troll field and the Smeaheia storage site are interconnected in terms of pressure, with production from the Troll field a decrease in Smeaheia site pressure below hydrostatic pressure levels is expected.

Despite the availability of production rates from the Troll field, these values cannot be directly applied to the pressure matching task due to the absence of the Troll field in our simulation model. To address this challenge, we introduced five dummy production wells into the model to simulate the production dynamics of the Troll field. However, it is important to recognize that simply adding wells to the model overlooks the spatial distance between the two sites. To emulate this spatial effect, cells surrounding the dummy wells were assigned significantly larger pore volumes. This adjustment delays the arrival of the pressure front at the Smeaheia site, more accurately reflecting the impact of distance on pressure propagation. All dummy wells commence production in 1991 at uniform rates.

---

Furthermore, the drilling of Well 32/4-3s, known as Galdsheim, in 2019 provides an opportunity for validation, as pressure data from this well is available. Leveraging Algorithm 2, we aim to minimize the difference between measured pressure data and simulated pressure data by iteratively adjusting production rates.

In summary, our approach integrates dummy wells, spatial adjustments using pore volume multipliers, and iterative change of production rate to pressure match the system and calibrate the simulation model effectively.

---

**Algorithm 2** FindBestProductionRate()

---

```

1: Input: WELLS_T.INC, SMH_TERM_TEST.in, MeasuredPressure, I, J, K
2: Output: Optimal injection rate
3: procedure MATCHBYRATE(RATE)
4:   Open WELLS_T.INC as file
5:   filedata  $\leftarrow$  file.read()
6:   filedata  $\leftarrow$  filedata.replace('<INJRATE>', str(int(RATE)))
7:   Write filedata to WELLS.INC
8:   Execute simulation with os.system
9:   sumdp  $\leftarrow$  0
10:  eclfile  $\leftarrow$  EclFiles('FILE_NAME')
11:  df  $\leftarrow$  grid.df(eclfile, rstdates='last')
12:  mat  $\leftarrow$  df[['I', 'J', 'K', 'PRESSURE', 'DEPTH']].to_numpy()
13:  for k in range(5) do
14:    target_values  $\leftarrow$  [I, J, K[k]]
15:    MeasuredPressure  $\leftarrow$  MeasuredPressure[k]
16:    matching_rows  $\leftarrow$  np.all(mat[:, :3] == target_values, axis=1)
17:    SimulationPressure  $\leftarrow$  mat[matching_rows, 3]
18:    dP  $\leftarrow$  (SimulationPressure - MeasuredPressure)2
19:    sumdp  $\leftarrow$  sumdp + dP
20:  end for
21:  Return sumdp
22: end procedure

```

---

### Input and Output:

#### Input:

- **WELLS\_T.INC:** Template file with a placeholder for the injection rate.
- **SMH\_TERM\_TEST.in:** Input file for the simulation.
- **MeasuredPressure:** Array of measured pressure values for the Gladsheim well.
- **I, J, K:** Indices for locating pressure values in the simulation grid.

**Output:** Optimal injection rate that minimizes the difference between simulated and measured pressures.

#### Procedure MatchByRate(RATE):

1. Open and read the template file WELLS\_T.INC.
2. Replace the placeholder <INJRATE> with the current RATE.
3. Write the modified data to WELLS.INC.
4. Run the simulation using os.system.
5. Initialize sumdp to zero.

- 
6. Extract the relevant data from the simulation output.
  7. For each of the five entries in K:
    - Find rows in the simulation output that match the target indices  $[I, J, K[k]]$ .
    - Calculate the pressure difference between simulated and measured pressures.
    - Accumulate the squared differences in sumdp.
  8. Return sumdp.

The workflow and algorithm presented above will be implemented and discussed in subsection 5.2.

### 4.3 Spill-point

As mentioned in the previous sections, ensuring the safe injection and storage of CO<sub>2</sub> is paramount for CCS projects. As elucidated in the preceding sections, various trapping mechanisms, including dissolution, mineralization, and residual trapping, offer greater safety assurances compared to structural trapping. However, it is notable that during the initial stages of injection, a significant proportion of the injected CO<sub>2</sub> becomes trapped within the geological structure in its free form as a secondary phase.

Furthermore, it has been underscored that accurate estimation of trapping capacity holds pivotal significance. Such estimations are indispensable for comprehending the economic viability of CCS projects by defining the permissible quantity of CO<sub>2</sub> that can be safely injected into storage reservoirs. However, the determination of trapping capacity necessitates knowledge of the height of the trap. Reservoir height is conventionally defined as the vertical distance between the top of the reservoir and a critical delineation known as the spill-point. This concept signifies the threshold at which the reservoir's capacity for containing free CO<sub>2</sub> is surpassed, prompting a consequential outflow from the structure [49].

Various methodologies exist for pinpointing the spill point within reservoirs. For instance, Nilsen et al. in [49], proposed a method to delineate spill paths by segmenting the reservoir into smaller discrete traps. This approach employs corner-based and center-based algorithms to partition the reservoir effectively, facilitating the identification of critical spill points and pathways for CO<sub>2</sub> migration.

In Figure 24, a simple illustration demonstrating the spill-point is provided. As depicted, due to the low density of CO<sub>2</sub> in comparison with the initial fluid in the reservoir, it will start filling the pores from the top of the reservoir, and the CO<sub>2</sub> plume height will increase, once the plume height within the reservoir reaches the reservoir height, it begins to escape from the reservoir domain.

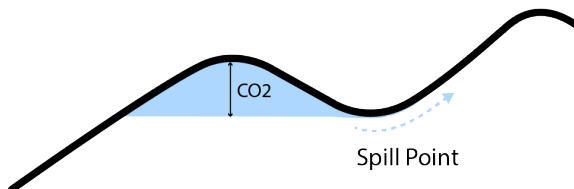


Figure 24: Simple illustration of spill-point

---

### 4.3.1 Spill-point Identification

As mentioned earlier, the Smeaheia aquifer comprises of two main structures, namely Alpha and Beta. Additionally, it has been highlighted that the eastern fault complex, known as Øygarden, presents risks of CO<sub>2</sub> vertical leakage. Hence, it is necessary to accurately identify the extent of the Alpha structure and pinpoint the spill point. To achieve this, the initial step involved a visual examination of the model, coupled with an analysis of depth values to determine a location in proximity to the spill point.

To identify the spill points, we will follow the following procedure: The depth of each cell is compared to that of its western neighbor; if the western cell is deeper, it is added to the region deemed unsafe for free CO<sub>2</sub>. Conversely, if the western cell is shallower than the eastern cell, the area from that cell to the westernmost part is included in the region deemed safe for injecting CO<sub>2</sub>. A pseudo-code for this method is given in Algorithm 3. This algorithm includes the following steps:

- The algorithm iterates over each layer ( $k$ ) in the grid and within each layer, it iterates over a range of Y-coordinates ( $j$ ).
- For each Y-coordinate range, it identifies cells within the same layer and with the same Y-coordinate.
- It then iterates over a range of X-coordinates ( $i$ ) for these cells, checking if each X-coordinate exists in the list of X-coordinates of the group of cells.
- If a cell's X-coordinate exists in the list, it marks the cell as part of the structure.
- It then checks the depth of neighboring cells to determine if they are part of the same structure, marking them accordingly.

---

#### Algorithm 3 Identifying Structure Extent in Geological Formation

---

```

1: Input: Grid DataFrame  $df$ , Layers  $k$ , Y-coordinate range  $[y_{\min}, y_{\max}]$ 
2: Output: Marked cells representing structure extent
3: for  $k$  in  $L$  do                                 $\triangleright$  Iterate over layers
4:   for  $j$  in  $Y_{\text{range}}$  do                 $\triangleright$  Iterate over Y-coordinates
5:      $same\_layer \leftarrow$  cells in  $df$  with layer  $k$ 
6:      $same_y \leftarrow$  cells in  $same\_layer$  with Y-coordinate  $j$ 
7:     for  $i$  in  $X_{\text{range}}$  do             $\triangleright$  Iterate over X-coordinates
8:       if  $i$  in  $X_s$  then
9:         Mark cell at  $(i, j, k)$  as part of structure
10:      end if
11:    end for
12:    for  $i$  in  $X_{\text{reverse}}$  do           $\triangleright$  Check depth of neighboring cells
13:      if  $\text{depth}(i - 1, j, k) > \text{depth}(i, j, k)$  then
14:        Mark cell at  $(i - 1, j, k)$  as part of structure
15:      else
16:        break
17:      end if
18:    end for
19:  end for
20: end for

```

---

Utilizing Algorithm 3, the reservoir was partitioned into two distinct regions. Finally, leveraging the FIPNUM keyword, these delineated regions were incorporated into the reservoir model. This algorithm is used in Subsection 5.3.

---

## 4.4 Optimization

Optimization methods have long been used in the oil and gas sector to help determine optimal well locations for injection or production, regulate variables such as injection or production pressures and rates, and sequence well drilling [12]. These methods include a variety of methodologies, both derivative and derivative-free, with the Net Present Value acting as the primary objective function in most cases. However, in certain scenarios, such as optimizing the sweep efficiency of the injection process, alternative objective functions may come into play, closely resembling NPV considerations.

### 4.4.1 Optimization Methods

Optimization methods can be divided into two categories, based on using or not using the derivative of the objective function, namely, derivative-based algorithms and derivative-free algorithms.

1. Derivative-based algorithms: Derivative-based optimization methods rely on the gradients or derivatives of the objective function to guide the search for the optimal solution [69]. These methods, such as gradient descent, Newton's method, and conjugate gradient descent, utilize information about the slope or curvature of the objective function to iteratively update the parameters towards the direction of the steepest descent or convergence. They are particularly effective for smooth, well-behaved functions and can often converge rapidly to a local minimum or maximum. However, they may struggle with non-smooth or discontinuous functions, and their performance can be sensitive to the choice of initial parameters and step size [69].
2. Derivative-free algorithms: Derivative-free optimization methods, on the other hand, do not rely on derivatives of the objective function. Instead, they explore the solution space using heuristic search strategies, such as simulated annealing, genetic algorithms, and particle swarm optimization. These methods are well-suited for problems with non-smooth, non-convex, or discontinuous objective functions, where derivatives may be unavailable or difficult to compute accurately [7]. While derivative-free methods may converge more slowly than derivative-based methods, they offer robustness and versatility in handling a wide range of optimization problems without requiring gradient information.

In this study for well placement optimization, the derivative-free method, compass search method is used. The compass search optimization method is a simple approach, making it easy to implement and suitable for non-differentiable or noisy functions. It is robust to the initial starting point and can handle various types of optimization problems. However, it can be slow to converge, especially for high-dimensional problems, and may get stuck in local optima. The algorithm's performance is sensitive to step size adjustments, and it can become inefficient for large-scale problems due to the need for multiple direction evaluations. Despite these drawbacks, its simplicity and flexibility are significant advantages.

## 4.5 Objective Function

In this study, one of the primary objectives is to optimize key parameters to achieve the best possible outcomes. While we could have chosen other metrics such as the amount of CO<sub>2</sub> injected, gas saturation in specific parts of the reservoir, trapping efficiency index, or sweep efficiency, we have chosen the Net Present Value (NPV) as our objective function. By focusing on NPV, we ensure that the optimization efforts are directed toward maximizing the financial return of the project. Additionally, by incorporating constraints such as the maximum bottom-hole pressure and penalties for CO<sub>2</sub> escaping the intended structure, we aim to integrate these considerations into the optimization process. This approach ensures that our decisions not only enhance NPV but also adhere to operational and environmental constraints, thereby driving the project towards optimal financial and practical performance.

---

#### 4.5.1 Net Present Value (NPV) Calculation

The Net Present Value is a financial metric used to evaluate the profitability of an investment or project. It represents the difference between the present value of cash inflows and the present value of cash outflows over a specified period. A simplified method of NPV calculation is represented by the equation 5.

$$NPV = -C_0 + \sum_{i=1}^T \frac{C_i}{(1+r)^i} \quad (5)$$

where:

- NPV : Net Present Value
- $C_0$  : Initial investment
- $C_i$  : Cash flow in period  $i$
- $T$  : Total number of periods
- $r$  : Discount rate

In this context, the NPV is calculated based on Capital expenditures (CAPEX), operational expenditures (OPEX), drilling expenditures (DRILLEX), income generated from CO<sub>2</sub> injection, and penalties.

$$OPEX = \dot{m} \cdot BHP \quad (6)$$

In which:

- $\dot{m}$  is the mass rate of CO<sub>2</sub> injected in standard conditions in ton per day.
- BHP is well bottom-hole pressure in bar.

$$DRILLEX = N \cdot DC \quad (7)$$

Where:

- N is the number of wells drilled.
- DC is drilling cost of an injection well.

$$INCOME = M \cdot I_R \quad (8)$$

Where:

- M is the total mass of injected CO<sub>2</sub> injected in tonne.
- $I_R$  is the amount of money earned per tonne of CO<sub>2</sub> injected.

$$PENALTY = M_{out} \cdot P_R \quad (9)$$

In which:

- $M_{out}$  is the mass of the CO<sub>2</sub> out the intended area, in Tonne.
- $P_R$  is the penalty that should be paid per tonne of CO<sub>2</sub>.

The final NPV is calculated by subtracting the total CAPEX, OPEX, DRILLEX, and PENALTY from the total INCOME:

$$NPV = INCOME - OPEX - DRILLEX - PENALTY - CAPEX \quad (10)$$


---

---

In this equation, each individual term has already been discounted by the discount rate.

Based on the equations presented above, Algorithm 4 has been developed. Note that the values used, e.g., for drilling cost, are just examples to test out the methodology and algorithms. If the methodology is to be implemented for a specific field case, these numbers need to be updated with accurate values for the given project. Such values are not commonly available outside the operator companies, therefore, some very rough estimates are used here.

---

**Algorithm 4** NPV Calculation Algorithm

---

```
1: Input: days_to_filter, WGIR1, BHP1, WGIT1, filtered_cells, NUMBEROFWELLS
2: Constants:
3: PENALTYRATE ← 10                                ▷ Norwegian Kroner per Tonne
4: discount_rate ← 8 %                               ▷ Norwegian Kroner per well drilled
5: Drilling_Cost ← 1 × 108                      ▷ Norwegian Kroner
6: Capital_Expenditure ← 1 × 109                ▷ Norwegian Kroner
7: InjectionRevenue ← 400                          ▷ Norwegian Kroner per Tonne
8: SC_Density ← 1.87                            ▷ kg per cubic meter
9: Initialize:
10: OPEX ← 0
11: INCOME ← 0
12: PENALTY ← 0
13: DRILLEX ← Drilling_Cost × NUMBEROFWELLS
14: CAPEX ← Capital_Expenditures
15: for i ← 0 to size(days_to_filter) - 1 do
16:   if i == 0 then
17:     opex ← (WGIR1[i] × BHP1[i] × 365 × SC_Density/1000) / (1 + discount_rate)i
18:     income ← (InjectionRevenue × WGIT1[i]/1000 × SC_Density) / (1 + discount_rate)i
19:   else
20:     opex ← (WGIR1[i] × BHP1[i] × 365 × SC_Density/1000) / (1 + discount_rate)i
21:     income ← (InjectionRevenue × (WGIT1[i] - WGIT1[i-1])/1000 × SC_Density) / (1 + discount_rate)i
22:   end if
23:   OPEX ← OPEX + opex
24:   INCOME ← INCOME + income
25: end for
26: PENALTY ← ∑(filtered_cells[:, 4] × filtered_cells[:, 5] × filtered_cells[:, 6]) × PENALTYRATE
27: NPV ← INCOME - OPEX - DRILLEX - PENALTY - CAPEX
28: Output: NPV
```

---

Explanation: The days\_to\_filter array contains cumulative day counts marking the end of each year in the simulation (e.g., [365, 730, 1095]). It is used to filter and process yearly data within the simulation.

### Constants and Initial Values

- **PENALTYRATE:** The rate applied to calculate the penalty costs, for the CO<sub>2</sub> leaked out of the intended region; 10 Norwegian Kroner per kilogram of CO<sub>2</sub> leaked out.
- **discount\_rate:** The discount rate used to calculate the present value, set to 1.08 (assuming an 8% discount rate).
- **Drilling\_Cost:** In this study, cost of drilling an injection well is assumed to be 100 million Norwegian Kroner.
- **Capital\_Expenditures:** Total initial investments, 1 billion Norwegian Kroner.
- **InjectionRevenue:** The rate used for calculating the income is 400 Norwegian Kroner per tonne of CO<sub>2</sub> injected, which is close to the CO<sub>2</sub> emission tax.

- 
- **SC\_Density:** The results captured from the reservoir simulator are in volumetric rate, to convert to mass rates, density of CO<sub>2</sub> in standard condition is used, which is 1.87 kg/m<sup>3</sup>.
  - **OPEX:** Initial operational expenditures, set to zero.
  - **INCOME:** Initial income, set to zero.
  - **PENALTY:** Initial penalty costs, set to zero.
  - **DRILLEX:** Drilling expenditures, calculated as 100 million Norwegian Kroner multiplied by the number of wells.
  - **CAPEX:** CAPEX set to Capital expenditures constant value.

### Iterating Over Days to Calculate OPEX and INCOME

- The code iterates over the number of days to filter, calculating the operational expenditures and income for each year.
- **WGIR1[i]:** Well gas injection rate for year i.
- **BHP1[i]:** Well bottom-hole pressure for year i.
- **WGIT1[i]:** Cumulative well gas injection for year i.
- **OPEX Calculation:**
  - For the first year ( $i == 0$ ), OPEX is calculated based on the gas injection rate and bottom-hole pressure.
  - For subsequent years ( $i > 0$ ), OPEX is similarly calculated.
- **INCOME Calculation:**
  - For the first year, income is based on the cumulative CO<sub>2</sub> injection.
  - For subsequent years, income is based on the amount of CO<sub>2</sub> injected in that specific year.
- Both OPEX and INCOME are discounted to their present values using the discount rate.

### Calculating PENALTY

- **PENALTY** is calculated using the formula:

$$\text{PENALTY} = \sum (\text{Cell Pore Volume} \times \text{Sgas} \times \text{Gas density}) \times \text{PENALTYRATE} \quad (11)$$

- **filtered\_cells:** Cells which are not in the safe region, but have the gas saturation value bigger than zero.
- The product is then summed and multiplied by the **PENALTYRATE** to obtain the total penalty costs.

### Final NPV Calculation

- The final NPV is calculated according to Eq. (10), by subtracting the total CAPEX, OPEX, DRILLEX, and PENALTY from the total INCOME after discounting.

This approach ensures that all cash flows are appropriately discounted and accounted for, providing a comprehensive measure of the project's profitability.

## 4.6 Well Placement Optimization

In this optimization problem, the well control parameters are held constant. Specifically, we focus on maintaining a consistent injection rate. Additionally, the optimization is subject to a constraint on the maximum bottom-hole pressure, ensuring that the pressure does not exceed predetermined safe limits.

$$\min_{x \in X} -\text{NPV}(x, u_0) \quad (12)$$

In this minimization process,  $u_0$  remains constant, representing the well control parameter, while  $X$  denotes the spatial domain within which the injection well can be drilled.

### 4.6.1 Lateral Well Placement Optimization

As mentioned earlier, compass search method is used in this work. This method entails initiating the search process from a designated starting point defined by its Cartesian coordinates  $(x, y)$ , alongside the selection of a stencil size parameter, both of which are determined in advance. The operation of the compass search algorithm is illustrated in Figure 25, where green dots show the current evaluated points, red for successful moves, blue for unsuccessful moves, and gray for previously evaluated points.

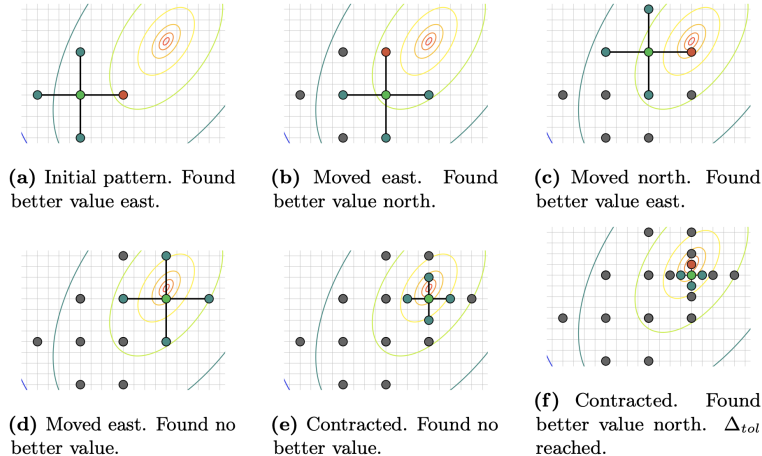


Figure 25: Steps of compass search optimization method (illustration from [39])

The selection of the starting point may be either randomized or guided by domain-specific engineering insights, aimed at positioning it in proximity to the anticipated optimum solution. Subsequently, the objective function, which in this case is NPV associated with this initial point is computed. Employing the specified stencil size, four additional points are systematically generated around the initial point at equidistant intervals. The NPVs corresponding to these new points are then evaluated, and any instances where a newly generated point demonstrates a higher NPV compared to the initial point, the point with the biggest NPV will be selected as the subsequent center point. This process is iterated until the center point exhibits a superior NPV relative to all neighboring points; in this condition, the stencil size is adjusted, and a fresh set of four points is generated accordingly. This iterative refinement process persists until the stencil size diminishes to a predetermined threshold, signifying the attainment of an optimal well location. A psuedo-code for this method is found in Algorithm 5.

---

**Algorithm 5** CompassSearch( $f$ ,  $\mathbf{x}_0$ ,  $\Delta_{tol}$ ,  $\Delta_0$ ,  $\mathcal{D}$ ) [39]

```
1:  $f_{best} \leftarrow f(\mathbf{x}_0)$                                 ▷ Set initial value for  $f_{best}$ .
2:  $\mathbf{x} \leftarrow \mathbf{x}_0$                                     ▷ Set initial value for  $\mathbf{x}$ .
3:  $\Delta \leftarrow \Delta_0$                                     ▷ Set initial step length.
4: while  $\Delta > \Delta_{tol}$  do                                ▷ Iterate while step length is greater than tolerance.
5:    $\mathcal{M} \leftarrow (\mathbf{x} + \Delta \cdot \mathbf{d}_k)$  for all  $\mathbf{d}_k \in \mathcal{D}$     ▷ Create list  $\mathcal{M}$  of moves  $\mathbf{x}_k$ .
6:    $\mathbf{x}_{min} \leftarrow \arg \min f(\mathbf{x}_k)$                             ▷ Find best move in iteration.
7:   if  $f(\mathbf{x}_{min}) < f_{best}$  then                                ▷ Found a better position.
8:      $\mathbf{x} \leftarrow \mathbf{x}_{min}$                                          ▷ Change the “best” position.
9:      $f_{best} \leftarrow f(\mathbf{x}_{min})$                                 ▷ Change the “best” objective value.
10:  else
11:     $\Delta \leftarrow \frac{1}{2}\Delta$                                      ▷ Reduce the step-length.
12:  end if
13: end while
```

---

#### 4.6.2 Coupled Well Placement and Perforation Length Optimization

In this section, we extend the well placement optimization method from 2D to 3D, introducing an additional dimension to enhance the optimization process. Previously, in the 2D optimization approach, the perforated interval of the well was kept constant, spanning from the top to the bottom of the formation. However, in the 3D optimization method, this perforation interval is also subject to optimization.

##### Methodology

The 2D optimization method involves generating four new cases in each iteration, with variations only in the  $x$  and  $y$  coordinates of the well placement. The perforated interval remains unchanged. In contrast, the 3D optimization method generates six new cases per iteration, considering variations in the  $x$ ,  $y$ , and  $z$  coordinates (where  $z$  represents the shallowest point of the perforation interval).

It is crucial to note that in all generated cases, only the shallowest perforation point is adjusted. The injection interval always continues to the deepest point of the formation. This ensures that the optimization process efficiently explores different perforation intervals, enhancing the overall placement and performance of the well.

Specifically, the six cases generated in each iteration for the 3D optimization are as follows:

Four cases with variations only in the  $x$  and  $y$  coordinates, similar to the 2D method. These cases maintain the same perforation interval as the central case.

Two additional cases where the  $x$  and  $y$  coordinates remain the same as the central case, but the perforation interval varies: One case has a larger perforation interval, extending the shallowest perforation point upwards while keeping the deepest point constant. The other case has a smaller perforation interval, moving the shallowest perforation point downwards while keeping the deepest point constant.

By incorporating the depth ( $z$ -coordinate) into the optimization process, the 3D method allows for a more comprehensive search for the optimal well placement. This results in potentially more efficient reservoir exploitation and improved overall performance compared to the 2D approach.

#### 4.6.3 Lateral Well Placement Optimization with Two Injection Wells

In this subsection, we extend the 2D well placement optimization method to scenarios involving two injection wells. Both wells are perforated from the top to the bottom of the formation and are operated with similar injection rates. The objective is to optimize the locations of both injection wells to maximize the NPV.

---

## Methodology

In each iteration of the optimization process, eight new potential well locations are evaluated. The procedure is as follows:

**First Set of Four Cases:** The location of Well 1 is kept constant, and four new locations for Well 2 are generated around its current position. These new locations are typically placed in the cardinal directions (north, south, east, and west) relative to the original position of Well 2.

**Second Set of Four Cases:** The location of Well 2 is kept constant, and four new locations for Well 1 are generated around its current position, similar to the first set.

For each of the eight generated cases, the NPV is calculated. The NPV values of these eight cases are then compared to the NPV of the central case, which has the original locations of both Well 1 and Well 2.

The new central point for the next iteration is determined by selecting the case with the highest NPV among the eight evaluated cases. If one of the eight new cases provides the highest NPV, this case becomes the new central point. However, if the central case itself provides the highest NPV, the stencil size is reduced to half. This procedure continues until reaching the stencil size equal to the size of a grid cell.

This reduction in stencil size allows for a more refined search around the current optimal point, enhancing the precision of the optimization process.

This iterative process continues until the optimal well placements are identified, ensuring that the locations of both injection wells are optimized to maximize the NPV.

By iteratively adjusting the positions of the two wells and comparing their performance, the optimization process effectively navigates toward the configuration that offers the best economic return for the two wells combined.

---

## 5 Results and Discussion

This section will present the results obtained from applying the different methodologies in the previous section. In addition, this section also discusses the obtained results.

### 5.1 Parallelization

The simulation times corresponding to varying numbers of requested CPUs are depicted in Figure 26. With perfect parallelization, a doubling of the number of cores should lead to a halving of the simulation time. Going from 1 to two cores yields a reduction in simulation time that is close to a halving; going from approximately 16 hours to a little more than 8 hours. Going from 2 to 4 cores yields a reduction that is more than half; this is a reduction that is more than the theoretical limit, and is attributed to noise occurring due to outside factors such as the heat of the processors, difference between processors, etc. It is assumed that if one conducted a higher number of runs and averaged the results, a larger reduction than 1/2 for doubling the number of processors would not occur.

Going from 4 to 8 and from 8 to 16 CPUs also shows an almost perfect parallelization, with the reduction in simulation time being close to 1/2. However, going above 16 cores (where  $\log_2(16) = 4$ , the reduction in simulation time is much reduced, indicating that we start to reach the maximum number of CPUs that gives an efficient parallelization. This work therefore used 16 CPUs for the individual simulations, as this was considered a fair balance between the speed-up of simulation and the computational cost.

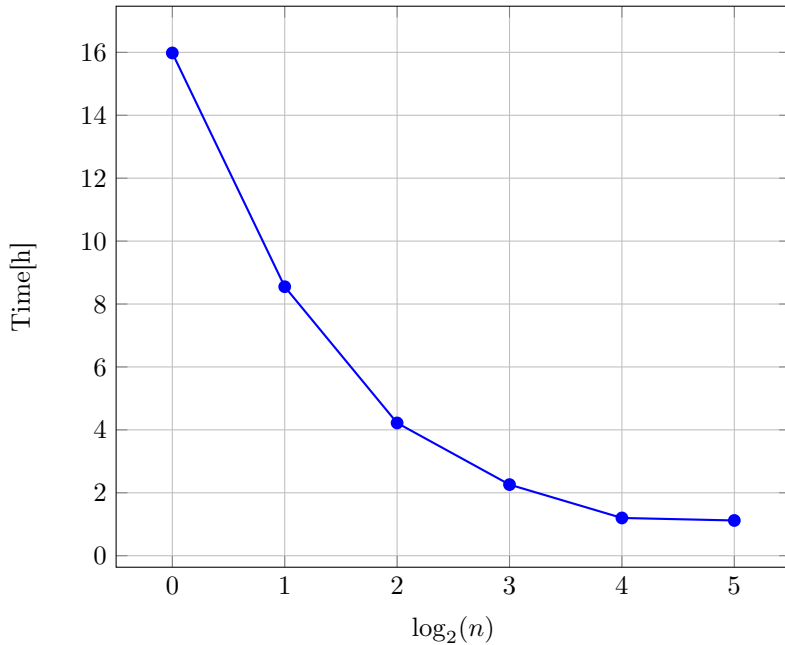


Figure 26: Simulation time versus number of cores requested. Here  $n$  is the number of CPUs

Consequently, increasing core count beyond 16 may yield minimal improvements in simulation duration. While understanding and mitigating these factors could enhance performance scaling, the current work's focus lies beyond pinpointing the root cause. The primary objective of this parallelization effort was to determine the optimal number of CPUs for subsequent work steps.

## 5.2 Pressure Matching

The pressure matching was conducted by coupling Pflotran-OGS with Python. The detailed methodology is explained in subsection 4.2.1, but to summarize:

First, the location of the Gladsheim well was identified within the reservoir model. Next, the depths of the pressure points were aligned with specific cells corresponding to the same location and depth. The simulation commenced on January 1, 1991, and ran until January 1, 2025, the assumed start date for CO<sub>2</sub> injection. By adjusting the rates of dummy production wells, the optimal match was achieved with the lowest pressure difference between the measured and simulated pressures.

### Results:

The results are illustrated in Figure 27. The figure displays five lines representing the pressures in the specified cells from the simulation, while the dots of similar colors indicate the measured pressures. As seen, three of the simulated pressures are higher than the measured pressures, and two are lower.

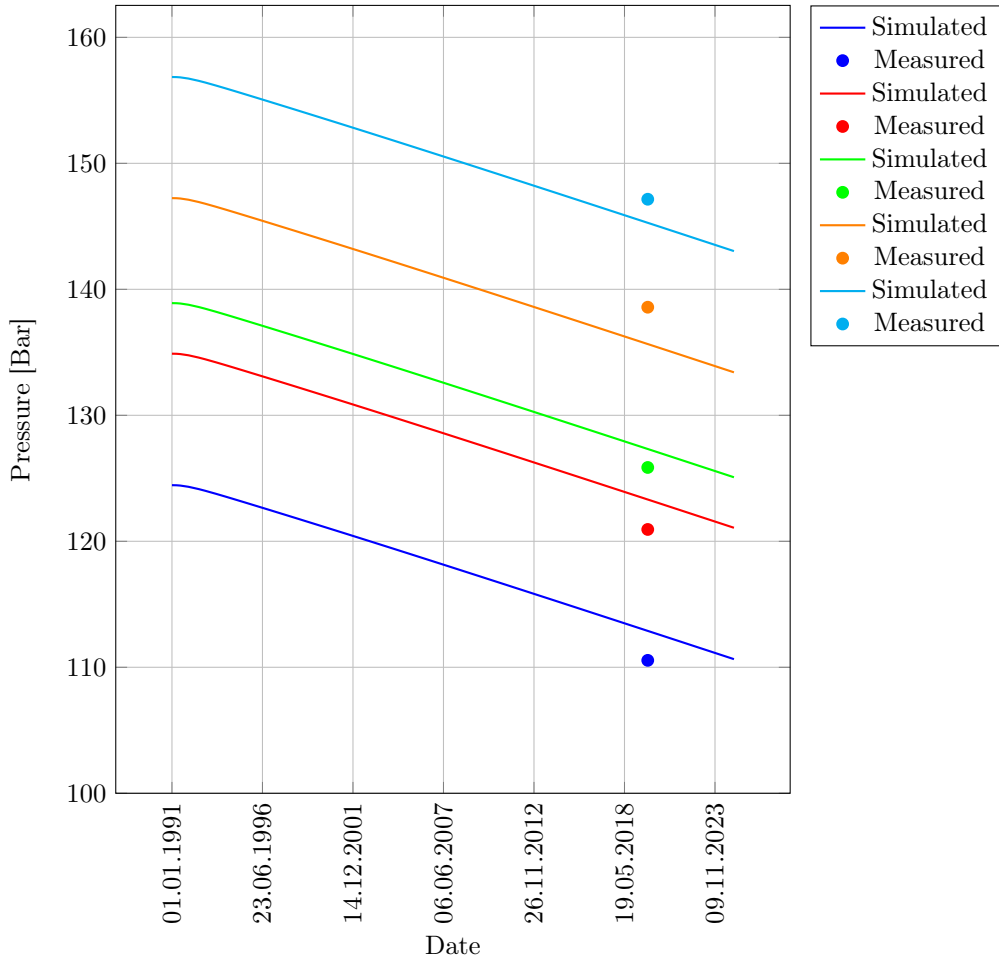


Figure 27: Lines showing pressure drawdown from start of production from Troll field in five different cells in the model and the points show the measured pressure points of the Gladsheim well.

### Discussion:

Several factors could explain why an exact pressure match was not achieved:

- Discrepancies Between Real-World Conditions and Model Setup: In our study, the dummy production wells are only active in the deeper parts of the model, specifically below the

deepest impermeable layer. This setup might not fully replicate real-world conditions, where pressure communication between Troll field and Smeaheia aquifer can vary. Consequently, this discrepancy could be a contributing factor to the challenges in achieving a perfect match in our simulations.

- Pressure Communication Between Layers: The Smeaheia aquifer contains several impermeable layers, which may impede uniform pressure transmission due to production activities from the Troll field. As previously mentioned, the permeability values for these layers are not accurate. Consequently, the pressure and flow communication between two parts of the aquifer separated by an impermeable layer can differ from real-world conditions. This discrepancy may hinder achieving the best match for all layers in our model.
- Brine Density and Salinity: The initial density of the brine in the aquifer, which depends on its salinity, can affect pressure measurements. While the salinity might have been measured, this data is not publicly available, potentially leading to inaccuracies in the pressure match. However, this is probably a second-order error compared to the points above, as the density variation with salinity is limited.

It is important to note that the rates obtained for the dummy wells cannot be interpreted as real rates. This is because the model used does not include the Troll field and the distance between the Troll field and Smeaheia is only mimicked by large pore volumes around the dummy wells. Achieving a perfect match is not within the scope of this work. For the purposes of this study, we will use the pressure match shown in Figure 27.

### 5.3 Spill Point Identification

A Python code utilizing Algorithm 3 was developed, dividing the reservoir into two separate parts. The results are displayed in Figure 28. Figure 28a depicts the depth map of the reservoir model where having free CO<sub>2</sub> is considered safe. Conversely, Figure 28b illustrates the region where free CO<sub>2</sub> poses a risk, since can then migrate upwards towards the Øygarden fault complex.

It should be noted that this method does not precisely delineate the region for the Alpha structure. In other words, this approach might overestimate the alpha region. However, the primary goal of this part of the work was to ensure that the CO<sub>2</sub> injected into the alpha structure would not reach the Øygarden fault complex, which poses a risk of leakage to shallower formations. This objective has been successfully achieved. These regions were added to the reservoir model to be used in the next simulations.

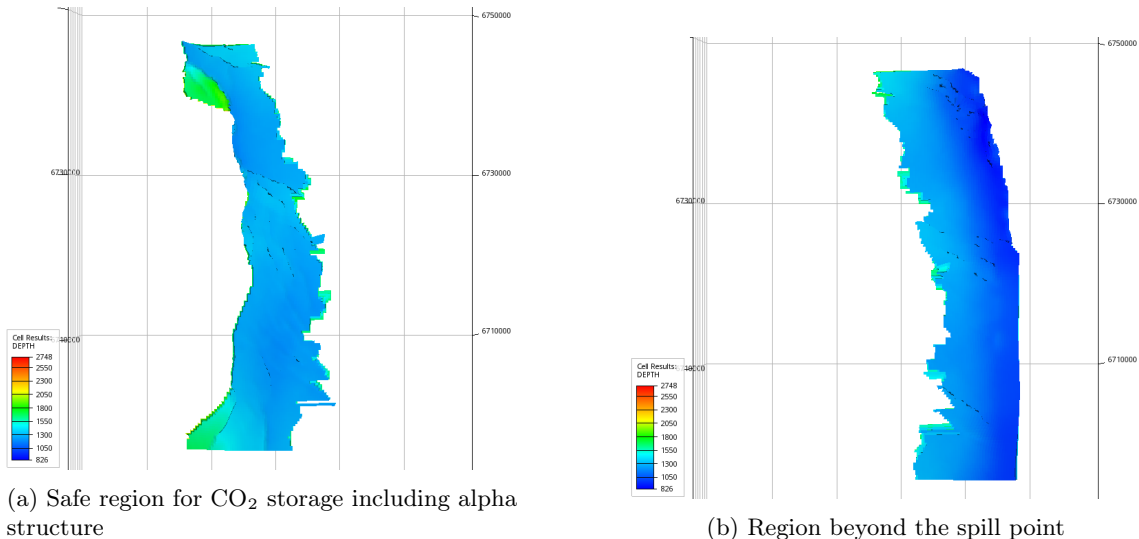


Figure 28: Reservoir divided into two main parts, safe and non safe regions for CO<sub>2</sub> storage

## 5.4 Sensitivity Analysis

In this section, we investigate the impact of various parameters on the NPV and other parameters through a sensitivity analysis. Before presenting the results of the sensitivity analysis, we will first introduce several figures that provide a comprehensive understanding of the underlying system. These visualizations will offer valuable insights and serve as a foundation for the subsequent analysis.

Figure 29 provides a snapshot of the total  $\text{CO}_2$  injected over time and the corresponding field average pressure over the injection period. The total volume of  $\text{CO}_2$  injected exhibits a linear increase over time, reflecting a constant injection rate sustained throughout the injection period without encountering the bottom-hole pressure limit. In contrast, the field average pressure curve may initially appear unconventional as it shows a decreasing trend over time while  $\text{CO}_2$  is being injected into the reservoir. This phenomenon, however, is attributed to ongoing production activities from dummy wells during the injection phase, representing gas production at the nearby Troll field. The pressure build-up resulting from the injection is outweighed by the pressure drawdown induced by the production at Troll, resulting in an overall decline in field average pressure.

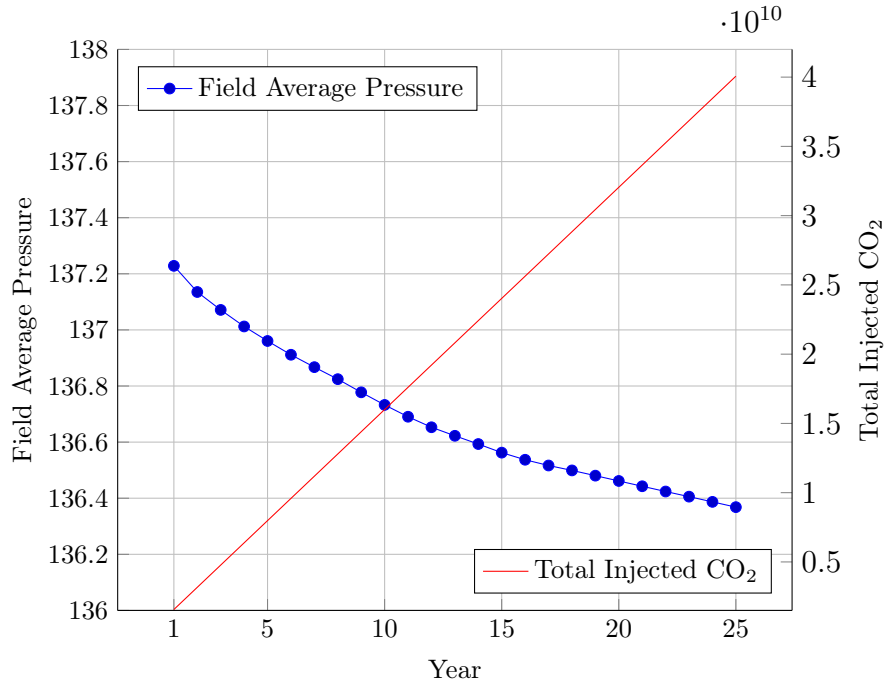


Figure 29: Field Average Pressure and Total Injected  $\text{CO}_2$  over 25 Years

The NPV versus time for one of the simulations is shown in Figure 30. This plot demonstrates the evolution of NPV over a 25-year period. It is important to note that the NPV plot presented here may not resemble a conventional NPV plot. This discrepancy arises because all costs are allocated to year 0, while the revenue generation also begins from year 0. Consequently, the NPV starts increasing from the outset.

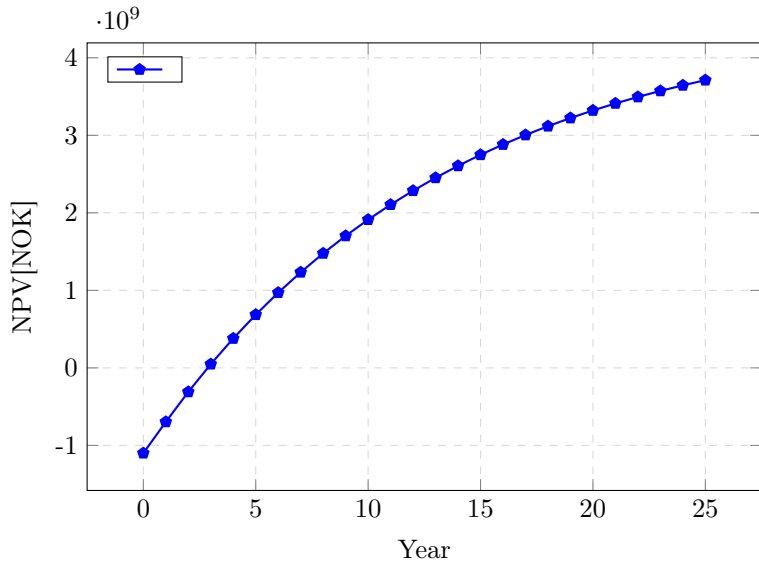


Figure 30: NPV vs Time for CASE 1

Figure 31 depicts the evolution of field average pressure over a simulation period spanning 560 years, segmented into distinct operational phases. Initially, from year 0 (corresponding to 1991) to year 35, production exclusively occurs from dummy wells. Subsequently, from year 35 to year 60, both CO<sub>2</sub> injection and production from dummy wells are concurrently operational. At year 60, CO<sub>2</sub> injection ceases, transitioning the phase to solely production from dummy wells until year 70. Beyond year 70, both injection and production activities halt, leading to a stabilization phase in pressure dynamics. The figure highlights the variations in field average pressure across these operational phases, illustrating the impact of injection and production activities on reservoir pressure over an extended timeframe.

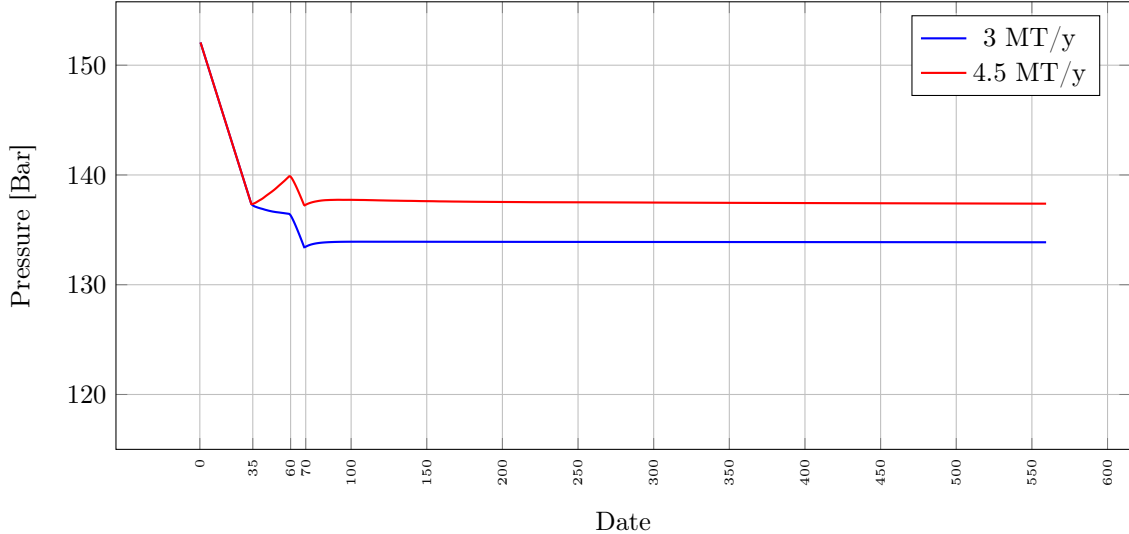


Figure 31: Field average pressure for a 560-year period, including production from Troll field, CO<sub>2</sub> injection, and post-injection for two cases, with injection rate of 3, and 4.5 MT/y.

Figure 32 depicts the mass of CO<sub>2</sub> dissolved in the aqueous phase, with dates corresponding to those in Figure 31. The data illustrates a dramatic increase in the dissolved CO<sub>2</sub> mass during the injection period. Following the injection phase, the dissolved CO<sub>2</sub> mass continues to rise but at a reduced rate, persisting until the end of the observation period.

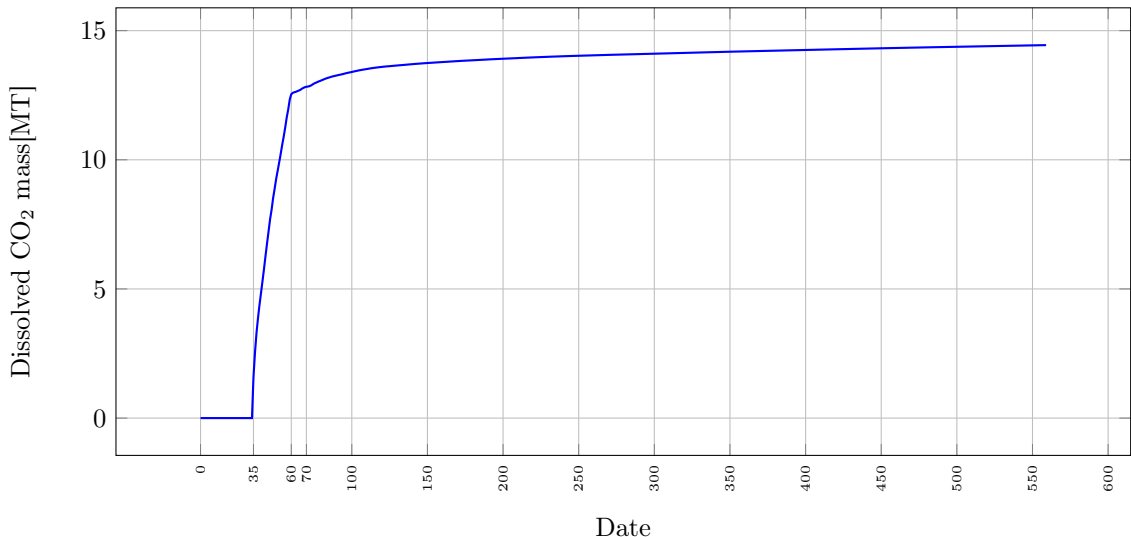


Figure 32: Total mass of CO<sub>2</sub> dissolved in the aqueous phase for a case with injection rate of 3 million ton per year

With the figures discussed, providing a foundational understanding, we now proceed to the sensitivity analysis. It is important to note a specific aspect of our methodology regarding pressure matching in our simulations. Initially, we achieved pressure matching using the technique detailed earlier in our study. However, when exploring the effects of altering different variables on the injection phase, employing previously established production rates from dummy wells was impractical. This is because adjustments in variables render these rates unsuitable for the new operational configurations. Ideally, we would have re-conducted the pressure matching process for each new variable setting to ensure accurate simulation. However, due to time constraints inherent in this study, repeated pressure matching was not feasible. To address this challenge, we utilized a pressure point obtained from previous pressure matching as the initial pressure distribution for subsequent simulations.

#### 5.4.1 Porosity

To investigate the influence of porosity distribution on NPV, the system's porosity values were scaled by factors of 0.75 and 1.25. These adjustments were compared against the base case, which in the next section will be introduced as CASE2. Higher porosity enables increased injection capacity and mitigates pressure buildup, resulting in lower bottom-hole pressure and consequently higher NPV. Surprisingly, both scenarios—lower and higher porosity—yielded lower NPV compared to CASE 2, contrary to initial expectations. To elucidate this phenomenon, a third case was formulated with reservoir properties identical to CASE 2, but adopting the pressure matching system employed in the current study. NPV from this case fell between the other two cases. Having a lower NPV compared to CASE 2, this scenario shares similar reasons as explained for the other two cases. Results for the four cases discussed are presented in Table 4. This table displays the final field average pressure for all cases. Three cases with a similar pressure matching system resulted in higher pressures because the dummy wells in these cases are not producing, making higher pressure levels expected. As anticipated, the effect of porosity on the field average pressure shows that cases with higher porosity yield lower pressures.

---

Table 4: Effect of Porosity on NPV and Field Average Pressure

| Case                                 | Factor | NPV [NOK] | Final Field Average Pressure [bar] |
|--------------------------------------|--------|-----------|------------------------------------|
| CASE 2                               | 1.00   | 8.26e9    | 136                                |
| Case with lower porosity             | 0.75   | 8.15e9    | 153                                |
| Case with similar porosity to CASE 2 | 1.00   | 8.19e9    | 150                                |
| Case with higher porosity            | 1.25   | 8.21e9    | 148                                |

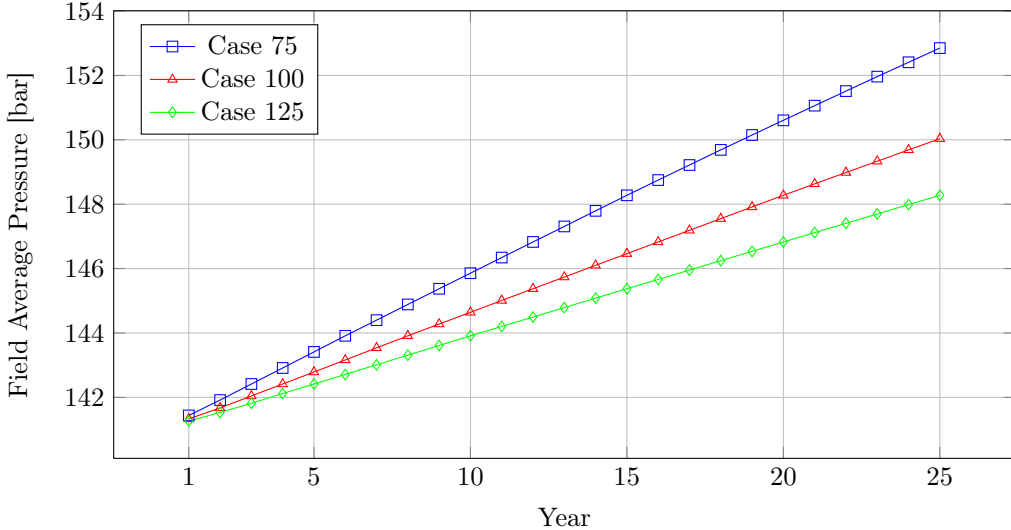


Figure 33: Field average pressure build-up versus time, for three cases with different porosity values.

#### 5.4.2 Saturation Functions

Two variations of saturation functions were employed, resulting in reduced Net Present Value compared to the base case. This decline primarily stems from alterations in the endpoint saturation at which gas mobility begins, residual gas saturation: the base case initiates gas movement at 12% saturation, while the new cases commence at 20% and 35%, respectively. The higher saturation thresholds in the new cases necessitate a higher injection pressure, leading to decreased NPV. Results are presented in Table 5

Table 5: Effect of Saturation Function on NPV and Field Average Pressure

| Case  | Residual Gas Saturation | NPV [NOK] | Final Field Average Pressure [bar] |
|---|-------------------------|-----------|------------------------------------|
| CASE 2  | 12%                     | 8.26e9    | 136                                |
| Case A  | 20%                     | 8.14e9    | 150                                |
| Case with similar saturation function to CASE 2 | 12%                     | 8.19e9    | 150                                |
| Case B  | 35%                     | 8.01e9    | 149.6                              |

Additionally, we examined the trends in field average pressure and bottom-hole pressure and plotted in Figure 34. Both new cases showed comparable increases in field average pressure due to consistent CO<sub>2</sub> injection volumes. However, Case B exhibited notably higher bottom-hole pressures compared to Case A. This disparity can be attributed to Case A's lower saturation threshold for CO<sub>2</sub> movement, which facilitates easier gas mobility and subsequently reduces bottom-hole pressure requirements. Moreover, the linear increase in relative permeability with saturation in Case A contributed to higher NPV by minimizing bottom-hole pressure demands, contrasting with Case B's flatter relative permeability curve and higher saturation thresholds.

This analysis underscores the critical role of saturation functions in shaping reservoir performance

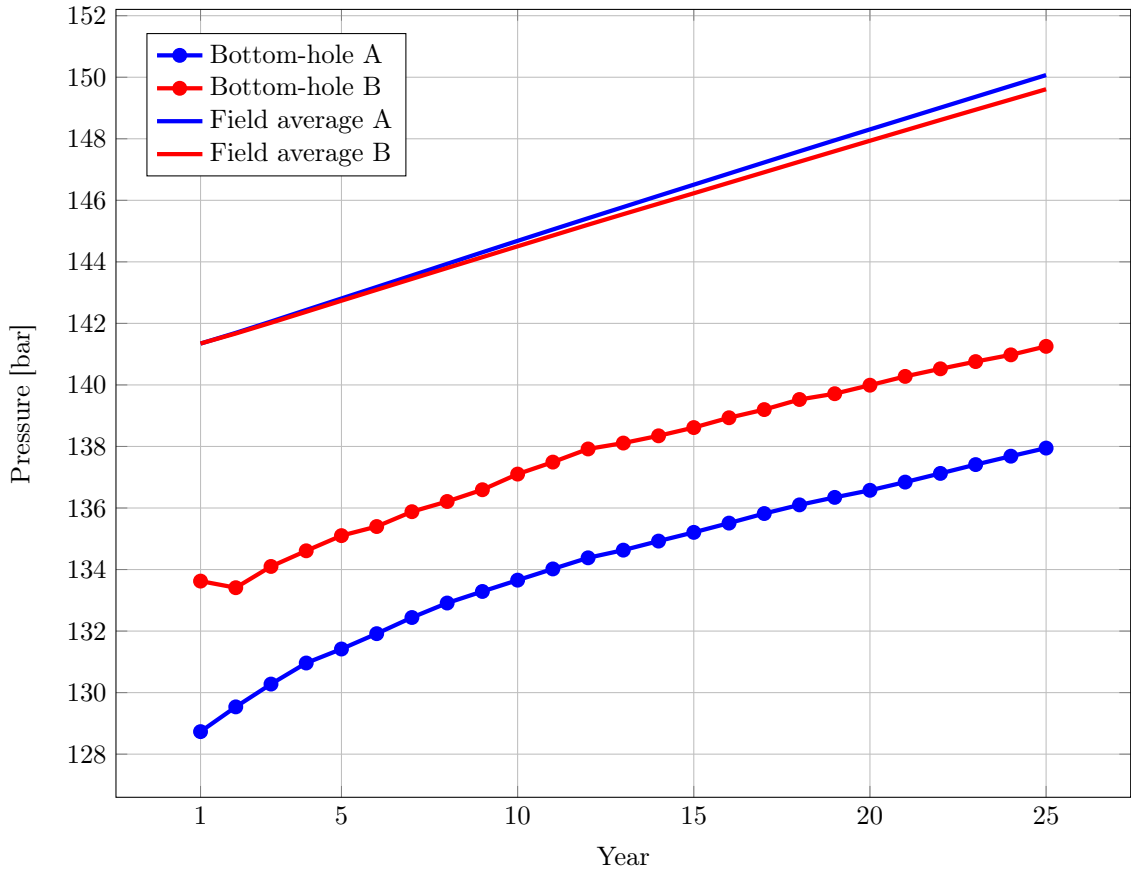


Figure 34: Field average pressure build-up during the injection period, and bottom-hole pressure for two cases with different saturation functions

and economic outcomes, highlighting the importance of accurately defining relative permeability curves in reservoir simulation studies.

#### 5.4.3 Permeability

To investigate the impact of permeability on Net Present Value, two distinct cases were analyzed with permeability values set at 0.75 and 1.25 times the initial values. The results demonstrate a higher NPV for the scenario with increased permeability and a lower NPV for the scenario with reduced permeability. This outcome can be attributed to the fact that greater permeability enhances injectivity factor, thereby reducing the required bottom-hole pressure.

The corresponding results for the NPV and final bottom-hole pressure are presented in Table 7.

Table 6: Effect of Permeability on NPV and Bottom-hole Pressure

| Case                                     | Factor | NPV [NOK] | Final Bottom-hole Pressure [bar] |
|--|--------|-----------|----------------------------------|
| CASE 2                                   | 1.00   | 8.26e9    | 126                              |
| Case with lower permeability             | 0.75   | 8.09e9    | 139                              |
| Case with similar permeability to CASE 2 | 1.00   | 8.19e9    | 136                              |
| Case with higher permeability            | 1.25   | 8.26e9    | 134                              |

Notably, although the case with higher permeability has a 25% increase in permeability, the change in NPV is approximately one percent. This suggests that even if the permeability data were not entirely accurate or precisely measured, having an approximation of the permeability could be sufficient for practical purposes. However, it is important to note that in this analysis, the permeability

---

values for the entire reservoir were altered uniformly. In a scenario where the permeability distribution varies spatially, the optimization results could be significantly affected, potentially leading to local optima in the area with higher permeability.

#### 5.4.4 Compressibility Factor

As in the previous sections, two distinct cases were established to examine the effect of rock compressibility factors on NPV and field pressures: one with a 25% decrease and the other with a 25% increase. The results indicate that a lower compressibility factor yields a lower NPV and higher bottom-hole pressure, whereas a higher compressibility factor results in a higher NPV and lower bottom-hole pressure. This phenomenon is explained by the relationship between the compressibility factor and the porosity. In this study, the Quadratic Rock Compressibility Model is used:

$$\phi = \phi(P_{\text{ref}}) \left( 1 + x + \frac{x^2}{2} \right)$$

where  $x$  is a function of the rock compressibility factor, given by:

$$x = C_{\text{rock}}(P - P_{\text{ref}})$$

According to this model, increasing the compressibility increases the porosity of the reservoir.

Table 7: Effect of Compressibility Factor on NPV and Bottom-hole Pressure

| Case  | Factor | NPV [NOK] | Final Bottom-hole Pressure [Bar] |
|---|--------|-----------|----------------------------------|
| CASE 2                                      | 1.00   | 8.26e9    | 126                              |
| Case with lower compressibility             | 0.75   | 8.17e9    | 137                              |
| Case with similar compressibility to CASE 2 | 1.00   | 8.19e9    | 136                              |
| Case with higher compressibility            | 1.25   | 8.21e9    | 135                              |

In summary, higher compressibility enhances NPV by higher increase in porosity values in constant pressure difference.

## 5.5 Optimization

In this section results for the well placement optimization are presented, and discussed. Results include five parts. Three first parts present the results and discuss the lateral well placement optimization, coupled well placement and perforation length optimization, lateral well placement optimization with two wells. Effect of the starting point, and pressure matching are also studied. Results for all cases are consolidated into a Table 8 to facilitate comparison.

### 5.5.1 Lateral Well Placement Optimization

In this section, we present the results of the optimization of lateral well placement within the Alpha structure of the reservoir.

#### Test Setup

The optimization of lateral well placement aimed to enhance reservoir performance by strategically positioning injection wells within the Alpha structure. The study commenced with a randomized initial location of (45, 120) in the reservoir model, which is perforated from top to the bottom of the reservoir. Three different cases with different injection rates, 1.5, 3, and 4.5 million tonne per year (MT/y), while maintaining a consistent higher bottom-hole pressure limit of 180 bar are set. This approach ensures that injection well operates at maximum efficiency, striving to maintain the specified injection rate until the bottom-hole pressure limit is reached, after which the injection rate decreases accordingly. In these tests the pressure distribution in the reservoir is matched with

the available pressure points, as explained in the previous section. Moreover, production from the dummy wells continue during the injection period, because the production from the troll field is expected to continue at least until the end of the injection process, which is January 1, 2050 in our cases. The injection starts from January 1, 2025.

The injection rate of 4.5 MT/y was chosen as it approximates the upper limit feasible for a standard injection well. The higher bottom-hole pressure limit, set at 180 bar, reflects industry experience in conventional reservoir management, as specific fracture pressure data for the formation are not publicly available.

Utilizing the Algorithm 5, we optimized the lateral placement of injection wells to maximize NPV. The algorithm iteratively adjusted well locations until reaching the configuration yielding the highest NPV.

## Results

Based on the results presented in Table 8, the optimal well locations for CASE1 and CASE2 were identical. However, a distinct final location was achieved for CASE3, indicating variability in optimization outcomes. In CASE 1 and 2, the final locations is on the northwest of the initial point, but for CASE 3 it is located on the southeast of the starting point.

### NPV Enhancement

For CASE1, CASE2, and CASE3, NPV increased by 3.6%, 2.7%, and 0.2%, respectively. These improvements underscore the effectiveness of optimized lateral well placement in enhancing economic viability and operational efficiency. Figure 35 illustrates the NPV values for all iterations in CASE 2, highlighting the improvement from the starting point to the final point. The blue bars represent positive NPV values, the red bars indicate negative NPV values due to penalties (with the absolute values plotted), the yellow bars denote values that have fallen outside the reservoir area, and the green bar indicates the highest NPV achieved.

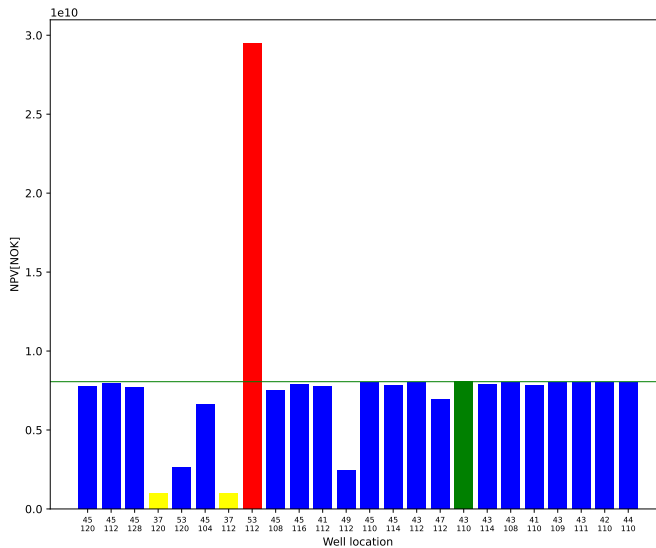


Figure 35: NPV values for all of well locations in the optimization loop for CASE 2

## Discussion

To gain a better understanding of the reasons behind the well movements, well locations from start to end are plotted on the permeability map of the reservoir in Figure 36. It should be noted that the values in the plot represent the average permeability along the z-axis. The analysis showed that in all cases, the wells moved towards cells with higher permeability values, aligning with

our understanding that higher permeability facilitates more efficient CO<sub>2</sub> injection and movement within the reservoir.

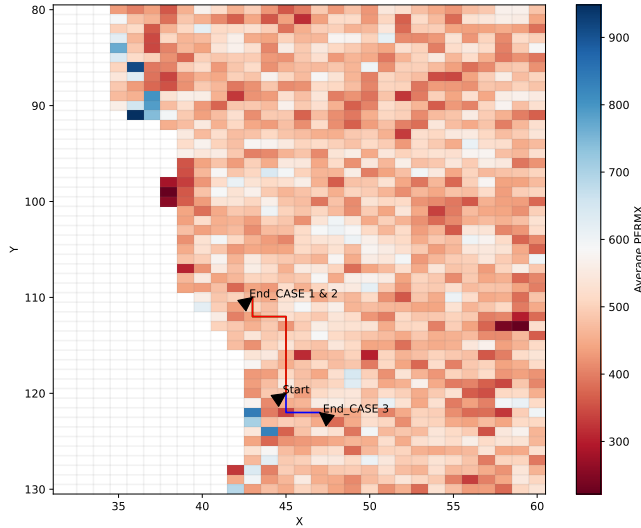


Figure 36: Well movement for CASE 1,2, and 3 plotted on the average permeability map

However, it is crucial to recognize that the permeability distribution in our model was randomly generated, which significantly differs from real-world permeability distributions. In reality, permeability values typically change gradually rather than abruptly from one cell to the next. This abrupt change in our model can cause the optimization process to miss some cells with higher permeability, which are located between two cells with low permeability.

This discrepancy between the modeled and real-world permeability distributions underscores the limitations of our current optimization approach. In practical scenarios, permeability gradients are smoother, leading to more predictable and reliable optimization outcomes. The random distribution in our model introduced a level of variability that can skew the optimization process, resulting in different final well placements and less consistent NPV improvements across cases.

To gain a deeper understanding of why CASE 3 ended in a different location, this issue will be further analyzed with additional data in subsequent sections.

### 5.5.2 Effect of Starting Point

To study the effect of the initial guess, CASE4 was configured identically to CASE3, except for the starting point. The initial point for CASE4 is located northeast of the initial guess used in the previous cases. The injection rate for CASE4 was selected based on the case that achieved the highest NPV in the previous set of cases.

## Results

With this configuration, the initial guess resulted in a negative NPV, indicating that a significant portion of the injected CO<sub>2</sub> moved out of the safe region. Similar to the previous cases, wells located in the northern and western parts of the reservoir yielded higher NPVs. Comparing the results from CASE3 and CASE4, the latter achieved a higher NPV.

## Discussion

One reason for the variability and the potential for getting trapped in a local optimum could be the distribution of porosity and permeability within the system. The porosity and permeability values

used in the simulation model appear to be randomly distributed. This randomness could cause the optimization process to converge to different local optima depending on the initial guesses and the specific scenario.

Moreover, the response surface for NPV in this optimization problem is relatively flat. This flatness means that small changes in well locations or operational parameters do not lead to significant changes in NPV, making it challenging to distinguish between different local optima. Importantly, this observation does not contradict our earlier statement regarding abrupt changes in permeability from one cell to the next. Even in cases of stark contrasts in permeability between adjacent cells, the resulting NPV values may not differ significantly. In such a landscape, the optimization algorithm might struggle to find the global optimum and instead settle on a locally optimal solution that is highly dependent on the initial conditions and the stochastic nature of the parameter distributions.

The NPV map for cases 3 and 4 is depicted in Figure X. In this figure, cells are colored based on NPV results: blue indicates positive values, while red indicates negative values. Yellow cells denote those outside the reservoir boundaries. Notably, cells located in the eastern part predominantly show negative NPVs, largely attributed to their proximity to the spill-point.

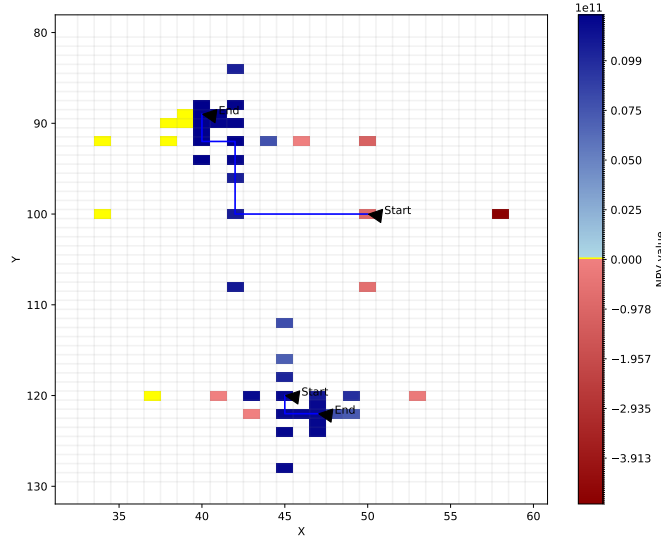


Figure 37: Results from CASE 3 and CASE 4, blue for positive NPV, red for negative NPV, and yellow for cells outside the reservoir domain.

To better understand why CASE 3 ended in a different location despite starting from the same point as CASE 1 and CASE 2, we plotted the penalty for each location in CASE 3 and CASE 4, as shown in Figure 38. The results indicate that for cases with higher injection rates, which inherently carry a higher risk of exceeding the reservoir capacity and allowing free CO<sub>2</sub> to migrate outside the safe region, the penalty values predominantly influence the optimal well location.

This finding aligns with our other results, which show that operational costs, primarily determined by reservoir parameters, remain relatively consistent across most cases. In contrast, penalty values vary significantly from case to case, underscoring their impact on determining the optimal well location in scenarios with higher injection rates.

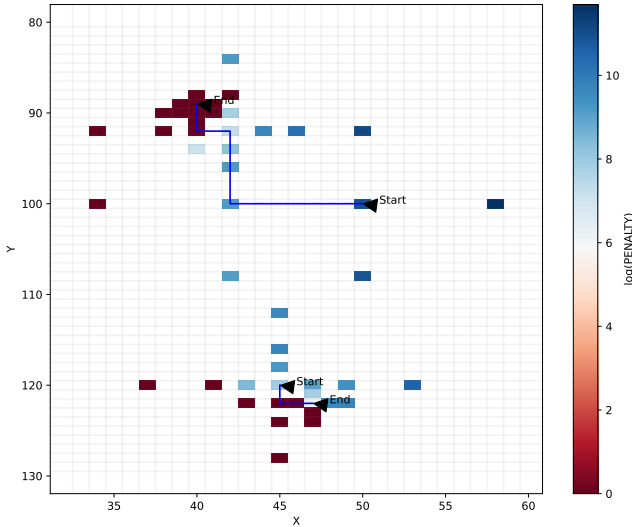


Figure 38: Results of well movement for CASE3 and 4 plotted on the map of the penalty of CO<sub>2</sub> leakage for each location

### 5.5.3 Effect of Pressure Matching

All of the four cases discussed above were done once again, but with no flow boundary conditions, meaning that the pressure distribution in the reservoir was initialized as the hydro-static pressure.

#### Results

For cases 1 and 2, the optimal well location were similar to the previous setup. On the other hand, for case 3 , and 4 different location were obtained. In all of the cases, NPVs for the pressure matched cases were higher than the no flow boundary cases.

#### Discussion

Results demonstrated that cases implementing pressure matching achieved higher NPVs. This advantage arises from lower initial reservoir pressure in pressure-matched cases, and maintaining lower reservoir pressures through continuous production from dummy production wells during injection. This translates to reduced bottom-hole pressure requirements, thereby lowering operational costs associated with maintaining injection rates. These findings underscore the economic benefits of pressure matching in optimizing CO<sub>2</sub> injection projects by ensuring more efficient operational conditions and cost-effectiveness.

It is important to acknowledge that in our specific cases, the bottom-hole pressure did not reach the higher limit of 180 bar that was chosen. This outcome could be attributed to factors such as the size of the reservoir or the initial reservoir pressure, potentially influenced by its depth. However, in scenarios where the reservoir size is smaller, or the bottom-hole pressure limit is lower, there is a heightened risk of reaching the upper pressure limit during injection operations. This scenario could necessitate a reduction in injection rates to avoid exceeding the pressure limits, potentially due to the reservoir's fracture pressure. Resulting in lower CO<sub>2</sub> injection volumes and potentially reduced revenue. In such cases, the critical importance of pressure matching becomes evident. Pressure matching ensures that the reservoir pressure is managed within safe operational limits throughout the injection process, thereby optimizing injection rates and maximizing CO<sub>2</sub> storage capacity while maintaining economic viability.

---

#### **5.5.4 Coupled Well Placement and Perforation Length Optimization**

In the previous sections, we discussed eight cases where wells were perforated from the top to the bottom of the reservoir. In this part, we present the results of an additional case where the wells were perforated from a specific point to the bottom of the reservoir.

In this new case, the optimization process included varying the top of the perforation interval to achieve the highest NPV. The objective was to determine whether adjusting the perforation interval, in addition to the lateral well placement, could enhance the results of CO<sub>2</sub> sequestration projects.

#### **Results**

During the optimization process, similar to the previous cases, the lateral movement of the well led to the identification of an optimum point located in the northwest direction relative to the initial guess. Additionally, the perforation interval in the optimum case was found to be larger compared to the initial configuration, to be more specific, in the initial configuration layers 15 to 25 were perforated, while in the optimum case perforation top was moved to layer 11.

Although this case did not necessarily result in a higher NPV compared to the previous cases, the approach of adjusting the top of the perforation interval provided valuable insights. The larger perforation interval allowed for increased exposure of the reservoir to the wellbore, which has implications for injected CO<sub>2</sub> flow in the reservoir and higher NPV values, which is mainly due to the lower operational costs.

#### **Discussion**

The primary reason the top of the perforation interval did not move further up to layer 1, but only to layer 11, can be attributed to the thickness and properties of the different reservoir layers. Most of the reservoir's pore volume is concentrated in the deeper layers. Injecting CO<sub>2</sub> into these deeper layers is effectively equivalent to injecting into the whole reservoir due to their higher storage capacity and permeability. The deeper layers, therefore, offer a more efficient pathway for CO<sub>2</sub> flow, resulting in lower operational costs and higher NPVs, even without extending the perforation interval to the uppermost layers.

Injecting closer to the cap rock can be a safer option because it minimizes the risk of CO<sub>2</sub> encountering thin, impermeable layers that could divert the CO<sub>2</sub> outside the intended safe region for injection. However, injecting too close to the cap rock might increase the pressure in this region, potentially endangering the containment integrity of the cap rock. Conversely, deeper injection has the advantage of utilizing more of the reservoir's pore volume for residual trapping, resulting in a larger CO<sub>2</sub> plume. This larger plume can enhance containment by providing a greater volume for CO<sub>2</sub> to be trapped, and consequently more dissolved CO<sub>2</sub>, thus improving the overall security of the storage site.

This finding highlights the importance of considering the distribution of pore volume and permeability within the reservoir during the optimization process. While increasing the perforation interval can expose more of the reservoir to the wellbore, it is crucial to target layers that contribute significantly to the overall storage capacity. Consequently, optimizing the top of the perforation interval to layer 11 strikes a balance between enhancing reservoir exposure and maintaining operational efficiency, given the specific characteristics of the reservoir in this study.

---

#### **5.5.5 Lateral Well Placement Optimization with Two Injection Wells**

The well placement optimization test began with two initial guesses, as outlined in the earlier sections. In each iteration, the case with the highest NPV among the eight possible scenarios was selected. The results indicated that the optimal configuration involved relocating both wells to the northwestern part of the reservoir, away from the spill-points. In this scenario, each injection well was injecting 2.25 million tonne of CO<sub>2</sub> per year.

#### **Discussion**

Despite the higher drilling costs associated with this setup, the NPV was higher compared to a scenario where the same amount of CO<sub>2</sub> was injected using a single well. This increase in NPV can be attributed to the reduced pressure buildup around each well when injecting from two wells at a lower rate. Lower pressure buildup necessitates a lower bottom-hole pressure, which in turn reduces operational costs. Consequently, the distribution of injection between two wells proved to be more cost-effective despite the initial higher drilling expenses.

Table 8: Optimization Results for different cases

| Case         | Initial Location  | Injection Rate | NPV     | Best Location    | Highest NPV | Improvement | No. of Runs |
|--------------|-------------------|----------------|---------|------------------|-------------|-------------|-------------|
| CASE1        | 45, 120           | 1.5            | 3.58e9  | 43, 110          | 3.71e9      | 3.6%        | 29          |
| CASE1_HS     | 45, 120           | 1.5            | 3.34e9  | 43, 110          | 3.49e9      | 4.5%        | 29          |
| CASE2        | 45, 120           | 3              | 8.04e9  | 43, 110          | 8.26e9      | 2.7%        | 29          |
| CASE2_HS     | 45, 120           | 3              | 7.57e9  | 43, 110          | 7.86e9      | 3.8%        | 29          |
| CASE3        | 45, 120           | 4.5            | 1.34e10 | 47, 122          | 1.34e10     | 0.2%        | 25          |
| CASE3_HS     | 45, 120           | 4.5            | 1.26e10 | 46, 119          | 1.27e10     | 0.3%        | 29          |
| CASE4        | 50, 100           | 4.5            | -8e10   | 40, 89           | 1.37e10     |             | 37          |
| CASE4_HS     | 50, 100           | 4.5            | -6e10   | 42, 92           | 1.29e10     |             | 25          |
| Place & Perf | 50, 110, 15       | 4.5            | 8.16e9  | 43, 108, 11      | 1.35e10     | 65.4%       | 61          |
| Two Wells    | 45, 120 & 50, 110 | 2.25 & 2.25    | 1.07e10 | 42, 108 & 43, 94 | 1.39e10     | 30.0%       | 65          |

In the end, two figures depicting the CO<sub>2</sub> saturation for Case 2 at different times are presented. Figure 39 illustrates the shape of the CO<sub>2</sub> plume at the end of injection, showing cells with gas saturation greater than zero. Figure 40 displays the CO<sub>2</sub> saturation results 500 years after injection cessation in the map of the safe region. It is evident from the second figure that free CO<sub>2</sub> has not migrated out of the safe area, indicating promising containment. It is noteworthy that a total of 75 million tonnes of CO<sub>2</sub> were injected into the reservoir in this case.

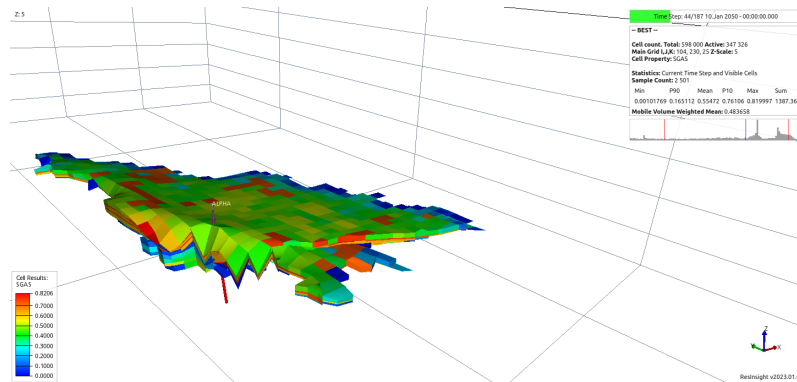


Figure 39: CO<sub>2</sub> plume shape at the end of injection for CASE 2, showing cells with gas saturation higher than zero.

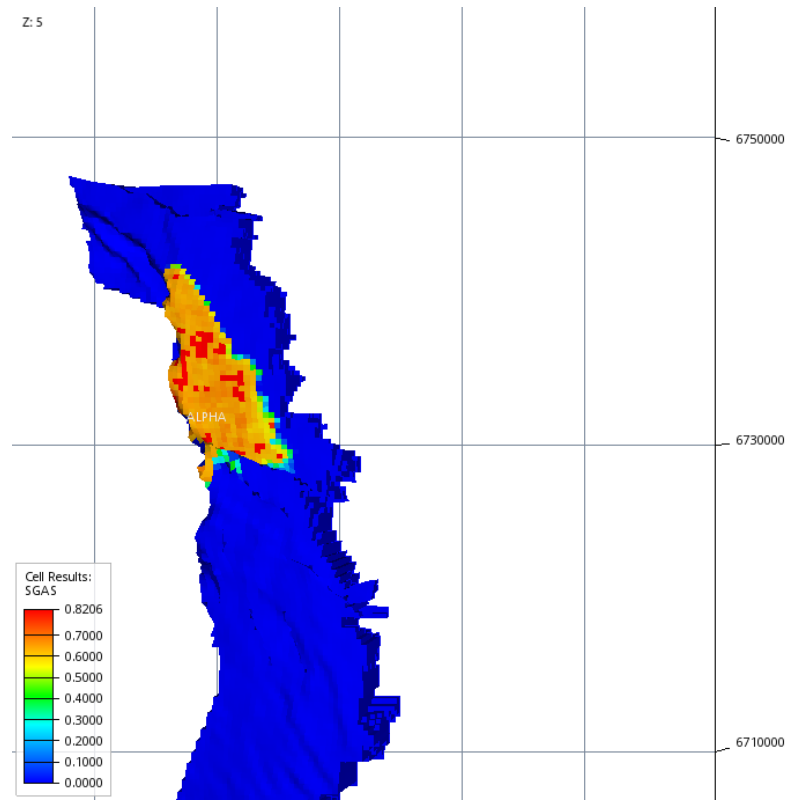


Figure 40: CO<sub>2</sub> saturation 500 years after injection cessation in the safe region map, demonstrating effective containment within the designated area

---

## 6 Conclusion

The primary objective of this research was to develop a workflow for optimizing injection well placement in CCS projects. Achieving this goal involved several critical subtasks, ensuring better and more reliable results. These subtasks addressed key issues related to initial reservoir pressure, CO<sub>2</sub> sequestration safety, data availability, and parameter sensitivity. Additionally, well placement optimization was approached for three different scenarios.

### 6.1 Key Findings and Implications

**Initial Reservoir Pressure:** Understanding initial reservoir pressure is vital, particularly when injecting into depleted hydrocarbon reservoirs or saline aquifers in pressure communication with producing fields. This aspect was thoroughly covered in our work.

**CO<sub>2</sub> Sequestration Safety:** For CO<sub>2</sub> sequestration projects, especially regarding containment and storage safety, identifying spill-points within the injection structure is necessary if one wants to include penalties for reaching the spill point into the NPV calculation. Our research successfully identified these spill-points, establishing a foundation for subsequent steps.

**Data Availability and Sensitivity Analysis:** In saline aquifer CCS projects, data availability poses significant challenges. We conducted a sensitivity analysis on four critical parameters: porosity, permeability, relative permeability (saturation function), and compressibility factor. This analysis demonstrated that while minor variations in these parameters do not significantly alter results such as optimal well location, larger deviations, especially in porosity and relative permeability, can substantially impact NPV and pressure distribution.

**Well Placement Optimization:** Optimization was executed in three approaches: lateral optimization with one well, two wells, and both lateral and perforation interval optimization. The derivative-free compass search method was employed, yielding several insights:

- For cases with the same starting point, lower injection rates converged to the same optimal point.
- Higher injection rates resulted in varied optimal points.
- Different starting points influenced the final optimal points, particularly in cases with flat response surfaces.
- Longer perforation intervals generally resulted in higher NPVs. However, the optimal solution was not the longest possible interval.
- Using two wells achieved the highest NPV, balancing initial investments with operational costs and bottom-hole pressure reductions. This result might be skewed by the use of an unrealistically low well cost in the optimization.
- For well placement, the optimization results indicated that well placement is primarily dominated by the penalties assigned for leaked CO<sub>2</sub>, followed by the petrophysical characteristics of the reservoir.

### 6.2 Limitations

**Data Availability:** The lack of complete data was a significant limitation. This is expected to be a common problem for CCS projects, as they are expected to have few wells compared to traditional hydrocarbon fields and therefore little available information about the subsurface.

**Computational Constraints:** High computational times and limited computational power hindered the efficiency of our research. One could have leveraged more starting points or optimization

---

routines that use more function evaluation if given more computation power. This might be necessary for optimization problems where the response surface is relatively flat, making it hard to localize the global optimum.

### 6.3 Recommendations for Future Work

**Enhanced Spill-Point Identification:** Future studies should perform spill-point identification in multiple directions for more robust results.

**Improved Pressure Matching:** Utilizing a larger model that includes the Troll field and its real data could enhance pressure-matching accuracy. Such a simulation could be conducted once, to estimate the boundary conditions of a smaller model used further for optimization of the sequestration.

**Comprehensive Sensitivity Analysis:** Conducting pressure matching for each sensitivity case and comparing the results would provide deeper insights.

**Refined Parameter Distribution:** Employing a more realistic permeability and porosity instead of a random distribution could yield more realistic outcomes. A simple improvement could be to use an ensemble of models with a Gaussian random field distribution for the porosity and permeability.

**Alternative Optimization Methods:** Exploring other optimization techniques that reduce the likelihood of falling into local optima and adjusting stencil sizes based on search space dimensions would likely improve optimization results. This is likely to increase computational costs.

**Joint Optimization:** Conducting both well placement and well control optimization could enhance overall efficiency. Additionally, performing a joint optimization while limiting the reservoir domain to the more important parts can help decrease computational costs.

### 6.4 Final Thoughts

In conclusion, this research has demonstrated the importance of initial reservoir conditions, safety considerations in CO<sub>2</sub> sequestration, and the impact of key parameters on injection strategies. While significant progress has been made in optimizing well placement, further enhancements in methodology and computational resources could lead to even more effective and reliable outcomes. This work could serve as a foundation for future research aimed at improving injection well optimization techniques and ensuring the safe and efficient sequestration of CO<sub>2</sub>.

Although the optimization methods used in petroleum production can be applied to CCS projects, additional actions and modifications are required to achieve optimal results in the context of CO<sub>2</sub> storage. This highlights the need for ongoing adaptation and refinement of these methods to address the unique challenges presented by CCS applications.

---

## Bibliography

- [1] URL: <https://docs.opengosim.com> (visited on 19th Dec. 2023).
- [2] Hisham Al Baroudi et al. ‘A review of large-scale CO<sub>2</sub> shipping and marine emissions management for carbon capture, utilisation and storage’. In: *Applied Energy* 287 (2021), p. 116510.
- [3] Muhammad Amjad. ‘Imaging Reservoir Geology of the Troll West Field in the North Sea by 3D Seismic Interpretation’. MA thesis. Institutt for petroleumsteknologi og anvendt geofysikk, 2014.
- [4] Yazan Arouri and Mohammad Sayyafzadeh. ‘An adaptive moment estimation framework for well placement optimization’. In: *Computational Geosciences* 26.4 (2022), pp. 957–973.
- [5] Masoud Babaee, Indranil Pan and Ali Alkhatab. ‘Robust optimization of well location to enhance hysteretical trapping of CO<sub>2</sub>: Assessment of various uncertainty quantification methods and utilization of mixed response surface surrogates’. In: *Water Resources Research* 51.12 (2015), pp. 9402–9424.
- [6] Masoud Babaee et al. ‘CO<sub>2</sub> storage well rate optimisation in the Forties sandstone of the Forties and Nelson reservoirs using evolutionary algorithms and upscaled geological models’. In: *International Journal of Greenhouse Gas Control* 50 (2016), pp. 1–13.
- [7] Einar Johan Moen Baumann. ‘Fieldopt: Enhanced software framework for petroleum field optimization-development of software support system for the integration of oil production problems with optimization methodology’. MA thesis. NTNU, 2015.
- [8] Larry Baxter, Andrew Baxter and Stephanie Burt. ‘Cryogenic CO<sub>2</sub> capture as a cost-effective CO<sub>2</sub> capture process’. In: *International Pittsburgh Coal Conference*. 2009.
- [9] RC Bissell et al. ‘A full field simulation of the In Salah gas production and CO<sub>2</sub> storage project using a coupled geo-mechanical and thermal fluid flow simulator’. In: *Energy Procedia* 4 (2011), pp. 3290–3297.
- [10] David A Cameron and Louis J Durlofsky. ‘Optimization of well placement, CO<sub>2</sub> injection rates, and brine cycling for geological carbon sequestration’. In: *International Journal of Greenhouse Gas Control* 10 (2012), pp. 100–112.
- [11] CCS Norway. *Feasibility Study: Full-scale CCS in Norway*. Accessed: 2024-06-27. 2016. URL: [https://ccsnorway.com/app/uploads/sites/6/2019/09/feasibilitystudy\\_fullscale\\_ccs\\_norway\\_2016.pdf](https://ccsnorway.com/app/uploads/sites/6/2019/09/feasibilitystudy_fullscale_ccs_norway_2016.pdf).
- [12] D Echeverría Ciaurri, Obiajulu J Isebor and Louis J Durlofsky. ‘Application of derivative-free methodologies to generally constrained oil production optimization problems’. In: *Procedia Computer Science* 1.1 (2010), pp. 1301–1310.
- [13] Abdullah Cihan, Jens T Birkholzer and Marco Bianchi. ‘Optimal well placement and brine extraction for pressure management during CO<sub>2</sub> sequestration’. In: *International Journal of Greenhouse Gas Control* 42 (2015), pp. 175–187.
- [14] Cal Cooper et al. ‘A technical basis for carbon dioxide storage’. In: *Energy Procedia* 1.1 (2009), pp. 1727–1733.
- [15] Norwegian Offshore Directorate. *4.1 - Geology of the North Sea*. Accessed: 2024-06-27. 2024. URL: <https://www.sodir.no/en/whats-new/publications/co2-atlases/co2-atlas-for-the-norwegian-continental-shelf/4-the-norwegian-north-sea/4.1-geology-of-the-north-sea/>.
- [16] Jr. Donald R. Burgess. ‘Thermochemical Data’. In: *NIST Chemistry WebBook*. Ed. by P.J. Linstrom and W.G. Mallard. NIST Standard Reference Database Number 69. Gaithersburg MD, 20899: National Institute of Standards and Technology, 2024. doi: 10.18434/T4D303. URL: <https://doi.org/10.18434/T4D303>.
- [17] Henhao Duan and Rui Sun. ‘An improved model calculating co<sub>2</sub> solubility in pure water and aqueous nacl solutions from 273 to 533 k and from 0 to 2000 bar’. In: *Chemical geology* (2003).
- [18] Zhenhao Duan et al. ‘Densities of the CO<sub>2</sub>-H<sub>2</sub>O and CO<sub>2</sub>-H<sub>2</sub>O-NaCl systems up to 647K and 100 MPa’. In: *Energy & Fuels* (2008).

- 
- [19] Celina Duong et al. ‘Quest carbon capture and storage offset project: Findings and learnings from 1st reporting period’. In: *International Journal of Greenhouse Gas Control* 89 (2019), pp. 65–75.
  - [20] Tobias Dyngeland and Anne C. Elster. ‘Accelerating PFLOTRAN-OGS on GPUs using PETSc’. In: <https://www.ntnu.no/ojs/index.php/nikt/article/view/5668/5108>. Trondheim, Norway: Norwegian University of Science and Technology, Dept. of Computer Science, 2023.
  - [21] Equinor. *Selected extracts from Statoil internal report on Subsurface Evaluation of Smeaheia as part of 2016 Feasibility study on CO<sub>2</sub> storage in the Norwegian Continental shelf*. Tech. rep. 2016.
  - [22] DN Espinoza et al. ‘Optimization of CO<sub>2</sub> Injector Location and Rate in Compartmentalized Reservoirs’. In: *ARMA US Rock Mechanics/Geomechanics Symposium*. ARMA. 2022, ARMA–2022.
  - [23] JE Evensen, Mari Skaug and Peter Goodey. ‘Production geological challenges of characterizing the thin oil rims in the Troll field’. In: *Offshore Technology Conference*. OTC. 1993, OTC–7172.
  - [24] PHM Feron and CA Hendriks. ‘CO<sub>2</sub> capture process principles and costs’. In: *Oil & Gas Science and Technology* 60.3 (2005), pp. 451–459.
  - [25] José D Figueroa et al. ‘Advances in CO<sub>2</sub> capture technology—the US Department of Energy’s Carbon Sequestration Program’. In: *International journal of greenhouse gas control* 2.1 (2008), pp. 9–20.
  - [26] Robert J Finley. ‘An overview of the Illinois Basin–Decatur project’. In: *Greenhouse Gases: Science and Technology* 4.5 (2014), pp. 571–579.
  - [27] Robert J Finley et al. ‘Early operational experience at a one-million tonne CCS demonstration project, Decatur, Illinois, USA’. In: *Energy Procedia* 37 (2013), pp. 6149–6155.
  - [28] Sofianos Panagiotis Fotias, Ismail Ismail and Vassilis Gaganis. ‘Optimization of Well Placement in Carbon Capture and Storage (CCS): Bayesian Optimization Framework under Permutation Invariance’. In: *Applied Sciences* 14.8 (2024), p. 3528.
  - [29] Anne-Kari Furre et al. ‘20 Years of Monitoring CO<sub>2</sub>-injection at Sleipner’. In: *Energy procedia* 114 (2017), pp. 3916–3926.
  - [30] Takashi Goda and Kozo Sato. ‘Global optimization of injection well placement toward higher safety of CO<sub>2</sub> geological storage’. In: *Energy Procedia* 37 (2013), pp. 4583–4590.
  - [31] Ana González-Nicolás et al. ‘Pressure management via brine extraction in geological CO<sub>2</sub> storage: Adaptive optimization strategies under poorly characterized reservoir conditions’. In: *International Journal of Greenhouse Gas Control* 83 (2019), pp. 176–185.
  - [32] E. K. Halland, W. T. Johansen and F. Riis. *CO<sub>2</sub> Storage Atlas North Sea*. Stavanger: Norwegian Petroleum Directorate, 2011.
  - [33] Olav Hansen et al. ‘Snøhvit: The history of injecting and storing 1 Mt CO<sub>2</sub> in the fluvial Tubåen Fm’. In: *Energy Procedia* 37 (2013), pp. 3565–3573.
  - [34] John Houghton. ‘Global warming’. In: *Reports on progress in physics* 68 1343 (2005).
  - [35] National centers for environmental information. *Annual 2023 Global Climate Report*. 2024. URL: <https://www.ncei.noaa.gov/access/monitoring/monthly-report/global/202313> (visited on 18th Nov. 2023).
  - [36] International Energy Agency. *CO<sub>2</sub> Storage Resources and their Development*. Accessed: 2024-06-27. International Energy Agency. 2022. URL: <https://www.iea.org/reports/co2-storage-resources-and-their-development>.
  - [37] Hoonyoung Jeong, Alexander Y Sun and Xiaodong Zhang. ‘Cost-optimal design of pressure-based monitoring networks for carbon sequestration projects, with consideration of geological uncertainty’. In: *International Journal of Greenhouse Gas Control* 71 (2018), pp. 278–292.
  - [38] Changhyeok Jun, Min Kim and Hyundon Shin. ‘Optimization of well placement and operating conditions for various well patterns in CO<sub>2</sub> sequestration in the Pohang Basin, Korea’. In: *International Journal of Greenhouse Gas Control* 90 (2019), p. 102810.

- 
- [39] Tamara G Kolda, Robert Michael Lewis and Virginia Torczon. ‘Optimization by direct search: New perspectives on some classical and modern methods’. In: *SIAM review* 45.3 (2003), pp. 385–482.
- [40] Deepanshu Kumar. ‘Optimization of well settings to maximize residually trapped CO<sub>2</sub> in geologic carbon sequestration’. In: *report submitted to the department of energy resources engineering of Stanford university* (2007).
- [41] Lawrence Berkeley National Laboratory. *ESS-DIVE – Deep Insight for Earth Science Data*. Accessed: 2024-06-27. 2024. URL: <https://ess-dive.lbl.gov/>.
- [42] DE Lumley. ‘4D Seismic Monitoring of Complex CO<sub>2</sub> Injection Effects for Carbon Sequestration Projects’. In: *AGU Fall Meeting Abstracts*. Vol. 2011. 2011, GC44A–01.
- [43] Jinfeng Ma et al. ‘Carbon capture and storage: history and the road ahead’. In: *Engineering* 14 (2022), pp. 33–43.
- [44] Allan Mathieson et al. ‘In Salah CO<sub>2</sub> Storage JIP: CO<sub>2</sub> sequestration monitoring and verification technologies applied at Krechba, Algeria’. In: *Energy Procedia* 4 (2011), pp. 3596–3603.
- [45] Alireza Mohsenifegandis. ‘Exploring the Impact of Thermal Considerations on CO<sub>2</sub> Plume Shape and Sensitivity Studies’. Specialization Project Report, Norwegian University of Science and Technology, 2023. 2023.
- [46] Kudrat Musayev, Hyundon Shin and Viet Nguyen-Le. ‘Optimization of CO<sub>2</sub> injection and brine production well placement using a genetic algorithm and artificial neural network-based proxy model’. In: *International Journal of Greenhouse Gas Control* 127 (2023), p. 103915.
- [47] Long Nghiem et al. ‘Optimization of residual gas and solubility trapping for CO<sub>2</sub> storage in saline aquifers’. In: *SPE Reservoir Simulation Conference?* SPE. 2009, SPE–119080.
- [48] Long Nghiem et al. ‘Simulation and optimization of trapping processes for CO<sub>2</sub> storage in saline aquifers’. In: *Journal of Canadian Petroleum Technology* 49.08 (2010), pp. 15–22.
- [49] Halvor Møll Nilsen et al. ‘Spill-point analysis and structural trapping capacity in saline aquifers using MRST-co2lab’. In: *Computers & geosciences* 75 (2015), pp. 33–43.
- [50] Batuhan Osmanoğlu et al. ‘Time series analysis of InSAR data: Methods and trends’. In: *ISPRS Journal of Photogrammetry and Remote Sensing* 115 (2016), pp. 90–102.
- [51] Indranil Pan et al. ‘A multi-period injection strategy based optimisation approach using kriging meta-models for CO<sub>2</sub> storage technologies’. In: *Energy Procedia* 63 (2014), pp. 3492–3499.
- [52] Changhyup Park et al. ‘Multi-objective optimization of CO<sub>2</sub> sequestration in heterogeneous saline aquifers under geological uncertainty’. In: *Applied Sciences* 11.20 (2021), p. 9759.
- [53] Kurt R Petvipsit et al. ‘Robust optimisation of CO<sub>2</sub> sequestration strategies under geological uncertainty using adaptive sparse grid surrogates’. In: *Computational Geosciences* 18 (2014), pp. 763–778.
- [54] K.M. Reinicke and C. Fichter. ‘Measurement strategies to evaluate the integrity of deep wells for CO<sub>2</sub> applications’. In: *Underground Storage of CO<sub>2</sub>, Energy* (2010), p. 67.
- [55] Philip Ringrose. *How to Store CO<sub>2</sub> Underground: insights from early-mover CCS Projects*. Springer, 2020.
- [56] PS Ringrose et al. ‘The In Salah CO<sub>2</sub> storage project: lessons learned and knowledge transfer’. In: *Energy Procedia* 37 (2013), pp. 6226–6236.
- [57] Hossein Shamshiri and Behnam Jafarpour. ‘Optimization of geologic CO<sub>2</sub> storage in heterogeneous aquifers through improved sweep efficiency’. In: *SPE International Conference on CO<sub>2</sub> Capture, Storage, and Utilization*. SPE. 2010, SPE–139643.
- [58] Roland Span and Wolfgang Wagner. ‘A new equation of state for carbon dioxide covering the fluid region from the triple-point temperature to 1100K at pressures up to 800 MPa’. In: *Journal of physical and chemical reference data* (1996).
- [59] Bachu Stefan. ‘Screening and ranking of sedimentary basins for sequestration of CO<sub>2</sub> in geological media in response to climate change’. In: *Environmental Geology* (2003).

- 
- [60] Jerzy Stopa et al. ‘Optimization of well placement and control to maximize CO<sub>2</sub> trapping during geologic sequestration’. In: *AGH Drilling, Oil, Gas* 33.1 (2016), pp. 93–104.
  - [61] Alexander Y Sun. ‘Optimal carbon storage reservoir management through deep reinforcement learning’. In: *Applied Energy* 278 (2020), p. 115660.
  - [62] Alexander Y Sun et al. ‘Using pulse testing for leakage detection in carbon storage reservoirs: A field demonstration’. In: *International Journal of Greenhouse Gas Control* 46 (2016), pp. 215–227.
  - [63] Rickard Svensson et al. ‘Transportation systems for CO<sub>2</sub>—application to carbon capture and storage’. In: *Energy conversion and management* 45.15-16 (2004), pp. 2343–2353.
  - [64] Yutaka Tanaka et al. ‘Tomakomai CCS demonstration project of Japan, CO<sub>2</sub> injection in process’. In: *Energy Procedia* 114 (2017), pp. 5836–5846.
  - [65] Daiji Tanase et al. ‘The post-injection phase of the Tomakomai CCS Demonstration Project’. In: *Proceedings of the 16th Greenhouse Gas Control Technologies Conference (GHGT-16)*. 2022, pp. 23–24.
  - [66] Mohammadali Tarrahi and Sardar Afra. ‘Optimization of Geological Carbon Sequestration in Heterogeneous Saline Aquifers through Managed Injection for Uniform CO<sub>2</sub> Distribution’. In: *Carbon Management Technology Conference*. CMTC. 2015, CMTC–440233.
  - [67] Caroline Wildbolz. ‘Life cycle assessment of selected technologies for CO<sub>2</sub> transport and sequestration’. In: *Diplom Thesis. Zurich: Swiss Federal Institute of Technology* (2007).
  - [68] S Wong. ‘CO<sub>2</sub> Compression and Transportation to Storage Site’. In: *Building Capacity for CO<sub>2</sub> Capture and Storage in the APEC region: A training manual for policy makers and practitioners* (2009).
  - [69] Stephen J Wright. *Numerical optimization*. 2006.
  - [70] Zheming Zhang and Ramesh Agarwal. ‘Numerical simulation and optimization of CO<sub>2</sub> sequestration in saline aquifers’. In: *Computers & Fluids* 80 (2013), pp. 79–87.
  - [71] Fangning Zheng et al. ‘Geologic CO<sub>2</sub> storage optimization under geomechanical risk using coupled-physics models’. In: *International Journal of Greenhouse Gas Control* 110 (2021), p. 103385.
  - [72] Amy Zou and Louis J Durlofsky. ‘Integrated framework for optimization of horizontal/deviated well placement and control for geological CO<sub>2</sub> storage’. In: *SPE Reservoir Simulation Conference?* SPE. 2023, D021S010R003.

